A Contemporary Study in the Theory of Traveling-Wave Tubes

by

Patrick Pat-Yeung Wong

A dissertation submitted in partial fulfillment
of the requirements for the degree of
Doctor of Philosophy
(Nuclear Engineering and Radiological Sciences)
in the University of Michigan
2018

Doctoral Committee:

Professor Yue Ying Lau, Chair
Dr. David P. Chernin, Leidos, Inc.
Professor Ronald M. Gilgenbach
Dr. Brad W. Hoff, Air Force Research Laboratory
Assistant Professor Louise Willingale

Patrick Y. Wong

pywong@umich.edu

ORCID iD: 0000-0002-8437-6990

Acknowledgements

"If I have seen further it is by standing on the shoulders of giants." I begin this thesis with a quote from Sir Issac Newton, my academic ancestor. Indeed, since I began the arduous process that is the PH. D program I have seen much further, and it is largely due to those who have kindly allowed me to stand on their shoulders. In particular, my academic advisor, Professor Y. Y. Lau, deserves many thanks for giving me the opportunity to study under him and for initiating me into the world of academia and my field of study. He has been not only a mentor but also a friend to me. I would also like to thank Dr. David Chernin for his invaluable advice and guidance throughout the years. None of what is presented in this thesis would be possible if it were not for his contributions and his infinite patience with a "green" fellow such as myself. Dr. Brad Hoff has been by my side since the beginning, and for that, I am truly grateful. His direct and tireless support in all aspects of my entire graduate education is decisive. He and his Air Force Research Laboratory colleague, Dr. David Simon, have aided at several points in this thesis with their simulation skills. Though our paths rarely intersected, Professor Ronald Gilgenbach has been a tremendous help to me, offering me support when I needed it most, especially towards the end of my tenure as a graduate student. Of course, it has always been very heart-warming to see Professor Louise Willingale's smile and hear her advice with regards to navigating the politics and pitfalls of the academic world. I will not forget the first couple of lectures in your laser-plasma diagnostics class.

I would also like to thank Professor John Foster and the whole plasma physics community in the Department of Nuclear Engineering and Radiological Sciences for teaching

and fostering my interest in the vast subject of plasma physics. I have learned much from attending your classes.

I would also like to express my deepest appreciations to my graduate coordinator, Peggy Jo Gramer, and the friends I have made here in graduate school and my friends back home. I greatly value all of the chats we have had and the emotional support you all have provided.

Lastly, but definitely not least, I would like to thank my parents, who have always been there for me without condition. Whether it is providing invaluable advice, taking me to and picking me up from school (yes, I am an 80-mile-a-day daily commuter), or simply listening to me when I needed to talk, your presence has not gone unappreciated. I am also proud to be a first-generation college PH. D student and for fulfilling my father's life-long dream. The last couple of years have been very rough in many more ways than one, but we have endured through the trepidations. Hopefully, things may shine in a more positive light.

This thesis work was supported by the Air Force Research Laboratory under Award FA9451-14-1-0374, Air Force Office of Scientific Research under Award FA9550-15-1-0097 and Award FA9550-14-1-0309, DARPA under contract HR0011-16-C-0080 with Leidos, Inc., Office of Naval Research under Award N00014-16-1-2353, and L3 Technologies Electron Devices Division.

A final note upon the suggestion of my thesis committee: the "we" that appears throughout this thesis refers to the various people that have contributed to the work. Specifically, Dr. David Chernin provided the circuit model of the tape helix and ran all simulations involving the CHRISTINE code; Dr. Brad Hoff initiated the problem of the Disk-on-Rod TWT as well as ran simulations of it using the ICEPIC code (with ANSYS HFSS). Dr. David Simon ran the simulations for the Disk-on-Rod TWT problem using the MAGIC code (with ANSYS HFSS).

Professor Y. Y. Lau conceived the harmonic generation problem underlying Chapter 2 and, with Dr. David Chernin, the tape helix problem underlying Chapter 3. Professor Lau also recognized the necessity for, and provided a physical interpretation of, the new parameter q.

Table of Contents

List of Tables

List of Figures

List of Appendices

Abstract

The traveling-wave tube (TWT) is a widely used amplifier in satellite communications and radar. An electromagnetic signal is fed into one end of the device and is amplified over a distance until it is extracted downstream at the output. The physics behind this spatial amplification of an electromagnetic wave is predicated on the interaction of a linear DC electron beam with the surrounding circuit structure. J. R. Pierce, known as the "father of communications satellites," was the first to formulate the theory for this beam-circuit interaction, which was since used in other electronic devices such as free-electron lasers, gyrotrons, and Smith-Purcell radiators. In this thesis, we extend the classic Pierce theory in two directions: harmonic generation and the effect of high beam current on both the beam mode and circuit mode.

The classical Pierce theory was formulated for a single (fundamental) frequency, same as the input signal. However, in a TWT with an octave bandwidth or greater, in particular the widely used helix TWT, the second harmonic of the input signal may also be within the amplification band and thus may also be generated and amplified. There is no input at this second harmonic frequency. An extension to the Pierce formulation that incorporates the generation of harmonics, including non-uniform taper, will be presented. We show that the second harmonic arises mostly from a newly discovered dynamic synchronous interaction instead of by the kinematic orbital crowding mechanism that is the most dominant harmonic generation mechanism in a klystron. The methodology provided may be applicable to the bi-frequency recirculating planar magnetron and other high-power microwave sources.

In beam-circuit interactions, the space-charge effect of the beam is important at high beam currents. In Pierce's TWT theory, this space-charge effect is modeled by the parameter which he called Q in the beam mode. A reliable determination of Q remains elusive for a realistic TWT. In this thesis, the author constructed the first exact small-signal theory of the beam-circuit interaction for the tape helix TWT, from which Q may be unambiguously determined. In the process of doing so, it was discovered that the circuit mode in Pierce's theory must also be modified at high beam current, an aspect overlooked in Pierce's original analysis. We quantify this circuit mode modification by an entirely new parameter that we call q, introduced here for the first time in TWT theory. For the example using a realistic tape helix TWT, we find that the effect of q is equivalent to a modification of the circuit phase velocity by as much as two percent, which is a significant effect equivalent to a detune of two percent.

Lastly, we apply the theory developed for Q and q to a high-power TWT amplifier of current interest, the disk-on-rod TWT. For this configuration, the exact analytical forms of these parameters are extracted from the exact dispersion relation, which the author has also constructed. Comparisons of the numerical solutions to the analytic results to simulations done in ANSYS HFSS, ICEPIC, and MAGIC are made.

Chapter 1 : Introduction

There is considerable current interest, for commercial and defense applications, in microwave and millimeter wave amplifiers with wide bandwidth and high-power capabilities. The traveling-wave tube (TWT) is one such device. This thesis provides a novel theoretical study of certain previously neglected physical mechanisms operating in a TWT.

1.1 Traveling-Wave Tubes

An electron beam may yield its kinetic energy to coherent electromagnetic radiation by passing through a periodic structure. One such source, widely used in satellite communications and radars, is the traveling-wave tube (TWT) [1-5]. In such a device, an electromagnetic signal is fed into one end and is amplified over some distance until it is extracted downstream. In between the input and output ends, there is a continuous interaction between the signal on the circuit and a linear DC electron beam.

Before the invention of the TWT, the klystron amplifier (1935) was one of the first microwave amplifiers used [1-2,4,5]. This device had several limitations. The most notable one is that the klystron had narrow bandwidth, as amplification is restricted to small intervals around the resonant frequencies of the klystron cavities. The idea then came about to couple the individual cavities of a multi-cavity klystron to a common transmission line so that there may be a continuous in-phase interaction between beam and circuit [4-5]. This eventually led to the development of the traveling-wave tube amplifier, abbreviated TWT, TWTA, or TWA

depending on context and usage. Figure 1.1 shows the evolution of the klystron to the traveling-wave tube.

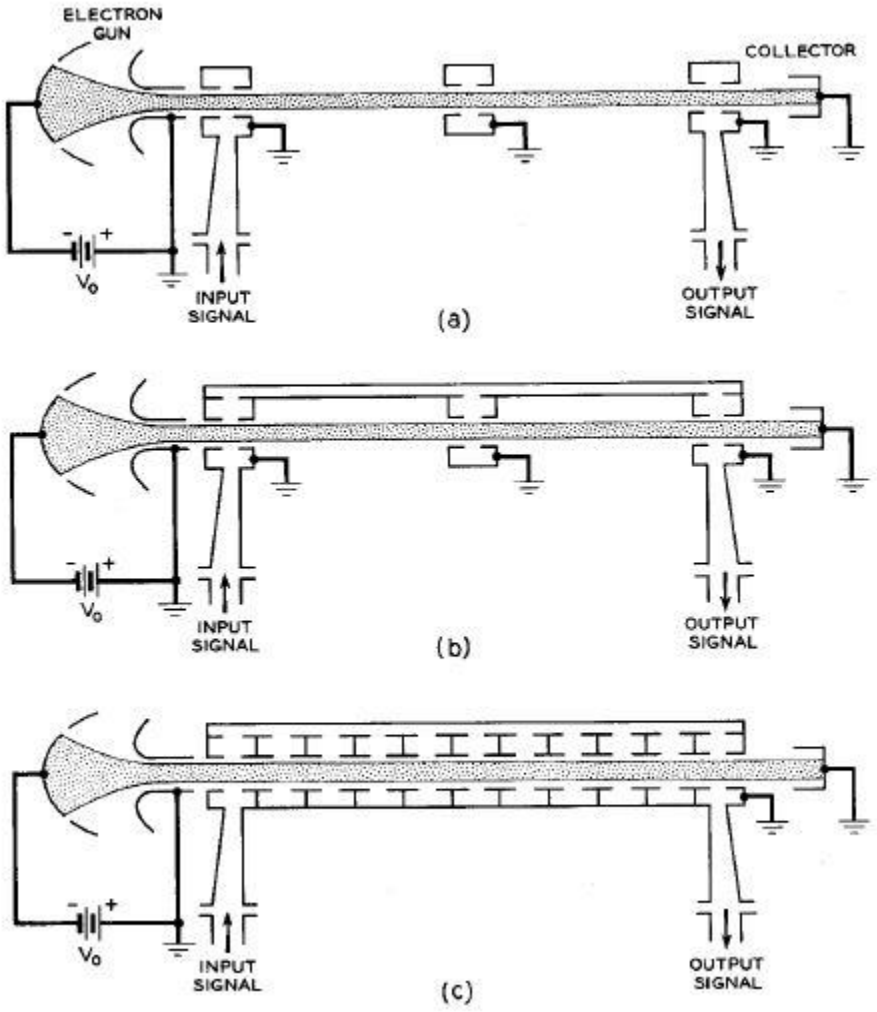

Figure 1.1. Schematic diagram showing the evolution of a multi-cavity klystron (a) to a traveling-wave tube amplifier (c). (b) shows the multi-cavity klystron with its cavities coupled to a common transmission line. Image from [4].

Rudolph Kompfner of England, interestingly an architect by profession, was the first to propose the idea of a traveling-wave tube. He and Nils Lindenblad of the United States used a metallic helix as the circuit structure for propagating the signal in phase with the centered

pencil electron beam in vacuum and are credited with being the first to create the TWT as it is known today [6-7]. Kompfner's invention of the TWT aroused the intense interest of John R. Pierce who laid the foundation of the TWT theory and was later known as the "father of communication satellites" [8]. A schematic diagram of a modern TWT is shown in Figure 1.2. Prior to this, Andrei Haeff, a doctoral student at Caltech at the time who later joined the Naval Research Laboratory, used a design where the beam propagated outside of the helix, which led to poorer gain [9].

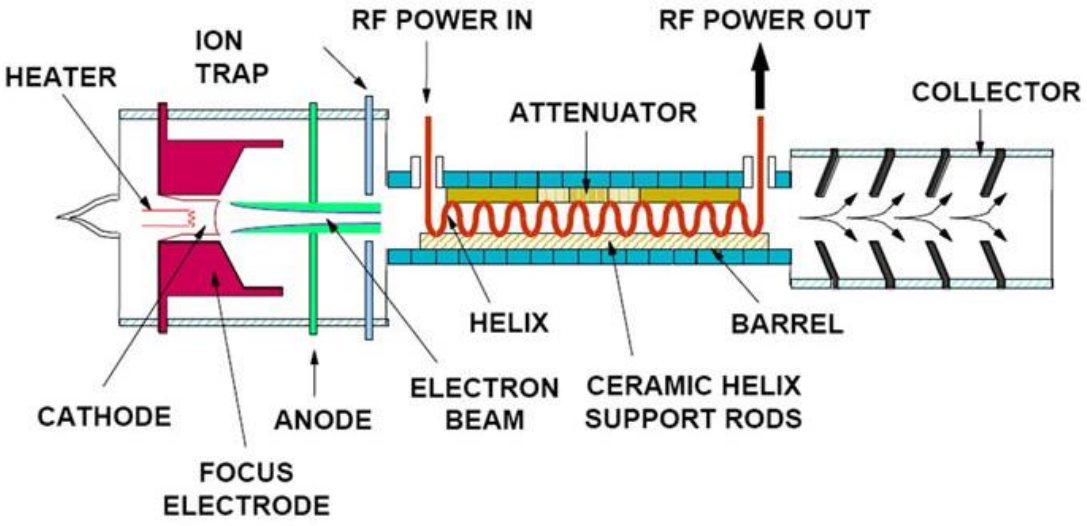

Figure 1.2. Schematic diagram of a traveling-wave tube amplifier. There are many components to a TWTA. In this thesis, we will concentrate only on the middle section, the helix, of the above figure: the beam-circuit interaction region. The slow-wave circuit referred to is the helix with support rods. Image from [10].

As can be seen in Figure 1.2, an actual TWT is a fairly complex device, consisting of components (left: cathode, electron gun, etc.) that create and form the electron beam, the beam-circuit interaction region (middle: helix, electron beam, attenuator, etc.), and components (right: collector) that collect the "spent" beam. In this thesis, we will exclusively focus on the physics in the beam-circuit interaction region containing the helix (Figure 1.2).

Like most beam-driven microwave sources and amplifiers, the operation of a TWT is predicated on the interaction between an electron beam propagating in vacuum and a circuit structure containing the signal to be amplified. In this chapter, we will first give a qualitative description of the beam and the circuit separately and then an explanation of the interaction (this section). The standard theory of Pierce analytically modeling this beam-circuit interaction will be presented in Section 2. Prior work will be described in Section 3, and Section 4 will outline the new work of this thesis in the subsequent chapters.

1.1.1 The Electron Beam

The electron beam is formed outside of the beam-circuit interaction region. Electrons are boiled off from a thermionic cathode (thermionic emission) or emitted from a material using strong electric fields (field emission). In either scenario, a voltage is externally applied to the cathode and this essentially dictates the kinetic energy of the beam entering the interaction region. We will denote the kinetic energy of this beam by voltage eV_b, corresponding to a DC beam velocity v_0.

Including relativistic effects, v_0 is determined from $(\gamma_0 - 1)m_e c^2 = eV_b$, where $\gamma_0 \equiv \frac{1}{\sqrt{1-\frac{v_0^2}{c^2}}}$ is the Lorentz relativistic mass factor. Solving this equation for v_0 gives: $v_0 = c\sqrt{1 - \frac{1}{\left(1+\frac{eV_b}{m_e c^2}\right)^2}} = c\left(1 - \frac{1}{\gamma_0^2}\right)^{\frac{1}{2}}$. In the non-relativistic regime, $v_0 \ll c$ or $eV_b \ll m_e c^2$ so that upon Taylor-expanding the last equation to first-order, one gets, as expected,

$$v_0 = \sqrt{\frac{2eV_b}{m_e}}. \tag{1.1}$$

For simplicity, it is assumed that there are no temperature effects on the beam so that the beam is "cold" or monoenergetic. We further assume that the DC beam motion is one-

dimensional, i.e., we implicitly assume that there is an infinite axial magnetic field confining the beam.

The current density of the beam is defined as: $\vec{J} = -en\vec{v}$, where *e* is the magnitude of the electron charge and *n* is the electron number density of the beam. This current density is related to the beam current, which is externally adjustable, given by $I_0 = JS = en_0v_0S$, where *S* is the cross-section of the beam. Solving for n_0 gives

$$n_0 = \frac{I_0}{ev_0S}. \tag{1.2}$$

The two externally adjustable parameters of the beam: the DC beam voltage V_b and the DC beam current I_0 control the unperturbed electron beam velocity v_0 and the electron number density n_0, respectively. In the absence of any perturbation, the electron beam travels through vacuum in the axial direction with these unperturbed properties.

An input signal of frequency ω would induce a density perturbation on the beam, whose characteristic propagation constant on the beam is $\beta_e = \frac{\omega}{v_0}$. That is, the wave-like density perturbation on the beam is carried along the beam with the beam's unperturbed velocity v_0. The simple relation, $\omega = \beta v_0$, is often known as the beam mode, where β is the wavenumber (usually designated as *k* in the plasma physics literature).

1.1.2 The Circuit

In vacuum, an electromagnetic signal, a transverse electric and magnetic (TEM) wave, propagates at the speed of light, *c*. However, for there to be appreciable gain for the input signal, the condition of synchronism between the wave and electrons in the beam must be satisfied. That is, $v_0 \approx v_{ph}$, where v_{ph} is the phase velocity component of the wave that co-propagates with the beam. This synchronism condition is required for the beam's kinetic energy to be effectively transferred to the wave energy of the electromagnetic signal. Since

the speed of the electrons cannot exceed *c*, one must slow down the phase velocity of the wave in the direction of beam propagation so that this condition of synchronism is achieved. This is realized through the use of a slow-wave structure (SWS). A good SWS is designed so that the signal has the axial projection of its phase velocity approximately equal to the beam velocity over a wide range of frequencies for broadband amplification. A metallic helix wire has such a property.

The reason why a helix TWT may offer a wide bandwidth is qualitatively illustrated in Figure 1.3.

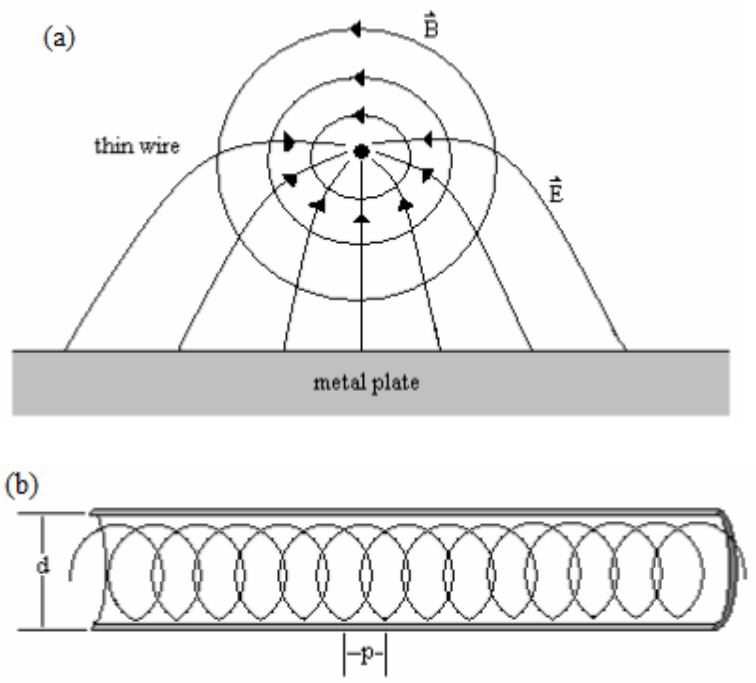

Figure 1.3. (a) Depiction of the TEM fields of a thin wire over a perfectly conducting metal plate. (b) The formation of a helix TWT from "wrapping" the set-up in (a).

Figure 1.3(a) shows a very thin metallic wire over a perfectly conducting plane. This idealized system admits a TEM wave that propagates along the wire at the speed of light, regardless of the frequency. Moreover, since the RF electric and RF magnetic fields of this

TEM mode decay like *1/r* from the wire, for a thin wire, the electromagnetic power carried along this thin wire will then be concentrated in the immediate vicinity of the thin wire. It is then easy to understand the figure shown in Figure 1.3(b): a thin helix inside a conducting cylindrical waveguide is able to transport electromagnetic energy in the vicinity of the wire at the light speed along the helix, for a very wide range of frequencies, i.e., wide bandwidth. The phase speed of this TEM mode along the *z*-axis is greatly reduced from *c* if the helix is tightly wound. From Figure 1.3(b), the incremental distance (*ds*) along the helix of radius *a* and pitch *p* is $ds = \sqrt{(ad\theta)^2 + (dz)^2} = dz\sqrt{1 + \left(a\frac{d\theta}{dz}\right)^2} = dz\sqrt{1 + \left(\frac{2\pi a}{p}\right)^2}$. Since $\frac{ds}{dt} = c$, for the TEM wave propagating along the helix, the phase speed of this local TEM wave projected along the *z*-axis is, $\frac{dz}{dt} = \left(\frac{ds}{dt}\right)\frac{1}{\sqrt{1+\left(\frac{2\pi a}{p}\right)^2}} = c\frac{p}{\sqrt{p^2+(2\pi a)^2}} \equiv v_{ph}$. Note that v_{ph} is independent of frequency in this approximation. Thus, the synchronism condition for beam-circuit interactions, $v_0 \approx v_{ph}$, may be maintained over a wide frequency band. Since this phase velocity is independent of the frequency of the injected signal ω, multiple octave bandwidths for the helix TWT are a reality. This fact prompted our study of harmonic generation (Chapter 2).

In Chapters 2 and 3 of this thesis, we will mainly concentrate on the helix for the SWS, but in Chapter 4, we will consider another circuit (and beam) configuration for high-power operation.

Because we are essentially dealing with the propagation of electromagnetic waves in some media, it should be expected that the governing equations will be the Telegrapher's Equations and hence the Wave Equation (or Helmholtz Equation with a wavenumber along

the direction of beam propagation, $\beta_{ph} \equiv \frac{\omega}{v_{ph}}$) with some modification due to the presence of the beam. This is indeed the case and will be quantified in Section 2.

1.1.3 The Beam-Circuit Interaction

Now that we have qualitatively described the beam and circuit separately, how do they interact in such a way to produce amplification of the injected signal? When the beam enters the beam-circuit interaction region and co-propagates with the circuit wave, the electrons in the beam will respond to the sinusoidal nature of the electric field of the signal. Consequently, one can imagine that some electrons will be accelerated by the accelerating portion of the wave and some electrons will be decelerated by the decelerating portion of the wave. This leads to the formation of electron bunches in the electron beam. These bunches in turn cause the electric field in the circuit to increase by inducing more current in the circuit. The resulting amplitude increase in the electric field in the circuit causes more bunching in the beam. The physical mechanism is illustrated in Gilmour [1-2].

From a wave mechanics picture, a pair of space-charge waves on the electron beam are created from interacting with the circuit wave. These space-charge waves on the beam are analogous to longitudinal pressure waves in air consisting of compressions and rarefactions. In this case, we have the fast and slow space-charge waves that co-propagate on the electron beam with the circuit wave. The energy difference from the slowing-down of the electrons in the beam to the slow space-charge wave phase velocity is given to the circuit, causing amplification of the circuit wave. This beam-circuit interaction has proven to be effective: the growth of the input signal, at least in the small-signal regime, is exponential with distance along the tube [1-2]. TWT power gain of 60 dB (1 million times) can be realized [11].

As more bunching occurs, the space-charge forces of the beam will cause the electron bunches in the beam to de-bunch. Furthermore, other effects, such as the slowing down of the beam as a whole due to the loss of energy to the circuit, will limit TWT gain because the synchronism condition ($v_0 \approx v_{ph}$) is no longer satisfied [1-2,5]. Phenomena such as saturation, wave-trapping of electrons, etc. constitute fully non-linear operation of the TWT and are beyond the scope of this thesis. The linear theory is important as it essentially feeds into the non-linear theory (the formulation of non-linear theory is predicated on the concepts introduced in the linear theory) and is stated to be able to accurately describe ~85% of the tube length [1-2,5]. Historically speaking, the linear theory was also the first comprehensive theory developed to describe the inner workings of the beam-circuit interaction. This thesis focuses mainly on the linear theory and its quasi-linear extension when we consider harmonic generation.

The classical theory of beam-structure interactions in a TWT was developed by Pierce [3], whose treatment also provided the foundations for the understanding and design of a wide range of contemporary sources such as free-electron lasers [5,12-17], Smith-Purcell radiators [5,13,17,18-19], gyrotron amplifiers [5,19-24], and metamaterials TWTs [25-27]. In this chapter, we will present the standard Pierce theory (Section 2). We further develop it to indicate other novel effects (Chapters 2 and 3) not previously considered by Pierce. Pierce described the energy transfer mechanism in terms of the interaction between the space-charge waves on the electron beam and the electromagnetic mode supported by the electromagnetic circuit. Amplification of a signal of frequency ω is described by the complex wavenumber β that is a solution of what is known as the Pierce dispersion relation, which, in its most basic form [1,3-5,12-16,19-24,27], is a third-degree polynomial for $\beta(\omega)$. This dispersion relation

describes the coupling between the beam mode and the circuit mode [28-29]. It has been used in the validation of non-linear, large-signal numerical codes in the small-signal regime.

1.2 The Pierce Theory of Traveling-Wave Tubes

Pierce adopted a mode coupling theory that has since found extensive use in a variety of other fields in electronics and in laser science [28-29]. We follow him and consider the beam mode and the circuit mode separately and will couple them at the end to arrive at the final result. It should be stressed that Pierce's theory is a linear, small-signal theory. The theory's relative simplicity and its validation of the non-linear, large-signal theories (in the small-signal regime) have allowed its extensive use for over sixty years.

1.2.1 The Electronic Equation

To start, we may analytically treat the electron beam using the cold fluid model (with zero temperature). The fluid force law for the electron beam in a general electromagnetic field then reads:

$$\frac{D\vec{v}}{Dt} = -\frac{e}{m_e}\left(\vec{E} + \vec{v} \times \vec{B}\right), \tag{1.3}$$

where $\frac{D}{Dt}$ is the operator for the convective derivative (using an Eulerian formulation) and $\vec{E}$ and $\vec{B}$ are the electric and magnetic fields. We assume an infinite axial magnetic field in this thesis so that the electrons move only one-dimensionally in the z-direction, even though, in practice, beam focusing and beam confinement are provided by external periodic permanent magnets or a solenoid. For 1D motion, $\vec{v} = v\hat{z}$, Eq. (1.3) reads

$$\left(\frac{\partial}{\partial t} + v\frac{\partial}{\partial z}\right)v = -\frac{e}{m_e}E, \tag{1.4}$$

where *E* describes the *z*-component of the electric field (which consists of the circuit electric field and the space-charge field of the beam, see Eq. (1.9) below) and the convective derivative has been explicitly written out. It is assumed that all dependent variables propagate in the *z*-direction. We may also write Eq. (1.4) in terms of the displacement of a fluid element in the beam *s* using the relation:

$$v = \left(\frac{\partial}{\partial t} + v\frac{\partial}{\partial z}\right)s. \tag{1.5}$$

Following Pierce (and standard first-order perturbation analysis), we linearize the force law and assume a wave-like dependence for the perturbation, as follows,

$$s = s_0 + \widetilde{s_1}e^{j\omega t - j\beta z}, \tag{1.6a}$$

$$v = v_0 + \widetilde{v_1}e^{j\omega t - j\beta z}, \tag{1.6b}$$

$$E = E_0 + \widetilde{E_1}e^{j\omega t - j\beta z}. \tag{1.6c}$$

The subscript "0" refers to the unperturbed or DC state, in which case, for a TWT, $s_0 = v_0 t$, $v_0 = \text{const.}$ given by Eq. (1.1) above assuming a non-relativistic beam, and $E_0 = 0$. The subscript "1" then refers to the perturbed state, and $\{\widetilde{s_1}, \widetilde{v_1}, \widetilde{E_1}\}$ are the complex amplitudes of their respective variables. The linearized force law, also known as the electronic equation [1-4], becomes algebraic,

$$\left(\frac{\partial}{\partial t} + v_0\frac{\partial}{\partial z}\right)v_1 = -\frac{e}{m_e}E_1 \rightarrow j(\omega - \beta v_0)\widetilde{v_1} = -\frac{e}{m_e}\widetilde{E_1}, \tag{1.7}$$

where

$$v_1 = \left(\frac{\partial}{\partial t} + v_0\frac{\partial}{\partial z}\right)s_1 \rightarrow \widetilde{v_1} = j(\omega - \beta v_0)\widetilde{s_1}. \tag{1.8}$$

We next separate the electric field E_1 into a component due to the circuit E_C and a component due to the space-charge in the beam E_{SC} (note we drop the subscript "1"):

$$\widetilde{E_1} = \widetilde{E_C} + \widetilde{E_{SC}}. \tag{1.9}$$

Equations (1.7) and (1.8) with (1.9) may now be combined to read:

$$(\omega - \beta v_0)^2 \tilde{s_1} = \frac{e}{m_e}\left(\widetilde{E_C} + \widetilde{E_{SC}}\right). \tag{1.10}$$

The circuit part of Eq. (1.9), $\widetilde{E_C}$, will be described in the next sub-section. We will only note here that the space-charge component $\widetilde{E_{SC}}$ is described through what is known as *QC*, a long-standing quantity of uncertainty that will be thoroughly discussed in Chapters 3 and 4. Here, we simply follow the most common notation, as given in virtually all microwave tube textbooks [3-5], and express the AC space-charge field $\widetilde{E_{SC}}$ as

$$\begin{aligned} \frac{e}{m_e}\widetilde{E_{SC}} &= \omega_q^2 \tilde{s_1} \\ &\equiv \omega_p^2 F^2 \tilde{s_1} \\ &\equiv \omega^2 (4QC^3)\tilde{s_1} \end{aligned} \tag{1.11a-c}$$

where ω_q is the reduced plasma frequency, F^2 is the plasma frequency reduction factor, $\omega_p = \sqrt{\frac{e^2 n_0}{m_e \varepsilon_0}}$ is the plasma frequency associated with the beam electrons, Q is the so-called dimensionless Pierce space-charge parameter, and C is the dimensionless Pierce gain parameter, defined by

$$C = \left(\frac{KI_0}{4V_b}\right)^{\frac{1}{3}} \tag{1.12}$$

in terms of the DC beam current I_0, DC beam voltage V_b, and the Pierce interaction impedance K which is defined in Eq. (1.15) below, where we consider the circuit wave.

The motivation of writing Eqs. (1.10) and (1.11) is that in the absence of the circuit electric field, $\widetilde{E_C} = 0$, Eq. (1.10) and Eq. (1.11b) yields the intuitive space-charge wave dispersion relation,

$$(\omega - \beta v_0)^2 = \omega_p^2 F^2 \tag{1.12a}$$

where F^2 is a dimensionless plasma frequency reduction factor mentioned above that depends only on ω, β, and on the geometry of the circuit and of the electron beam. Setting $F^2 = 1$ in Eq. (1.12a) is the familiar space-charge wave dispersion relation $(\omega - kv_0)^2 = \omega_p^2$ that appears in plasma physics textbooks ($k \equiv \beta$, see for example, [30-32]), whose two solutions $\omega = kv_0 \pm \omega_p$ represent the fast (+ sign) and slow (- sign) space-charge waves mentioned above.

From Eqs. (1.11b) and (1.11c), we may express the beam mode Eq. (1.12a), including the "space-charge effect," as

$$(\omega - \beta v_0)^2 - \omega^2 4QC^3 = 0 \tag{1.12b}$$

in Pierce's notation. Upon using Eq. (1.11c) into Eq. (1.10), we arrive at the electronic equation, in Pierce's notation,

$$[(\omega - \beta v_0)^2 - \omega^2 4QC^3]\widetilde{s_1} = \frac{e}{m_e}\widetilde{E_C}. \tag{1.12c}$$

As a final note on beam dynamics, the equation of continuity for the beam electrons gives

$$\frac{\partial n}{\partial t} + \vec{\nabla} \cdot n\vec{v} = 0 \rightarrow j(\omega - \beta v_0)\widetilde{n_1} = j\beta n_0 \widetilde{v_1} \tag{1.13}$$

upon linearizing. The AC beam current I_1 becomes

$$I_1 = J_1 S = -e(n_0 v_1 + n_1 v_0)S = -jen_0 S\omega s_1, \tag{1.14}$$

upon using Eq. (1.8) and Eq. (1.13).

1.2.2 The Slow-Wave Circuit Equation

Pierce treated the circuit structure, whatever it may be (helix, coupled-cavity, folded waveguide, etc.), as an idealized transmission line. An equation for the electric field in this transmission line will now be derived [3-5].

Recall that in basic circuit theory, the power P into a pair of terminals is $P = IV = \frac{V^2}{Z}$, where I is the current in, V is the voltage across, and Z is the impedance looking into the terminals. Analogously, we may write the power flowing along the slow-wave circuit as: $P = -IE_zL = \frac{|E_z|^2}{\beta_{ph}^2 K}$ in terms of the (axial) electric field. Here, L is the equivalent length of the circuit (TWT). In writing the last expression, we used the fact that the induced current on the circuit is proportional to the axial circuit electric field E_z, and K is Pierce's interaction impedance defined as:

$$K \equiv \frac{\iint |E_z|^2 dS}{2\beta_{ph}^2 P_r S}, \qquad \beta_{ph} = \frac{\omega}{v_{ph}}, \tag{1.15}$$

where P_r is the power flow on the slow-wave circuit and S is the cross-section of the slow-wave structure. Note that K is a function only of the geometry and frequency ω.

Dividing the beam into infinitesimal segments of length dz, the differential power from each segment is: $dP = -I_1 E_z dz = \frac{2E_z}{\beta_{ph}^2 K} dE_z \rightarrow dE_z = -\frac{\beta_{ph}^2 K I_1}{2} dz$. This differential electric field is the field that is induced from the current of the beam on the circuit at an axial location z. There are two waves launched at z due to the beam: a forward wave dE_{z+} and a backward wave dE_{z-}. Because of symmetry, one can see that $dE_{z+} = dE_{z-}$.

Thus, the total electric field in this system at an arbitrary location is:

$$E_z(z,t) = \left(E_{10}e^{-j\Gamma_0 z} + \int_0^z dE_{z+}e^{-j\Gamma_0(z-z')} + \int_z^L dE_{z-}e^{-j\Gamma_0(z'-z)} \right) e^{j\omega t}$$

$$= \left(E_{10}e^{-j\Gamma_0 z} - \frac{\beta_{ph}^2 K}{2} \int_0^z I_1(z')e^{-j\Gamma_0(z-z')}dz' \right. \tag{1.16}$$

$$\left. - \frac{\beta_{ph}^2 K}{2} \int_z^L I_1(z')e^{-j\Gamma_0(z'-z)}dz' \right) e^{j\omega t}.$$

Equation (1.16) is an integral equation giving the electric field at a point *z* from all possible sources: (1) the electric field from the input signal E_{10} located at $z = 0$ (first term), (2) the electric field from the beam segments before *z* (middle term), and (3) the electric field from the beam segments after *z* (last term). To be completely general, the traveling waves from each source have propagation constant $\Gamma_0 \equiv \beta_{ph} - j\mathrm{Im}(\Gamma_0)$, where the imaginary part accounts for attenuation in the circuit ($\mathrm{Im}(\Gamma_0) > 0$). We may readily convert this equation into a differential equation by twice differentiating the equation with respect to *z*. Doing so and using Eq. (1.16) gives,

$$\frac{d^2E_z(z)}{dz^2} + \Gamma_0^2 E_z(z) = j\Gamma_0\beta_{ph}^2 K I_1(z) \tag{1.17}$$

where E_z and I_1 have an $e^{j\omega t}$ dependence. Equation (1.17) is given in p. 150 of Chodorow and Susskind [33]. Physically, Eq. (1.17) describes the excitation of the circuit wave, whose cold-tube AC electric field at the location of the beam is E_z, by an AC beam current I_1.

Assuming time and spatial harmonic dependence for E_z, $E_z = E_C = \widetilde{E_C}e^{j\omega t - j\beta z}$ in Eq. (1.17) yields Eq. (10.1-34) of [4]:

$$\widetilde{E_C} = \frac{j\Gamma_0\beta_{ph}^2 K}{\Gamma_0^2 - \beta^2}\widetilde{I_1}, \tag{1.18}$$

which gives the circuit electric field $\widetilde{E_C}$ excited by the beam's AC current $\widetilde{I_1}$ at frequency ω. Note that if there is no electron beam, $\widetilde{I_1} = 0$, there will be a non-zero circuit electric field $\widetilde{E_C}$ only if $\beta = \Gamma_0$, which is the vacuum circuit mode dispersion relation, and this circuit electric field $\widetilde{E_C}$ is then simply the vacuum mode solution. In other words, if $\beta = \Gamma_0$, any finite AC current on the beam will yield an infinite response on the circuit electric field $\widetilde{E_C}$, a well-known fact for synchronous excitation, as clearly shown in Eq. (1.18). It should be noted that this analysis of the circuit, following Pierce, deals only with the fundamental passband and its interaction with the beam. In general, there are an infinity of passbands and space harmonics of the circuit mode *and* the beam mode. Pierce's theory is also used for the interaction between a single space harmonic of the circuit and the fundamental mode of the beam to assess the strength of interaction at that space harmonic. The major objective in Chapters 3 and 4 is to relax these restrictions.

A sample Brillouin or cold-tube dispersion diagram (ω vs. β plot, obtained from $\beta = \Gamma_0$) is shown in Figure 1.4 for the tape helix (Figure 1.5). In this example, no cold-tube circuit loss is assumed ($\mathrm{Im}(\Gamma_0) = 0$). This tape helix has a period p whose property will be fully discussed in Chapter 3. Here, we simply note the multiple passbands (two shown in Figure 1.4) in blue and the periodic nature of each passband corresponding to the space harmonics n. The propagation constant, β_n, of the nth spatial harmonic is:

$$\beta_n = \beta_0 + \frac{2\pi n}{p}, n = 0, \pm 1, \pm 2, ..., \tag{1.19}$$

where p is the period of the periodic structure (Figure 1.5). β_0 is called the fundamental and β_n ($n \neq 0$) is called the nth space harmonic.

The beam mode $\omega = \beta v_0$ is also shown in Figure 1.4 in red. As can be seen, the synchronism condition ($v_0 \approx v_{ph}$) between the beam mode and the circuit mode is satisfied

for a wide range of frequencies. This is what gives the tape helix its characteristic wide bandwidth.

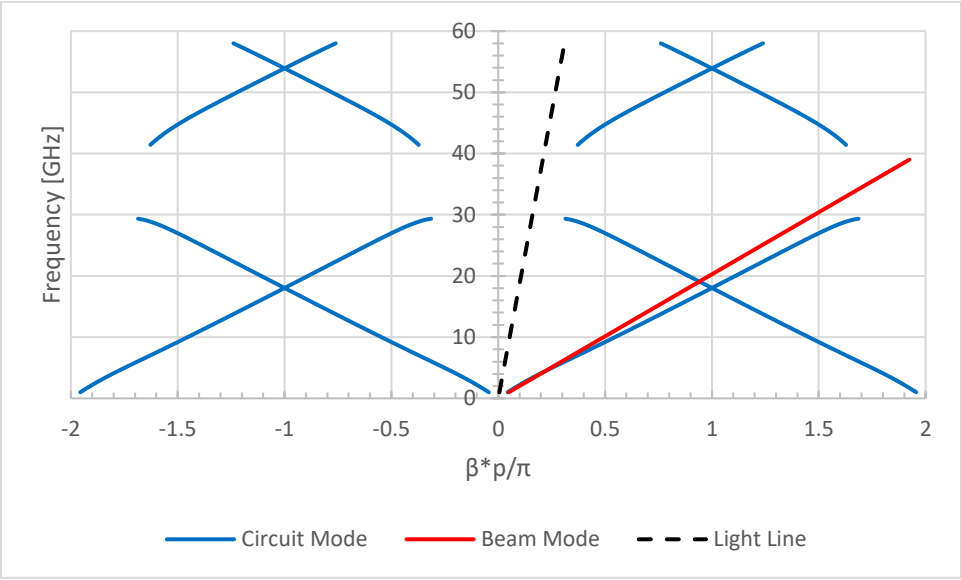

Figure 1.4. Dispersion diagram for a tape helix showing several circuit modes ($\beta = \Gamma_0$, blue) and the beam mode ($\beta = \frac{\omega}{v_0}$, red). Also included in the Figure is the light line ($\beta = \frac{\omega}{c}$, black, dashed).

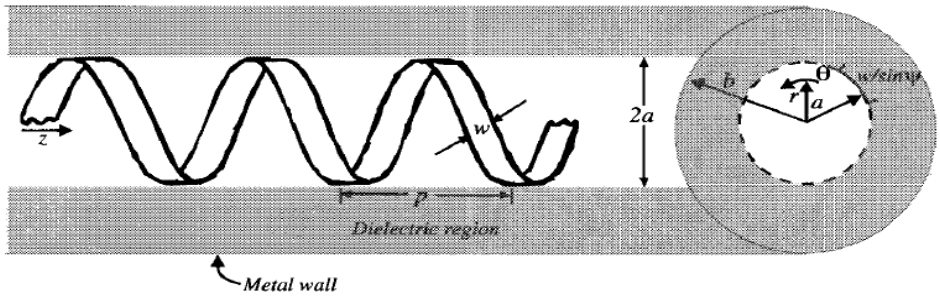

Figure 1.5. Schematic depiction of a thin tape helix radially stratified by a dielectric to represent the support rods. The parameters and details are given in Chapter 3 below (see first paragraph of Section 3.3). Image from [34].

1.2.3 The General Pierce Dispersion Relation and the Pierce Parameters

We combine the electron dynamics in Section 1.2.1 and the circuit response in Section 1.2.2 to derive the Pierce dispersion relation, as follows.

Inserting Eq. (1.14) into Eq. (1.18) yields

$$\widetilde{E_C} = \frac{j\Gamma_0\beta_{ph}^2 K}{\Gamma_0^2 - \beta^2}[-jen_0 S\omega\tilde{s_1}], \tag{1.20a}$$

which expresses the excitation of the circuit electric field $\widetilde{E_C}$ by the beam's perturbation displacement $\tilde{s_1}$. Multiply Eqs. (1.20a) and (1.12c) and cancel $\tilde{s_1}\widetilde{E_C}$ to yield Pierce's four-wave dispersion relation:

$$[(\beta - \beta_e)^2 - \beta_e^2 4QC^3][\beta^2 - \Gamma_0^2] = -2\beta_e\beta_{ph}^2\Gamma_0 C^3, \tag{1.20b}$$

where $\beta_e = \frac{\omega}{v_0}$ and $\beta_{ph} = \frac{\omega}{v_{ph}}$, v_0 is the beam velocity and v_{ph} is the cold-circuit wave phase velocity. The first square bracket on the LHS represents the beam mode, the second bracket represents the cold-tube circuit mode, and the RHS represents the coupling of the two.

To derive the three-wave dispersion relation of Pierce, we ignore the reverse propagating circuit mode in Eq. (1.20b), by assuming $\beta \approx \Gamma_0 = \frac{\omega}{v_{ph}} \equiv \beta_{ph}$. To include the cold-tube loss rate (represented by the Pierce parameter d defined in Eq. (1.21d) below), we approximate the second square bracket of Eq. (1.20b) as

$$\left[\beta^2 - \beta_{ph}^2\right] \approx 2\beta_{ph}\left[\beta - \beta_{ph} - jCd\beta_e\right]. \tag{1.20c}$$

Inserting Eq. (1.20c) into (1.20b), we obtain the traditional Pierce three-wave dispersion relation:

$$[(\beta - \beta_e)^2 - \beta_e^2 4QC^3]\left[\beta - \beta_{ph} - jCd\beta_e\right] = -\beta_e\beta_{ph}^2 C^3. \tag{1.20d}$$

This equation thus only admits two forward-propagating space-charge waves (first square bracket) and one forward-propagating circuit wave (second square bracket). Typical numerical values are: $\beta \sim \beta_e \sim \beta_{ph} \sim O(1)$, $C \sim O(10^{-3} - 10^{-1})$, $Q \sim O(1 - 10)$, and $d \sim O(1)$.

Pierce expresses his three-wave dispersion relation, Eq. (1.20d), in dimensionless form, in terms of his incremental propagation constant, δ, and the cubic polynomial for δ then reads

$$(\delta^2 + 4QC)(\delta + jb + d) = -j \tag{1.21}$$

where[1]

$$\delta = \frac{\beta - \beta_e}{\beta_e j C} \tag{1.21a}$$

$$b = \frac{v_0 - v_{ph}}{C v_{ph}} \tag{1.21b}$$

$$C^3 = \frac{K I_0}{4 V_b} \tag{1.21c}$$

$$d = \frac{1}{40\pi \log_{10} e} * \frac{Loss}{C} = \frac{\mathrm{Im}(\Gamma_0)}{\beta_e C}, \tag{1.21d}$$

In Eq. (1.21c), the interaction impedance *K* is defined by Eq. (1.15), and "Loss" in Eq. (1.21d) is the cold-tube circuit attenuation (in dB) per unit axial wavelength of the beam mode. The three solutions of δ in Eq. (1.21) depends only on the four dimensionless parameters, *C*, *b*, *Q*, and *d*, representing respectively the strength of mode coupling in the beam-circuit interaction (also known as the Pierce gain parameter or coupling constant), the degree of synchronism between the beam motion and the cold-circuit wave (velocity mismatch or detune parameter), the space-charge effect (Pierce's AC space-charge parameter), and the cold-tube circuit loss [1,3,4]. Among these four parameters, *Q* is the most

[1] The full form of the RHS of Eq. (1.21) should read: $-j \rightarrow -j(1 + Cb)^2$. That is, Eq. (1.21) is obtained by approximating $\beta_{ph} = \beta_e$ in the RHS of Eq. (1.20d). This approximation is valid only for small *C* or close to synchronism ($b \approx 0$).

difficult to evaluate accurately [35-37]. In this thesis, we present a new, precise method to calculate Q for a TWT based on a tape helix structure [34]. In so doing, we find that the circuit mode – like the beam mode – is modified by a *new* space-charge parameter, which we call q, and this is a major finding of this thesis.

In this thesis, we will deal solely with the Pierce three-wave dispersion relation. Reflection from the ends and waves near the band edges cannot be accounted for by Pierce's three-wave theory. A classical look into Pierce's four-wave theory and its reduction to the three-wave theory is provided by Birdsall and Brewer [38] (The importance of the four-wave description, and the effects of reflection on the TWT stability may be found in [39-41].).

1.3 Prior Work

Now that the ground work for the Pierce theory of TWTs has been laid out, we now turn our attention to extending the classic theory in two directions to account for effects not covered by Pierce's theory: harmonic generation and beam loading on the circuit. These theories are described in Chapters 2 and 3 respectively. First, we will review previous work on these subjects.

1.3.1 Harmonic Generation

The subject of harmonic generation in a TWT has traditionally been studied in the non-linear, large-signal regime. We will not delve into large-signal theory in this thesis as it is beyond the scope of this text. We will note that large-signal TWT theory and also the study of harmonics of the input signal can be traced back to the classical paper by A. Nordsieck [42], who provided the first analysis of TWT efficiency. References may be made to Tien et

al. [43], Rowe [44], Giarola [45], and Dionne [46] whose subsequent works heavily relied on Nordsieck's theory.

Linearized orbital motion due to an input signal may lead to orbital crowding, which leads to harmonic generation kinematically (See Figure 2.1 below). This effect is well-known in klystrons and is the dominant cause for harmonic generation in klystrons. It was not until recently that such a theory on harmonic content in the beam current of a TWT was developed by Dong et al. [47] in the small-signal regime. In that work, the linearized electron orbits might lead to a second harmonic AC current as high as 25% of the DC beam current, and this was favorably compared to the large-signal TWT code CHRISTINE [48].

In this thesis, we discover another source of harmonic content in a TWT: weak non-linearities in the electron orbits. It turns out, with respect to the RF power output, that this source of harmonic generation is much more important as it possesses the property of synchronism between the beam and circuit in both space and time. The effect of orbital crowding described in the preceding paragraph is negligible in comparison.

1.3.2 Evaluation of the Pierce Parameters

As we have stated, the weakest aspect of Pierce's theory of mode coupling concerns the modification of the beam mode at high beam currents; this modification was characterized by Pierce's space-charge parameter, Q, for which no general calculation has been given (c.f. Eqs. (1.20d) and (1.21)).

Many theories have been proposed that attempt to give a general formulation for calculating Q for a general beam and circuit structure. A treatise of the subtlety of this problem is given by Lau and Chernin [36], who ultimately advance the idea that Q is due to the interaction of the beam with the higher-order circuit modes (passbands higher than the

fundamental). This interpretation was actually also proposed by Pierce [3], who quickly abandoned such an interpretation [36].

Physically speaking, the calculation of the space-charge parameter boils down to calculating the "reduced" plasma frequency ω_q, as mentioned in the previous section (see Eqs. (1.11a) and (1.11c)). By "reduced," we mean only the axial component of the RF electric field (not the total RF electric field which has a radial component and possibly an azimuthal component as in the tape helix) could exchange energy with the linear electron beam. We seek to calculate the reduction factor to the plasma frequency that accounts for the circuit structure (including the SWS, taking into account, for example, the "field leakage" in the opened sections of a helix). This calculation is intimately tied to the higher-order circuit modes mentioned in the preceding paragraph. Prior to our work, no general formulation exists, but many approximations have been developed. Here, we will look at perhaps the most widely used one for the also widely used helix TWT.

The most widely used space-charge parameter *QC* is prescribed by Branch and Mihran [49]. In the particular case of a thin tape helix TWT (Figure 1.5) with a pencil electron beam, Branch and Mihran assume that the helix is replaced with a perfectly conducting metallic cylinder of the same radius. Hence, they then calculate the plasma frequency reduction factor $F = \frac{\omega_q}{\omega_p} = \sqrt{\frac{1}{1+\left(\frac{T}{\beta_e}\right)^2}}$, where the radial propagation constant T is given explicitly in terms of Bessel functions by solving Maxwell's equations in this simplified geometry (we shall also adopt the Branch and Mihran calculation for the disk-loaded TWA with an annular electron beam in Chapter 4, for comparison.). An improved model for the helix structure makes use of what is known as a sheath helix, in which current is allowed to travel on the circuit in a

helical direction. While there are more elaborate models [37,48,50-52] on the AC space-charge effects in a helix TWT, none give the procedure of evaluating *QC*.

Prior to our analytic calculation of *Q* in Chapter 4 for a realistic structure, a study using the pedagogical model of a dielectric TWT that consists of a planar dielectric slab and sheet electron beam was done by Simon et al. [35]. In that model, where an *exact* dispersion relation may be readily derived, the idea of the higher-order circuit modes yielding *Q* was established conclusively. In addition, that paper showed how to accurately evaluate the Pierce parameters once a closed analytic form was found. This model is deficient in that there is no periodic structure in this dielectric TWT, so higher harmonics in the beam mode are excluded. Thus, the new parameter $q = 0$ in this dielectric TWT model.

1.4 Thesis Organization

The focus of this thesis is on the modeling of some aspects of the beam-circuit interaction in a TWT that are of current interest, namely, harmonic generation and accurate modeling of the space-charge effects.

At the University of Michigan Plasma, Pulsed Power, and Microwave Laboratory, there is an on-going experiment on a bi-frequency recirculating planar magnetron, where output powers of up to 44 MW and 21 MW at 1 GHz and 2 GHz respectively are being generated [53-54]. The physical process that generates second harmonic is explored in this thesis for a much simpler model, that of a TWT.

Our study of Pierce's space-charge parameter *Q* was initially motivated by the disk-on-rod TWA studied by Hoff and French [55-56] at the Air Force Research Laboratory. The analysis of backward wave oscillations in a helix TWT motivated us to study *QC* in a helix

TWT also [57-58]. An accurate determination of Q (and q) is important for at least three reasons:

(i) A small discrepancy in Q can lead to a large change in the predicted small-signal gain.

(ii) An accurate value of Q (or QC) is required by the non-linear TWT simulation codes such as CHRISTINE [48] in order to compute large-signal quantities like saturated output power and efficiency.

(iii) In Johnson's classical theory for the onset of backward wave oscillations in TWT [57], the threshold conditions depend only on QC and on d [4,57], which implies that prediction of BWO threshold current requires accurate values of QC and d.

In response to these objectives, a quasi-linear theory on second harmonic generation extending the classic Pierce theory will be considered in Chapter 2. We will next examine Pierce's AC space-charge parameter Q for a realistic TWT, a tape helix, via the exact hot-tube dispersion relation. In Chapter 4, another TWA, the disk-loaded rod with annular electron beam, will be subjected to a similar exact, small-signal analysis. Chapter 5 concludes with a summary of the main results and suggested future work.

Chapter 2 :
The Origin of Second Harmonic Signals in Octave Bandwidth Traveling-Wave Tubes

2.1 Introduction

We shall now present our first extension to the classic Pierce three-wave theory for the traveling-wave tube (TWT): harmonic generation. Besides its fundamental nature, this work was motivated by current experiments on harmonic generation in a bi-frequency recirculating planar magnetron (RPM) [53-54,59]. We would like to model the harmonic generation that is present in such a device, and we start first with the TWT in order to understand the dynamical nature of harmonic generation. A TWT has a well characterized beam. In particular, we will consider a helix TWT, which has a wide bandwidth that is unmatched [5], for reasons qualitatively explained in Chapter 1. With such a wide bandwidth, the second harmonic of an input signal could be generated and amplified. There are also contemporary simulations and experiments of harmonic generation in a TWT (see for example, [60]). This chapter might provide a new theoretical framework for such works.

In a helix TWT with octave bandwidth, the electrons can synchronously interact with the circuit wave over a wide range of frequencies, when the beam's velocity is about equal to the phase velocity (which is roughly independent of frequency; see e.g. Figure 1.4) an input signal near the low frequency end of the amplification band may then generate a second harmonic signal if the beam current carries a second harmonic component. This chapter analyzes the generation of second harmonic in a TWT, due solely to an input signal at the

fundamental frequency, ω_0, in the case that the second harmonic experiences a finite small-signal gain. Here, we focus on the physical mechanism by which the second harmonic is generated, its analytic description, and its validation with a simulation code.

First, a well-known non-linear process in vacuum electronics that leads to harmonic beam current, due to an input signal of a single frequency, ω_0, is crowding of the electron orbits [4], in which neighboring electrons are getting closer together, as shown in Figure 2.1. Here, if there are no perturbations, the electrons leaving the input, located at $z = 0$, simply stream down the axis following $z(t) = v_0(t - t_0)$, where t_0 is the departure time from the input and v_0 is the DC electron velocity. Adding in a perturbation in the form of the input signal, the electron orbits are consequently altered so that $z(t) = v_0(t - t_0) + z_1(t, t_0)$, where the linear perturbation z_1 accounts for the effects. In this scenario, one can see that at a later time t and at a downstream position L, the perturbed orbits may come closer together, as depicted in Figure 2.1. This occurs in the drift tube of a klystron and the harmonic content in the AC current has been calculated *exactly* in a one-dimensional (1D) model [4,61]; this calculation has been explicitly shown to be valid even for the case where the electron orbits have crossed, i.e., when charge overtaking has occurred [61]. *Significant harmonic current appears even if the electron perturbation velocity is strictly in the linear regime*, that is, the velocity of an electron has only a DC component, plus a fundamental frequency component at a very low level [4,62-63]. The non-linearity in the AC current arises *kinematically*, from the exact solution to the *non-linear* continuity equation that accounts for orbital crowding (including charge overtaking) in the *linearized* electron orbits [61-62]. While this orbital crowding process has been well-known for a klystron in generating harmonic AC current, this process was relatively unknown to the TWT literature until Dong et al. adopted the

theory [47]. From that study, the second harmonic AC current in the beam in a TWT was found to be quite high, reaching 1/4 of the DC beam current, even though the electron's AC velocity is in the *linear* regime (as in the klystron analysis). This level of second harmonic current in a TWT, due to orbital crowding, was corroborated by the code, CHRISTINE [48].

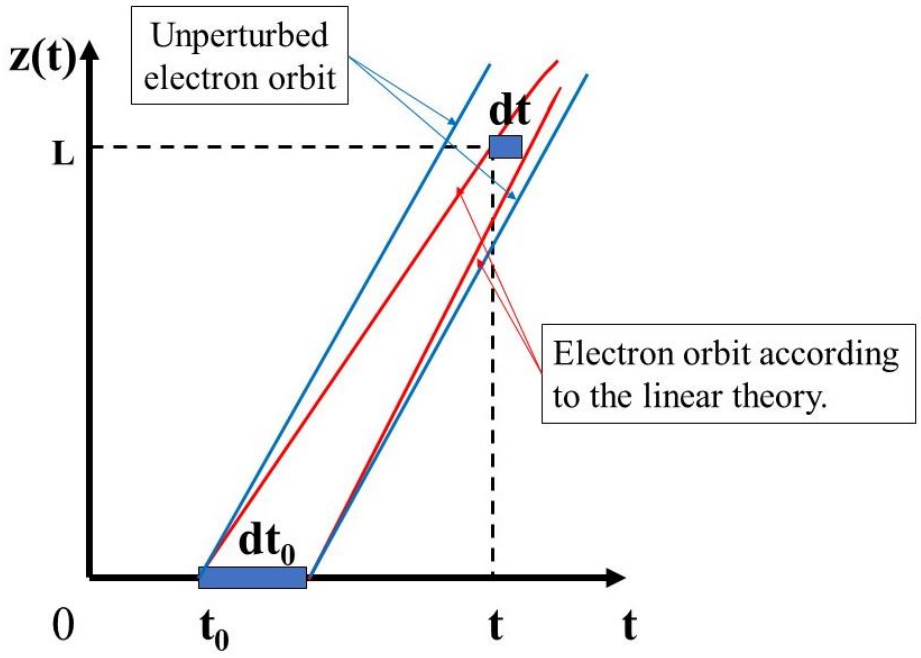

Figure 2.1. An (exaggerated) illustration of harmonic generation due to orbital crowding. Crowding in the linear orbits may lead to harmonic current generation, as shown in klystron theory [4] and TWT theory [47].

Despite the high harmonic current due to orbital crowding that was described in the preceding paragraph, in this chapter, we report another non-linear effect that is far more important in the generation of second harmonic power in a wideband TWT. The latter is due to the quasi-linear correction in the electron orbit, which is described by the non-linear convective derivative in the force law, $v_1 \frac{\partial v_1}{\partial z}$, where $v_1 = v_{10} e^{j\omega_0 t - j\beta_0 z}$ is the *linearized* electron fluid velocity at the fundamental frequency, whose wavenumber $\beta_0 \approx \frac{\omega_0}{v_0}$ where v_0 is

the DC beam velocity. This convective derivative, $v_1 \frac{\partial v_1}{\partial z}$, then contributes a "force" proportional to $v_{10}^2 e^{j2\omega_0 t - j2\beta_0 z}$ (analogous to the "ponderomotive force" in the latter's derivation [64]). This "force" is a traveling wave at the second harmonic frequency. It has a phase velocity also synchronized with the electron beam because $\frac{\omega}{\beta} = \frac{2\omega_0}{2\beta_0} = \frac{\omega_0}{\beta_0} \approx v_0$, the condition for synchronism in a TWT. This "force" may then synchronously excite a second harmonic wave, *both in time and space*, which makes it a much more powerful contributor to second harmonic generation. The AC harmonic current due to orbital crowding, described in the preceding paragraph, does not possess this property of synchronization in both time and space, and is therefore a much weaker contributor in the generation of RF power at the second harmonic. This is a rather unexpected finding, because it was not anticipated that the quasi-linear term $v_1 \frac{\partial v_1}{\partial z}$ would be so important, as v_1 is admittedly in the linear regime (and hence $v_1 \frac{\partial v_1}{\partial z}$ is second-order in nature). Comparison with CHRISTINE simulations confirmed these facts, as we shall show in the numerical examples in Section 2.3.

It should be mentioned that, largely based on Nordsieck's seminal paper [42] on non-linear TWT theory, harmonic generation in broadband TWT was extensively studied [43-46]. These works did not identify the physical origin of the harmonic generation, even though they have all included the effect of orbital crowding (including charge overtaking). It is also not immediately clear how these works could be applied to a realistic tube that has a spatially non-uniform circuit loss, and a sever region. The analytic approach, based on a straightforward expansion given here (Section 2.2), is a marked departure from the Nordsieck formulation [42]. It readily includes spatially non-uniform circuit loss and a sever, in addition to the discovery that orbital crowding (including charge overtaking) is not the dominant

cause for harmonic generation. The numerical examples presented below validated our approach, whose results were favorably compared with the non-linear simulation code, CHRISTINE [48]. Other works on harmonic generation in a TWT may be referenced, which either used an Eulerian [65-66] or Lagrangian description [67]. None of these prior works recognized the main result of this chapter, namely, the dominant influence of synchronous excitation, over orbital crowding, in harmonic generation in a wideband TWT.

In Section 2.2, the classical TWT theory of Pierce [3] is extended to include the generation of second harmonic. We shall indicate how the nonsynchronous charge overtaking effect, and the synchronous excitation due to $v_1 \frac{\partial v_1}{\partial z}$, would enter in our formulation of harmonic generation. Numerical examples for a TWT with a sever and spatially non-uniform cold-tube loss are given in Section 2.3, and compared with simulation results. Section 2.4 presents the concluding remarks.

2.2 Formulation

The Eulerian description will be used to formulate the force law and the circuit equation. We shall indicate how harmonic current due to orbital crowding can be accounted for in such a formulation. We shall closely follow, but extend Pierce's classical three-wave theory of TWTs [3-4] to include harmonic generation. The lowest order (linear) theory is identical to Pierce's. The force law (electronic equation) and the circuit equation will be considered separately.

We digress to remark that we shall use Pierce's classical three-wave theory of TWT, instead of the more complete Pierce's four-wave theory (Eq. (1.20b)), for the following reasons:

(i) We shall compare our analytic formulation with the CHRISTINE code, which is a well-validated large-signal helix TWT simulation code. The governing equations solved by CHRISTINE reduce to those of Pierce's three-wave theory for small-signal amplitudes.

(ii) A careful case study of a dielectric TWT [35] showed that the value of the space-charge parameter, *QC*, would be different between the three-wave and four-wave theory.

(iii) Perhaps most importantly, since the four-wave theory includes the reverse-propagating circuit mode, an absolute instability could arise if the beam current is sufficiently high [68-69], and such a possibility is beyond the scope of this thesis. Pierce's three-wave theory of TWT rules out the excitation of absolute instability (in the absence of reflections, as we assumed in this thesis).

2.2.1 Electronic Equation

We assume that the electron beam is cold, confined by an infinite axial magnetic field, and drifts at constant velocity v_0 in the unperturbed (DC) state. In the 1D model, the non-linear force law for the electron fluid reads

$$\left(\frac{\partial}{\partial t} + v(z,t)\frac{\partial}{\partial z}\right) v(z,t) = -\frac{e}{m_e} E(z,t), \tag{2.1}$$

where the fluid velocity $v(z,t)$ is related to the fluid displacement $s(z,t)$ by

$$v(z,t) = \left(\frac{\partial}{\partial t} + v(z,t)\frac{\partial}{\partial z}\right) s(z,t), \tag{2.2}$$

and the total electric field $E(z,t)$ consists of circuit and space-charge electric fields (c.f. Eq. (1.9)),

$$E(z,t) = E_C(z,t) + E_{SC}(z,t). \tag{2.3}$$

The circuit field E_C is excited by the AC current, as modeled by Pierce (c.f. Eq. (1.17)), and the space-charge field E_{SC} will also be modeled by Pierce through his space-charge parameter, *QC* (c.f. Eq. (1.11c)). Note that all quantities in Eqs. (2.1)-(2.3) are expressed in the Eulerian description.

The dependent variables $\{s,v,E\}$ may be expanded as follows:

$$s(z,t) = s_0 + \varepsilon s_1(z,t) + \varepsilon^2 s_2(z,t) + \cdots \tag{2.4a}$$

$$v(z,t) = v_0 + \varepsilon v_1(z,t) + \varepsilon^2 v_2(z,t) + \cdots \tag{2.4b}$$

$$E(z,t) = E_0 + \varepsilon E_1(z,t) + \varepsilon^2 E_2(z,t) + \cdots \tag{2.4c}$$

where ε is a small expansion parameter in harmonics, which measures the ratio of the beam's perturbation velocity to its DC velocity. We substitute Eqs. (2.4a)-(2.4c) into Eqs. (2.1) and (2.2) and collect terms of the same order in ε. The ε^0 terms describe the DC state. The ε^1 terms describe the familiar linearized force law,

$$\left(\frac{\partial}{\partial t} + v_0 \frac{\partial}{\partial z}\right) v_1 = -\frac{e}{m_e} E_1, \tag{2.5}$$

$$v_1 = \left(\frac{\partial}{\partial t} + v_0 \frac{\partial}{\partial z}\right) s_1. \tag{2.6}$$

The ε^2 terms then give,

$$\left(\frac{\partial}{\partial t} + v_0 \frac{\partial}{\partial z}\right) v_2 = -\frac{e}{m_e} E_2 - v_1 \frac{\partial v_1}{\partial z}, \tag{2.7}$$

$$v_2 = \left(\frac{\partial}{\partial t} + v_0 \frac{\partial}{\partial z}\right) s_2 + v_1 \frac{\partial s_1}{\partial z}, \tag{2.8}$$

which describe the generation of second harmonic on account of the $v_1 \frac{\partial v_1}{\partial z}$ in the right-hand member of Eq. (2.7). Such a term represents the quasi-linear correction on the electron orbit.

If the ε^1 terms give the linearized response to the fundamental frequency ω_0, we may write the ε^n terms as

$$\{s_n, v_n, E_n\} = \{s_n(z), v_n(z), E_n(z)\}e^{j(n\omega_0)t}. \tag{2.9}$$

Thus, the operator $\frac{\partial}{\partial t}$ in Eqs. (2.5) and (2.6) may be replaced by $j\omega_0$ for v_1 and s_1, whereas the operator $\frac{\partial}{\partial t}$ in Eqs. (2.7) and (2.8) may be replaced by $j2\omega_0$ for v_2 and s_2, i.e. Eqs. (2.5)-(2.8) then become first-order ordinary differential equations in z.

We next follow Pierce and decompose the total electric field E into the circuit electric field E_C and space-charge electric field E_{SC}, for the nth harmonic fields (c.f. (1.11c)):

$$E_n = E_{nC} + E_{nSC} = E_{nC} + \frac{4(n\omega_0)^2 Q_n C_n^3 s_n}{e/m_e}. \tag{2.10}$$

In Eq. (2.10), Q_n and C_n are, respectively, Pierce's space-charge parameter and gain parameter at the nth harmonic. The last equality in Eq. (2.10), giving the explicit form of the space-charge electric field, follows Pierce's definition of the QC parameter (as applied to a wave at the nth harmonic frequency, $\omega_n = n\omega_0$). In Pierce's notation, we use Eq. (2.10) into Eq. (2.5) to write the electronic equation at the fundamental frequency (n = 1) as [3-4,47],

$$\left[\left(\frac{d}{dz} + j\frac{\omega_0}{v_0}\right)^2 + 4\left(\frac{\omega_0}{v_0}\right)^2 Q_1 C_1^3\right] s_1(z) = -\frac{e}{m_e v_0^2} E_{1C}(z). \tag{2.11}$$

Similarly, Eqs. (2.7) and (2.8) yield the electronic equation at the second harmonic (n = 2), see also Eq. (1.12c),

$$\left[\left(\frac{d}{dz}+j\frac{2\omega_0}{v_0}\right)^2+4\left(\frac{2\omega_0}{v_0}\right)^2 Q_2 C_2^3\right] s_2(z)$$

$$= -\frac{e}{m_e v_0^2} E_{2C}(z) - \frac{v_1(z)}{v_0^2}\frac{dv_1(z)}{dz} \tag{2.12}$$

$$-\left(\frac{d}{dz}+j\frac{2\omega_0}{v_0}\right)\frac{v_1(z)}{v_0}\frac{ds_1(z)}{dz}.$$

The linear theory for the fundamental frequency, Eq. (2.11), is identical to Pierce's theory (Eq. (1.12c)). Equation (2.12) then is the quasi-linear extension of Pierce's theory for the second harmonic. Note that Eq. (2.12) is similar in form to Eq. (2.11), except for the additional non-linear forcing terms at the end of the RHS of (2.12). These non-linear terms, comprised of quantities from the fundamental, are what generate and drive the evolution of the second harmonic.

The excitation of the circuit electric field, E_{nC}, also follows the classical TWT theory and is considered next.

2.2.2 Circuit Equation

The excitation of the circuit wave electric field, E_{1C}, at the fundamental frequency (n = 1) is the same as the classical, linear theory of TWTs. In Pierce's notation, it reads,

$$\left(\frac{d}{dz}+j\frac{\omega_0}{v_0}[1+(b_1-jd_1)C_1]\right)E_{1C}(z) = j\frac{m_e}{ev_0}\omega_0^3 C_1^3(1+C_1 b_1)^2 s_1(z). \tag{2.13}$$

In Eq. (2.13), b_1 and d_1 are, respectively, Pierce's detune parameter and circuit loss parameter at the fundamental frequency (n = 1). See Eqs. (1.21b) and (1.21d).

Note that the RHS of Eq. (2.13) represents the AC current at the fundamental frequency, which is proportional to the electronic displacement at the fundamental frequency, s_1. It is this AC current, at the fundamental frequency, that excites the circuit field, E_{1C}. The Pierce

three-wave dispersion relation (Eq. (1.20d)) may readily be obtained from Eqs. (2.11) and (2.13) by assuming a wave-like solution for $s_1(z), E_1(z) \propto e^{-j\beta z}$ [70].

The AC current at the second harmonic frequency would similarly excite the circuit wave electric field at the second harmonic, E_{2C}. The composite electronic displacement, s_1 and s_2, now both contribute to the second harmonic current, kinematically. The displacement s_2, at the second harmonic frequency, will contribute to a second harmonic current that is represented by the first term in the RHS of the circuit equation, now constructed for the second harmonic,

$$\left(\frac{d}{dz} + j\frac{2\omega_0}{v_0}[1 + (b_2 - jd_2)C_2]\right)E_{2C}(z) = j\frac{m_e}{ev_0}(2\omega_0)^3(1 + C_2b_2)^2C_2^3 s_2(z) + j\frac{m_e}{ev_0}\Lambda I_2(s_1), \tag{2.14}$$

which may readily be compared with Eq. (2.13). The last term in Eq. (2.14) represents the second harmonic current due solely to the displacement s_1. It is denoted as $I_2(s_1)$, and its physical origin comes from orbital crowding from the first-order (linearized) electron orbit, s_1. Dong et al. [47] provided the procedure to compute the spatial evolution of $I_2(s_1)$, which is also valid even if charge overtaking occurs. Λ here is a coupling coefficient that is defined as: $\Lambda \equiv -j\frac{(2\omega_0)^2 v_0}{I_0}C_2^3$. It turns out that quasi-linear contributions to the s_2 term (that are described by the last two terms in the RHS of Eq. (2.12)) in the RHS of (2.14) are much more important than the $I_2(s_1)$ term.

Equations (2.11) and (2.13) may be solved for the evolution of the fundamental frequency solutions, $s_1(z)$ and $E_{1C}(z)$, subject to the boundary conditions at $z = 0$ (TWT input),

$$s_1(z=0)=0,$$

$$\left.\frac{\partial s_1}{\partial z}\right|_{z=0}=0, \qquad (2.15a,b,c)$$

$$E_{1C}(z=0)=E_{10},$$

where E_{10} is the circuit electric field at the input, which is at the fundamental frequency. Equation (2.15b) states that there is no velocity perturbation at the input, as can be seen from $v_1 = j\omega_0 s_1 + v_0 \frac{\partial s_1}{\partial z}$ and using Eq. (2.15a). Once $s_1(z)$ and $v_1(z)$ are obtained, Eqs. (2.12) and (2.14) may be solved for the evolution of the second harmonic solutions, $s_2(z)$ and $E_{2C}(z)$, subject to the boundary conditions at $z = 0$,

$$s_2(z=0)=0,$$

$$\left.\frac{\partial s_2}{\partial z}\right|_{z=0}=0, \qquad (2.16a,b,c)$$

$$E_{2C}(z=0)=0.$$

Equations (2.16c) and (2.15c) state that all second harmonic quantities are generated by the input signal at the fundamental frequency. Note further that the second harmonic signal that is generated will have a definite phase relation with respect to the input signal.

2.3 Numerical Examples

We shall consider several test cases involving a helix TWT with parameters tabulated below (Table 2.1). This example includes a sever and spatially non-uniform cold-tube loss.

Table 2.1. Tabulation of parameters for test cases.

Parameter	**Value**
Input power (P_{in})	1 mW
Length of circuit (L)	9.5758 cm
Beam radius (R_b)	0.05 cm
Beam voltage (V_b)	3 kV
Beam current (I_0)	0.170 A

Frequency [GHz]	v_{ph}/c	K [Ω]	b	C	QC
4.5	0.103818	111.27	0.337	0.116	0.281
9.0	0.093908	8.97	2.961	0.050	1.053

Here v_{ph} is the wave phase velocity (normalized to the speed of light in vacuum, c), K, b, C, and QC are the Pierce interaction impedance, detuning parameter, gain parameter, and AC "space-charge" parameter, respectively. For the Pierce circuit cold-tube loss parameter d (c.f. Eq. (1.21d)), we consider the cases of (i) a spatially uniform profile (d = constant) given by the gray line and (ii) an attenuation profile given by the black line, as shown in Figure 2.2.

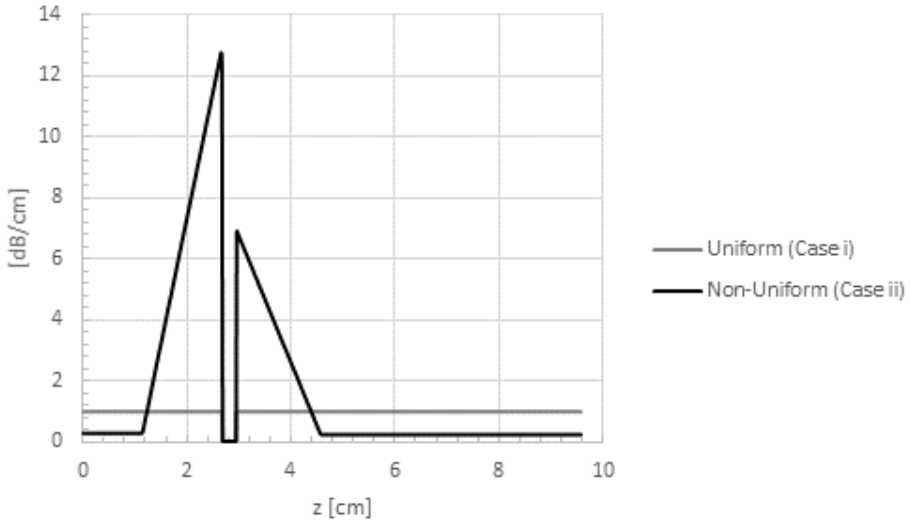

Figure 2.2. Attenuation profile of a helix TWT used for the test cases. The mid-stream sever of radius R_{sever}=0.2794 cm is located between z=2.667 cm and z=2.921 cm.

As can be seen in Figure 2.2, there is an addition of a sever mid-stream. The modeling of the sever region is given in Appendix A.

The results for the RF power profile for both test cases (uniform and non-uniform attenuation profile) are shown in Figure 2.3.

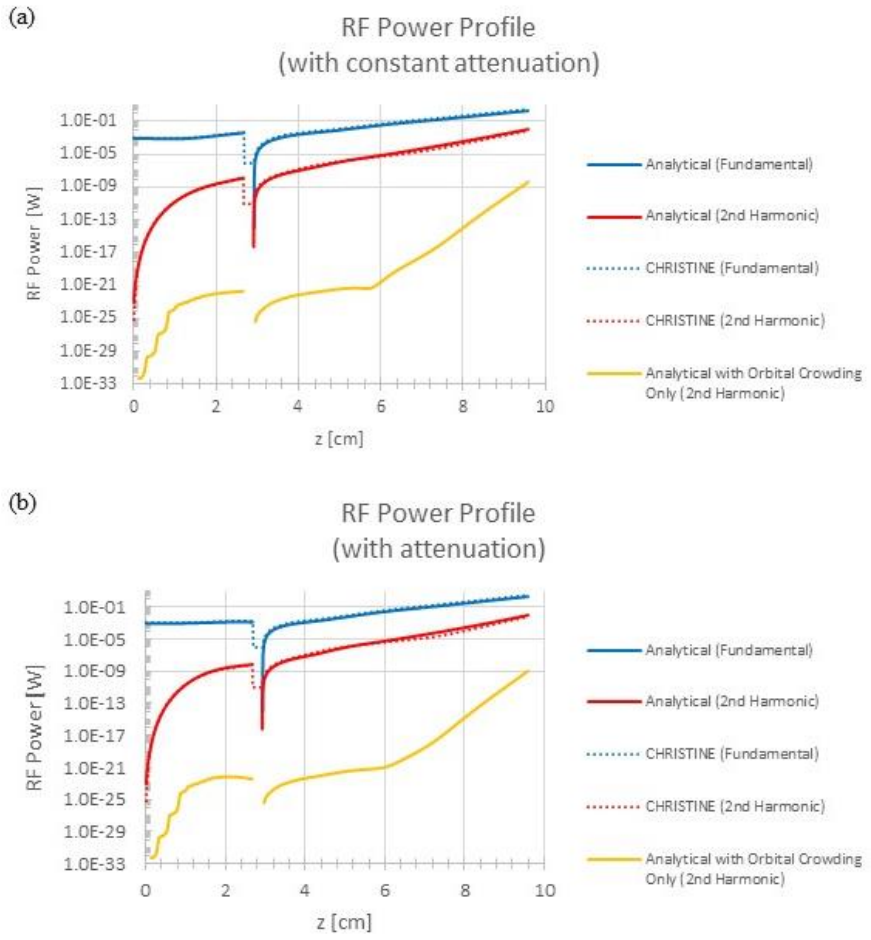

Figure 2.3. RF power profile in semi-log plot for (a) the case with constant attenuation and (b) the case with the attenuation profile. The bottom curves show second harmonic RF power due only to the orbital crowding term, $\Lambda I_2(s_1)$, in Eq. (2.14).

The top four curves in Figure 2.3(a) and Figure 2.3(b) show the RF power profile for both test cases and for both the fundamental and second harmonic in semi-log plot. There is excellent agreement between the analytical calculation (blue solid curves) and the CHRISTINE code (blue dashed curves) for the evolution of the fundamental, as is expected. For the second harmonic, it may be seen that there is also reasonable agreement. This may be more explicitly seen in the linear plots of the second harmonic RF power profile (Figure 2.4).

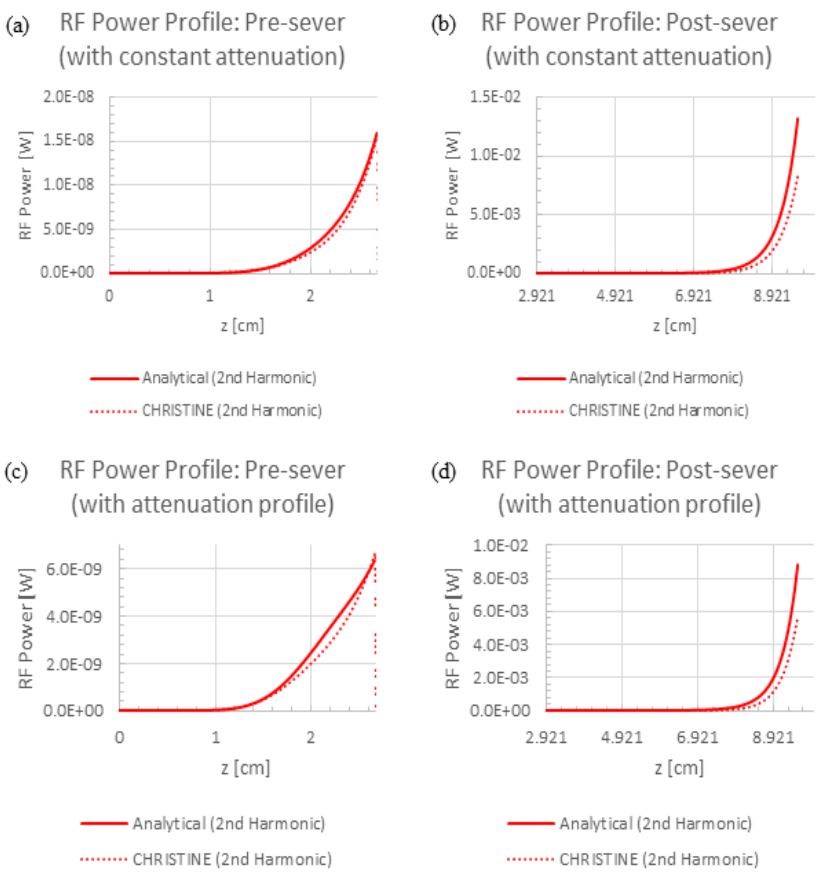

Figure 2.4. RF power profile for the second harmonic in linear plot for (a) and (b) case with constant attenuation and (c) and (d) case with the attenuation profile.

As can be seen from Figure 2.4, there is reasonable agreement between the analytic theory (red solid curves) and CHRISTINE (red dashed curves) for the second harmonic RF power profile. In the pre-sever region, (Figures 2.4a and 2.4c), there is excellent agreement for both constant attenuation and spatial taper (attenuation profile). In the post-sever region, (Figures 2.4b and 2.4d), the analytic formulation differs from CHRISTINE by only 50 percent, after the second harmonic RF power exponentiates by six orders of magnitude beyond the sever region. This difference might well be attributed to the differences in modeling the sever region in CHRISTINE and in the analytic theory (Appendix A). These tests may then be taken as a validation of both the CHISTINE code and the analytic theory,

for both the fundamental and second harmonic, with and without the effects of spatial tapers.

It should be noted that the synchronous non-linear terms in s_2 (i.e., the $v_1 \frac{\partial v_1}{\partial z}$ and $v_1 \frac{\partial s_1}{\partial z}$ terms in Eq. (2.12)) are the main contributors to describing the growth of the second harmonic RF power. Without these non-linear terms for s_2, but retaining only the orbital crowding term $\Lambda I_2(s_1)$ in the RHS of Eq. (2.14), the second harmonic RF power is orders of magnitude lower, as shown in the bottom curve in Figures 2.3(a) and 2.3(b). The non-synchronicity of the orbital crowding term means that the second harmonic RF power does not grow beyond its initial value (0 W). In other words, the top four curves in Figures 2.3(a) and 2.3(b), and all curves in Figure 2.4, are hardly changed if we drop the $\Lambda I_2(s_1)$ term in the RHS of Eq. (2.14), when we solve Eqs. (2.12) and (2.14). It should also be noted that from no initial power at the second harmonic frequency and an input power of 1 mW at the fundamental frequency, RF power on the order of 10 mW is derived at the second harmonic for this example.

2.4 Conclusions

In a helix TWT that has an octave bandwidth (or greater), the second harmonic of the input signal at the fundamental frequency may be within the tube's amplification band and thus may also be generated and amplified. In such a case, there are two possible sources of harmonic content: the process of orbital crowding from the linear orbits (similar to that in klystrons) and non-linearities in the electron orbits. Much to our surprise, it was found that orbital crowding did not play as important of a role as was initially thought. Rather, quasi-linear terms in the force law that drive the second harmonic electronic displacement played a much more important role in describing the second harmonic RF power growth. These

terms represent synchronous excitation, in both time and space, between the beam mode and the circuit mode at the second harmonic frequency.

This chapter has provided a method to ascertain the synchronous non-linear terms in the governing equations for the beam-circuit interaction. In so doing, we extend Pierce's original formulation to quantify harmonic contents in the electron beam. The method in this chapter also recovers Pierce's original equations for the beam-circuit interaction at the fundamental (input) frequency and allows for axial variations in the Pierce parameters. Since we used an Eulerian description, the theory is applicable only when the electronic displacement is small.

Several test cases were considered and compared with the large-signal, non-linear CHRISTINE simulation code. In these test cases, a helix TWT with a mid-stream sever and a spatial attenuation profile was considered. As was expected, excellent agreement in the RF power profiles was found between theory and CHRISTINE at the fundamental. We have also validated the second harmonic RF power profile in the pre- and post-sever regions for the cases of uniform and non-uniform attenuation.

Future work may include extension to higher harmonics, and application of this theory to harmonic generation in other devices.

Chapter 3 :
A Modification of Pierce's Classical Theory of Traveling-Wave Tubes

3.1 Introduction

In the previous chapter, we extended Pierce's classical three-wave theory for the beam-circuit interaction in a traveling-wave tube to include the generation of harmonics in a perturbation analysis. We had assumed that his theory of mode coupling was correct as is and that we have information on all of the Pierce parameters to be used in the governing equations (c.f. the electronic and the slow-wave circuit equations). In general, the calculation of the Pierce parameters is not trivial, especially for the so-called "Pierce AC space-charge parameter," *Q*, which has remained an open question for over sixty years [35]. Here, we attempt to provide an answer to the exact calculation of the Pierce parameters in a realistic TWT: the tape helix.

An accurate determination of *Q* is important for at least three reasons:

(i) A small discrepancy in *Q* can lead to a large change in the predicted small-signal gain.

(ii) An accurate value of *Q* (or *QC*) is required by the non-linear TWT simulation codes such as CHRISTINE [48] in order to compute large-signal quantities like saturated output power and efficiency.

(iii) In Johnson's classical theory for the onset of backward wave oscillations in TWT [57], the threshold conditions depend only on *QC* and on *d* [4,57],

which implies that prediction of BWO threshold current requires accurate values of QC and d.

We may also add that, when the free-electron laser dispersion relation is cast in Pierce's form [5,12-17], the parameter Q characterizes the so-called "Raman regime"; setting $Q = 0$ corresponds to operation in the "Compton regime".

Approximate models of Q have been presented in the literature [35,49-51]. One widely used model is due to Branch and Mihran [49], in which the helix is replaced with a perfectly conducting metallic cylinder. This model does not take into account the higher-order circuit modes or field leakage through the helix windings. An improvement to this model is the sheath helix model [48,50,52] which allows current to flow in the helical direction. However, this model still does not fully take into account the field leakage in a finite width tape or wire helix. A general formulation that does take the circuit geometry and field leakage into account exactly has been given by Cooke, et al. [37], but these authors do not specify how to extract a value for Q from their approach. These models have been implemented in the large-signal helix TWT code CHRISTINE [48,50,52].

For a realistic case of an electron beam interacting with the electromagnetic fields supported by a thin perfectly conducting tape helix, the author derives the *exact* dispersion relation, from which an unambiguous determination of Q is made. In the process of doing so, we discover that the circuit mode in the equivalent three-wave theory of Pierce must be modified at high beam current also, an aspect overlooked in Pierce's original analysis. We quantify this circuit mode modification by an entirely new parameter that we call q, introduced here for the first time in TWT theory. In a realistic example, we find that the

effect of q is equivalent to modification of circuit phase velocity by as much as two percent, which is a significant effect - equivalent to a detune of two percent.

The aforementioned exact dispersion relation captures the complete information on the geometry, the circuit, the beam, and their interaction. It not only provides an exact value of Q by the method we describe below, it also demands that the circuit mode as represented in Pierce's three-wave form be modified by the introduction of a new dimensionless parameter q when the beam current is high. We have evaluated both Q and q numerically for a realistic tape helix TWT model. We compare our exact value of Q with those of the Branch and Mihran and sheath helix models.

Section 3.2 contains a presentation of our beam-wave interaction model and the numerical results obtained from the exact dispersion relation. The modified Pierce dispersion relation including the new parameter q is presented in Section 3.2. Sections 3.3 and 3.4 include a test case study and concluding remarks. Details of the derivation of the exact dispersion relation of an electron beam interacting with an electromagnetic mode of a thin tape helix is provided in Appendix B.

3.2 Modification of Pierce's Classical TWT Theory

Pierce's classical dispersion relation (Eq. (1.21)) reads,

$$[(\beta - \beta_e)^2 - 4\beta_e^2 Q C^3]\left[\beta - \beta_{ph}\right] = -\beta_e^3 C^3 \tag{3.1}$$

where $\beta_e = \frac{\omega}{v_0}$, $\beta_{ph} = \frac{\omega}{v_{ph}}$, v_0 is the beam velocity, and v_{ph} is the phase velocity of the circuit wave on the cold helix. This equation quantifies the coupling of the beam mode [first bracket on the LHS, which includes the so-called "space-charge effect" represented by Q] with the

cold-tube circuit mode [second bracket, assuming zero circuit loss, i.e., $d = 0$]. The quantity C^3 on the RHS is a measure of the strength of the coupling between the beam and the circuit; it is proportional to the DC beam current (c.f. Eq. (1.21c)).

To illustrate explicitly why Eq. (3.1) must be modified, we consider the realistic model of a helix circuit [34], shown in Figure 1.5 and redrawn in Figure 3.1 with the electron beam. It consists of an infinitesimally thin tape helix of radius a, pitch p, and width w, surrounded by a stratified dielectric and an outer perfectly conducting metallic cylinder of radius b (Figure 3.1). The pitch angle ψ of the helix is defined by $\cot\psi \equiv k_H a$, where $k_H \equiv 2\pi/p$. A stratified (layered) dielectric is included between the outer cylinder and the helix in order to represent the dielectric effects of the support rods in an approximate way. It has been shown (see refs. [12,13] of [34]) that this model is a good approximation to an actual helix TWT circuit without dispersion control elements (vanes).

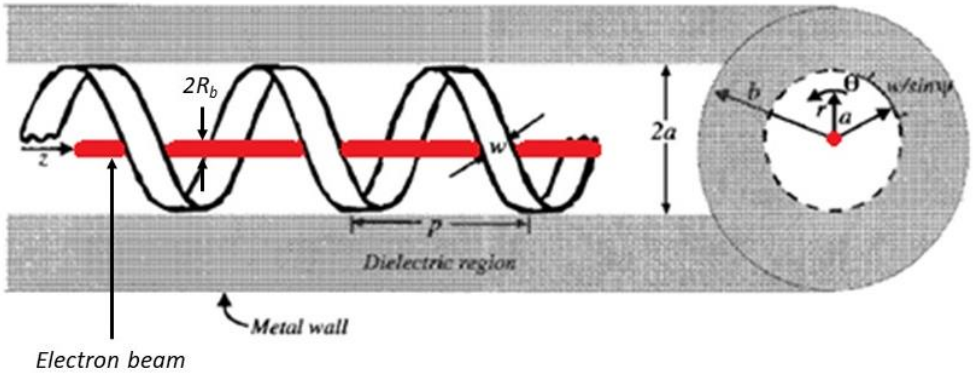

Figure 3.1. Schematic diagram of tape helix TWT model.

An exact dispersion relation for this helix in the absence of a beam (the cold-tube dispersion relation) was obtained by Chernin et al. [34]. This dispersion relation may be solved numerically for the propagation constant β given the signal frequency ω. This cold-

tube dispersion relation is shown by the blue curves in Figure 1.4. For simplicity, we assume as in [34] that the dielectric layers are lossless and the tape helix is perfectly conducting; consequently there is no cold-tube loss (the Pierce loss parameter $d = 0$) for the cases considered in this study.

We next consider the addition of a mono-energetic electron beam of radius R_b and uniform density n_0 centered on the axis of the helix and confined by an infinite axial magnetic field so that electrons move only axially. We denote the DC beam current by I_0 and the beam velocity by v_0. We assume that the beam is non-relativistic, $v_0 \ll c$.

Outside the beam region, the calculation in [34] for the vacuum electromagnetic fields carries over. Within the beam region, we may calculate the small-signal AC current and the electromagnetic fields. At the interface between beam and vacuum all components of the RF electric and magnetic fields are continuous [71]. Applying these conditions we find that the dispersion relation in the presence of the beam (the hot-tube dispersion relation) may be written in a form very similar to that in [34], namely,

$$D(\beta; \omega) = \det(M) = 0, \tag{3.2}$$

where the infinite matrix M is given in Eq. (B34) of Appendix B.

We note that Eq. (3.2) does not have the form of Eq. (3.1); it is much more complicated and must be solved numerically for β, given the frequency ω. However, for all examples that we have tried, we find that Eq. (3.2) always admits three roots for β with positive real parts, corresponding to positive phase velocity, that is, phase velocity in the direction of propagation of the beam; two of which (β_1, β_3) are complex conjugates (corresponding to spatial decay and growth, respectively) and the third root (β_2) is purely real (see Figure 3.3 below). Thus, the exact dispersion relation may be represented in a three-wave theory as:

$$D(\beta;\omega) \equiv (\beta-\beta_1)(\beta-\beta_2)(\beta-\beta_3) = 0. \tag{3.3}$$

An equivalent form of Eq. (3.3) may be written in a form similar to Eq. (3.1),

$$[(\beta-\beta_e)^2 - 4\beta_e^2 QC^3]\left[(\beta-\beta_{ph}) - 4\beta_{ph} qC^3\right] = -\beta_e^3 C^3, \tag{3.4}$$

where q is a new parameter introduced to account for the space-charge effect on the circuit mode. This new term is necessary to make Eqs. (3.3) and (3.4) equivalent, whose three roots of β are identical to the numerical roots obtained from the exact theory, Eq. (3.2). Note from Eq. (3.4) that q produces a circuit phase velocity change due to a space-charge effect, by a fraction equal to $4qC^3$. This new parameter, q, is introduced here for the first time in the literature of TWTs. Physically, Eq. (3.4) describes the modification of the beam mode at high current through Q, and the modification of the cold-tube circuit mode through q. In terms of the numerically obtained roots β_1, β_2, and β_3 of Eq. (3.2) the parameters qC^3, QC^3, and C^3 may be obtained by equating coefficients of β^2, β^1, and β^0 in Eqs. (3.3) and (3.4),

$$\begin{aligned} qC^3 &= \frac{1}{4}\left(\frac{\beta_1+\beta_2+\beta_3-2\beta_e}{\beta_{ph}} - 1\right), \\ QC^3 &= \frac{1}{4}\left(1 - \frac{\beta_1\beta_2+\beta_2\beta_3+\beta_1\beta_3-2\beta_e\beta_{ph}(1+4qC^3)}{\beta_e^2}\right), \\ C^3 &= \frac{\beta_e^2(1-4QC^3)\beta_{ph}(1+4qC^3)-\beta_1\beta_2\beta_3}{\beta_e^3}. \end{aligned} \tag{3.5a-c}$$

Numerical solutions for C, Q, and q will be presented next, and compared with previous, approximate theories.

3.3 Numerical Examples

We consider the first test case in [34] with the following circuit parameters: tape helix radius a = 0.12446 cm, pitch p = 0.080137 cm, helix pitch angle ψ = 5.851 deg, tape width w = 0.0159 cm, wall radius b = 0.2794 cm, and dielectric constant of supporting layer $\varepsilon_r^{(2)}$ =

1.25. For the electron beam, we assume beam radius R_b = 0.05 cm, DC beam voltage V_b = 3.0 kV, and DC beam current I_0 = 0.17 A.

We first confirm that the cold-tube dispersion relation [34] is recovered from our hot-tube dispersion relation if we set the DC beam current very close to zero numerically. This is demonstrated in the phase velocity vs. frequency plot of Figure 3.2.

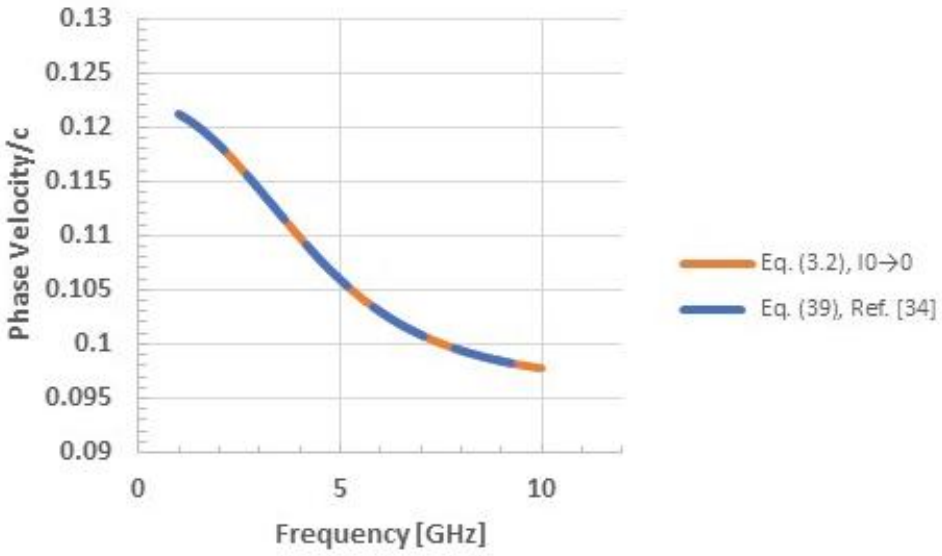

Figure 3.2. Plot of the phase velocity/c, as a function of frequency.

The cold-tube limit of the hot-tube dispersion relation may also be verified analytically. This is shown explicitly in Appendix B.

Figure 3.3 shows the solutions of Eq. (3.2) as functions of frequency along with the solutions of Pierce's classical three-wave dispersion relation Eq. (3.1) with different models of Q (Branch and Mihran [49] and sheath helix [48]). The solutions of Eq. (3.1) were used as initial guesses in the iterative numerical solution of Eq. (3.2).

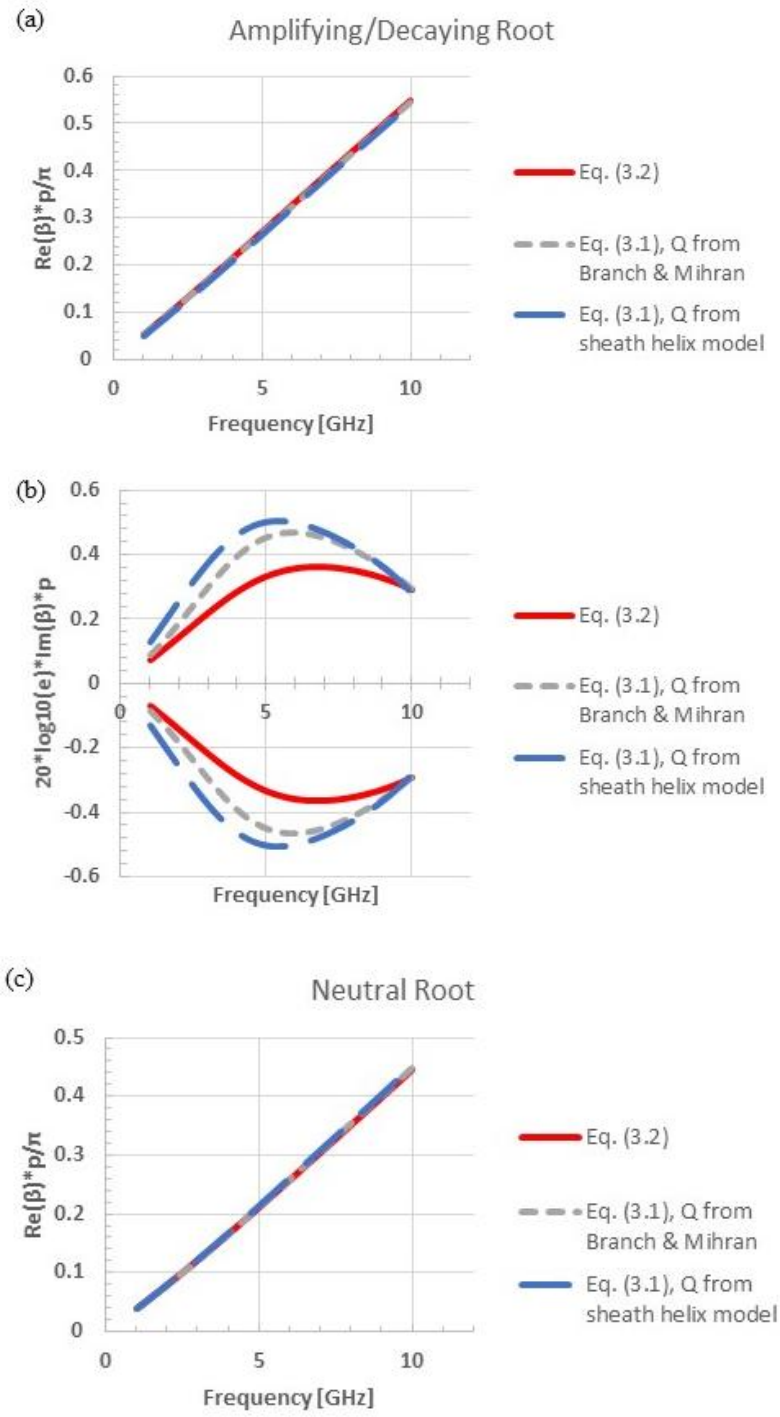

Figure 3.3. Roots of the hot-tube dispersion relation Eq. (3.2) for a tape helix TWT, along with the solutions of Eq. (3.1) for different models of *Q*. The quantity plotted in (a) and (c) is the phase shift per period/π; the quantity plotted in (b) is the growth or attenuation in dB per period.

The *exact* values of the Pierce parameters obtained from Eq. (3.5) are plotted against

frequency in Figure 3.4, along with results using various previous models of Q. In Figure 3.4a the 'classical' value of C is obtained from $C = (KI_0/4V_b)^{1/3}$ (c.f. Eq. (1.21c)), where K is the Pierce impedance, averaged over the beam cross-section (c.f. Eq. (1.15)). From the hot-tube results, we see that the new q parameter is required in order to obtain sensible results for the Pierce parameters. For example, we see in Figure 3.4a that the value of C obtained from Eq. (3.5c) by setting $q = 0$ is at least a factor of 2 too large. Likewise, Figure 3.4b shows that the value of Q is too small if we set $q = 0$ in Eq. (3.5b). The values of C, Q, and q at 4.5 GHz as functions of the beam current are plotted in Figure 3.5(a,b,c). Note that both Q and q depend on the beam current by this theory.

For $q = 5$ and $C = 0.1$ (Figure 3.5), we have $4qC^3 = 0.02$, which is equivalent to a change of circuit phase velocity of two percent according to Eq. (3.4). This is equivalent to a detuning between the beam velocity and the circuit phase velocity of two percent which is very significant.

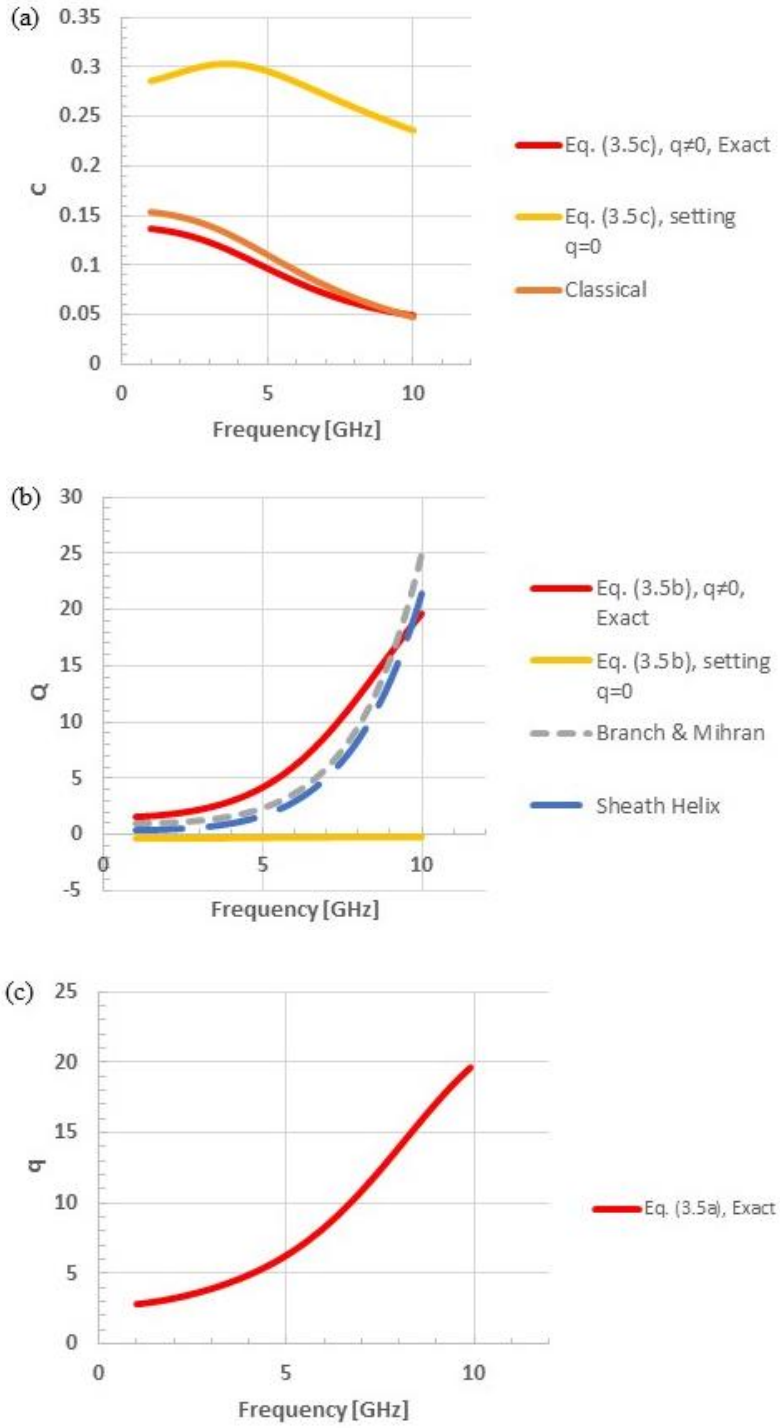

Figure 3.4. Plots of the exact Pierce parameters [(a) *C*, (b) *Q*, (c) *q*] and their traditional definitions as a function of frequency.

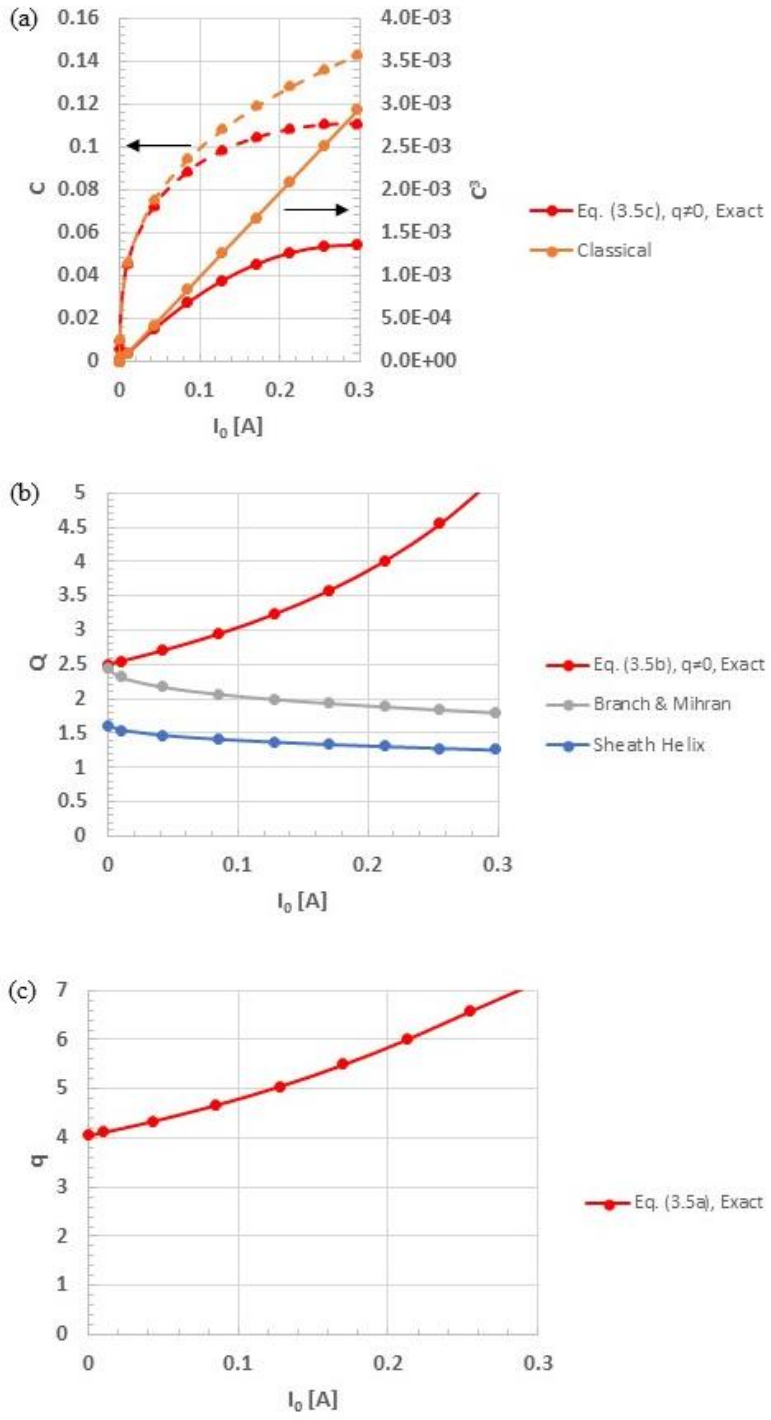

Figure 3.5. Plot of the Pierce parameters [(a) C, (b) Q, (c) q] at 4.5 GHz, and their traditional definitions as functions of DC beam current. Also shown in (a) is the plot of C^3.

3.4 Conclusions

From a study of the numerical solutions of the exact dispersion relation for a beam interacting with the electromagnetic fields of a tape helix, we have concluded that the phase velocity of the circuit mode is affected by the beam current. This effect may be represented by a new parameter q defined in Eq. (3.4), and is equivalent to a change of circuit phase velocity by the fraction of $4qC^3$.

The space-charge parameters Q and q appear symmetrically in Eq. (3.4) as modifications of the beam mode and the circuit mode, respectively. In their earlier work [36], Lau and Chernin have shown explicitly for a sheet electron beam propagating inside a corrugated waveguide (c.f. Figure 3a and Eq. (C17) of Ref. [36]) that

(i) Q originates from the higher-order circuit modes, as noted by Pierce [3],

(ii) though not explicitly pointed out in [36], there is a hidden effect like q that originates from the higher-order beam modes (this will be explicitly demonstrated in Chapter 4 for the disk-on-rod TWT), and

(iii) both Q and q depend on ω and β.

The present work here demonstrates that the 'q' term is important for the tape helix. It is anticipated that a finite value of q is generally required for the accurate representation of the dispersion relation of an electron beam interacting with the electromagnetic fields of any periodic structure.

Chapter 4 :
A Traveling-Wave Amplifier Using a Disk-on-Rod Slow-Wave Structure and an Annular Electron Beam

4.1 Introduction

In Chapters 2 and 3, we concentrated on a particular type of slow-wave structure and electron beam: a thin tape helix SWS and a pencil electron beam. While this combination of circuit structure and beam-type is the most commonly used in industry [1-2,4], its power handling capabilities is severely limited because of its very small size. In this chapter, we will analyze another traveling-wave amplifier that may operate at much higher power levels and is of current interest [55-56]. This TWA features an on-axis disk-loaded or Disk-on-Rod (DoR) SWS and an outer annular electron beam; these components are enclosed by a cylindrical metallic waveguide. Figure 4.1 shows a schematic diagram of the DoR TWA.

This DoR geometry was first introduced by Field [72], where he experimentally tested an X-band variant. A U.S. patent [73] for this device was filed in 1953, but since then, this design seems to have been abandoned in the TWT literature in favor of other designs. Recently in the simulation papers by Hoff and French [55-56], this design was revisited. However, instead of using an annular beam as in Field's original work (and here), a set of pencil beams at a constant radius from the center conductor and equally spaced azimuthally are used to form a discretized version of the annular beam. This was done to enable better separation of the electron gun and the support points of the centered SWS, which also serve as the injection and extraction ports upstream and downstream respectively. This in turn may

enable higher beam voltages than originally designed by Field. Since multiple pencil beams necessarily make the geometry three-dimensional, in this Chapter, we use the simpler model of an annular beam to enable a much more tractable two-dimensional analytic treatment.

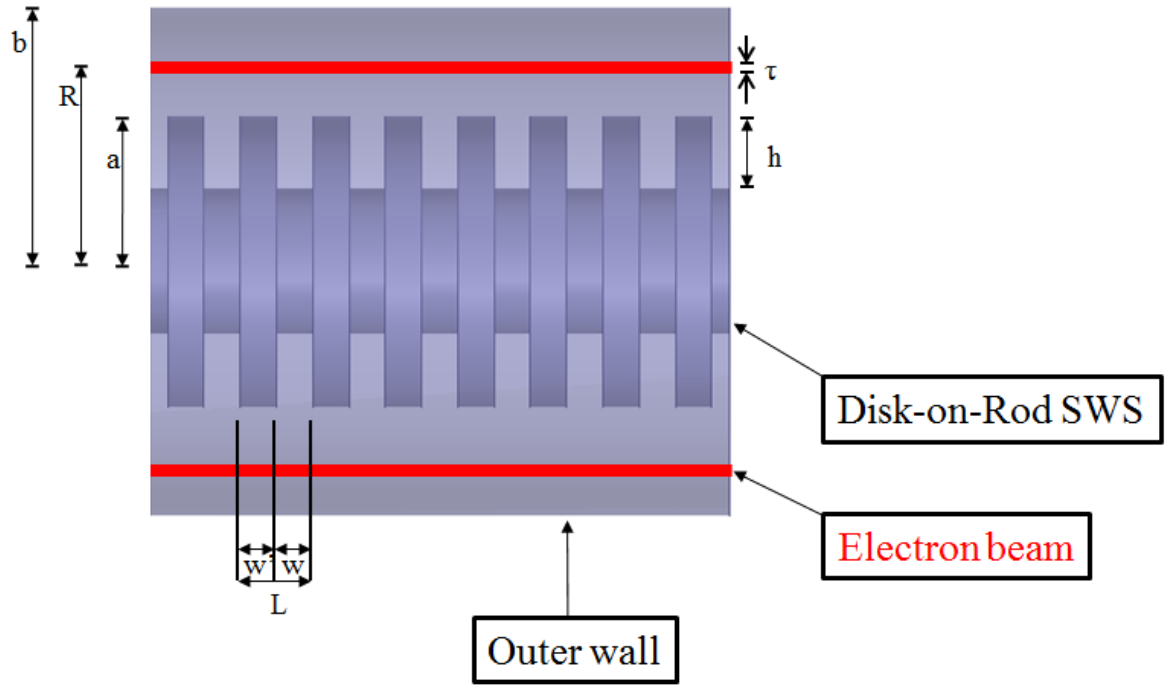

Figure 4.1. Schematic diagram of the Disk-on-Rod TWA. A thin annular electron beam at radius *R* is assumed.

With the exception of a helix TWT (which has wide bandwidth), most other amplifiers concentrate on high power output and, in doing so, sacrifice bandwidth. The DoR TWA has garnered interest because this particular device may provide both high power and moderate bandwidth by virtue of its annular electron beam and the DoR slow-wave structure. A large diameter annular beam may produce high power for two reasons: (a) its large cathode area, and (b) its much higher limiting current than a pencil beam, especially if the annular beam is

placed close to the outer wall [74-76]. This leads to much higher output power than the use of a pencil beam.

The objective of this chapter is to provide an in-depth analytic study of the Disk-on-Rod TWA. A case study will be considered. In particular, we consider the exact dispersion relation and the values of the Pierce parameter Q and our new parameter q for this DoR TWA. The design values of this case study are tabulated below (Tables 4.1 and 4.2). A small-signal (linear) analysis will be cast into Pierce's three-wave TWT theory, similar to our treatment of the helix TWT in Chapter 3. We will also derive traditional TWT metrics such as C and QC so that comparisons may be made with existing theories. In so doing, we will investigate several theories on QC in greater detail and look further into the new space-charge parameter qC introduced in the previous chapter. Comparisons with ICEPIC [77] and MAGIC [78] simulations will also be made.

Table 4.1. Dimensions for the Disk-on-Rod TWA for a case study.

Dimensions [cm]	
b	3.5
R	2.8
a	2.3
h	1.3
L	0.6
w'	0.3
w	0.3
τ	0.1

Table 4.2. Operating parameters for a case study of the Disk-on-Rod TWA.

Operating Parameters	
V [kV]	124
β_{01} [m^{-1}]	100
f_1 [GHz]	2.832

4.2 The Cold-Tube Dispersion Relation

To begin, the electron beam is removed to characterize the cold-tube structure of the DoR TWA. We will consider transverse magnetic (TM) electromagnetic waves in regions (Figure 4.1) outside of the vanes ($r > a$) and assume transverse electric and magnetic (TEM) waves inside the cavities ($a - h < r < a$). The TM modes admit an axial electric field, which is required for axial bunching of the beam. The assumption of TEM modes in the cavities, which is commonly used, turns out to be a good assumption [79-81]. Inhomogeneous wave equations for the magnetic and electric fields (decoupled) can be derived from combining Maxwell's Equations. Assuming $e^{j\omega t - j\beta_n z}$ (time and n^{th} spatial harmonic) dependence for the fields and employing the Floquet Theorem for periodic structures, the equations for the fields (up to arbitrary constants) may be derived. We next apply the appropriate boundary conditions: (1) tangential electric field must be zero at $r = a - h$, (2) tangential electric field must be continuous at $r = a$, (3) the spatially-averaged (across the cavity opening) magnetic field must be continuous at $r = a$, and (4) the electric field must be zero at $r = b$. By boundary conditions (1) and (4), we assume that the metallic structures in the problem are perfectly conducting. In so doing, the Pierce cold-circuit loss parameter *d* is zero (c.f. Eq.

(1.21d)). With some algebra, the field solutions with the above boundary conditions may be rearranged to give a dispersion relation of the form:

$$G(\omega,\beta_0) \equiv \frac{U'\left(\frac{\omega a}{c}\right)}{\left(\frac{\omega a}{c}\right)U\left(\frac{\omega a}{c}\right)} - \sum_{n=-\infty}^{\infty} \frac{(sin\,\theta_n)^2}{\theta_n'\theta_n} \cdot \frac{V'(p_n a)}{(p_n a)V(p_n a)} = 0, \tag{4.1}$$

where

$$\beta_n = \beta_0 + \frac{2\pi n}{L}, n = 0, \pm 1, \pm 2, \ldots \tag{4.2}$$

$$\theta_n = \frac{\beta_n w}{2}, \theta_n' = \frac{\beta_n L}{2} \tag{4.3}$$

$$p_n = \sqrt{\beta_n^2 - \frac{\omega^2}{c^2}} \tag{4.4}$$

$$U\left(\frac{\omega r}{c}\right) = J_0\left(\frac{\omega(a-h)}{c}\right) Y_0\left(\frac{\omega r}{c}\right) - J_0\left(\frac{\omega r}{c}\right) Y_0\left(\frac{\omega(a-h)}{c}\right) \tag{4.5}$$

$$U'\left(\frac{\omega r}{c}\right) = J_0\left(\frac{\omega(a-h)}{c}\right) Y_1\left(\frac{\omega r}{c}\right) - J_1\left(\frac{\omega r}{c}\right) Y_0\left(\frac{\omega(a-h)}{c}\right) \tag{4.6}$$

$$V(p_n r) = I_0(p_n r)K_0(p_n b) - I_0(p_n b)K_0(p_n r) \tag{4.7}$$

$$V'(p_n r) = I_1(p_n r)K_0(p_n b) + I_0(p_n b)K_1(p_n r). \tag{4.8}$$

J and *Y* are the Bessel functions of the order of the subscript, and *I* and *K* are the corresponding modified Bessel functions. Equation (4.1) is the dispersion relation for the vacuum mode; it is also known as the cold-tube dispersion relation.

In obtaining Eq. (4.1), the continuity of the spatially-averaged magnetic field across the cavity opening is assumed. This assumption is commonly used for treatments of SWS's, and it provides significant simplification [82]. Unlike the previous study of the tape helix where

the goal was to give a formally exact dispersion relation for the purposes of numerically obtaining exact values of the space-charge parameter *Q*, here we seek to analytically manipulate the equations to give closed-form analytic expressions for the Pierce parameters. To that end, we may represent the cold-tube dispersion relation, Eq. (4.1), as $\omega^2 - \omega_c^2(\beta_0) = 0 \rightarrow \omega = \omega_c(\beta_0)$, where ω_c are the cold-tube eigen-frequencies corresponding to a propagation constant β_0. This cold-tube dispersion relation is shown in Figure 4.2.

We digress to remark that our formulation presented here differs from that presented by Field [72] in that we consider *all* spatial harmonics in the structure. This was not done in his brief analysis of the "disk-loaded rod." Furthermore, we will go one step further and look at the "hot-tube" dispersion relation that has the effects of the beam incorporated. We will evaluate the derived analytic forms of the Pierce parameters and the newly discovered space-charge parameter *q*, something that Chen [83] did not consider. In other words, Field's and Chen's analyses cannot yield reliable values of *Q*.

4.2.1 Comparison with ANSYS HFSS and ICEPIC

The solutions to the cold-tube dispersion relation, Eq. (4.1), are next considered. The fundamental circuit mode for the case study and the second passband are shown (Figure 4.2). To validate that this dispersion relation derived from field theory is correct, Dr. David Simon of the Air Force Research Laboratory [84] designed the Disk-on-Rod TWA in the program High Frequency Structural Simulator (HFSS from ANSYS) [85] and ran simulations to determine the eigen-frequencies. Validation was also done by comparing with the data furnished by Dr. Brad Hoff, also of the Air Force Research Laboratory, who used the Electromagnetic Particle-in-Cell (PIC) code ICEPIC (Improved Concurrent Electromagnetic

Particle In Cell) [77]. Shown in Figure 4.3 are the plots of the results from HFSS and ICEPIC compared to the analytic field theory. The beam line for the case study is also included here.

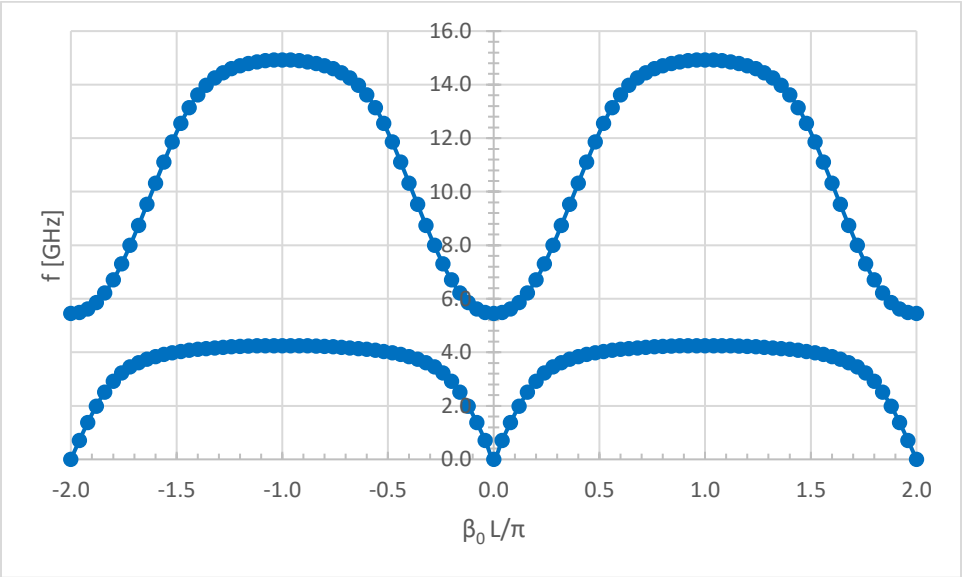

Figure 4.2. Plot of the numerical roots of the analytical cold-tube dispersion relation for the case study of the DoR TWA. $\beta_0 L$ is the phase shift per period.

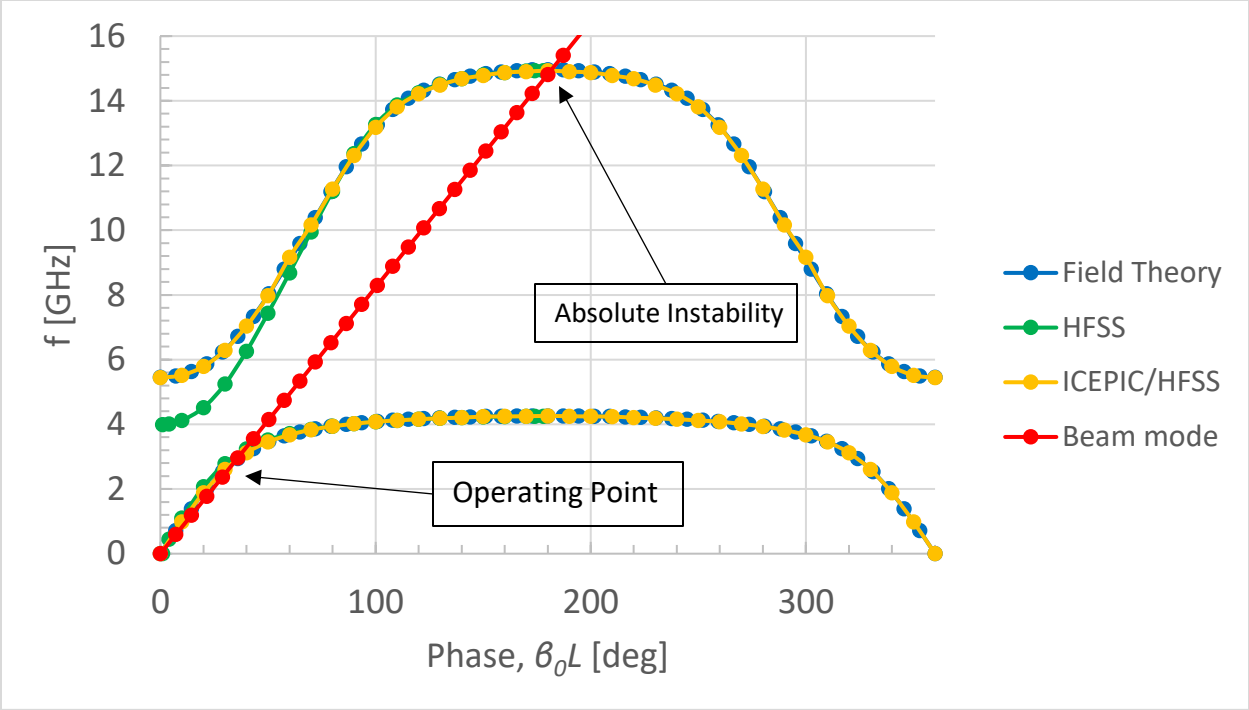

Figure 4.3. Comparison of the solutions of the cold-tube dispersion relation between analytic field theory, HFSS, and ICEPIC for the case study of the DoR TWA.

As can be seen in Figure 4.3, the HFSS and ICEPIC simulations agree well with the analytic field theory. There is a slight discrepancy in the second passband between the analytic theory and ICEPIC with HFSS for low phase advances. This may be due to the limitation of resolution for the HFSS simulations. It may also be due to the identification of TE and/or "hybrid" modes that are not TM.

The beam line intersects the fundamental passband at $(\frac{\omega_1}{2\pi}, \beta_{01}) \approx (2.832\ \text{GHz}, 100\ \text{m}^{-1})$, which denotes the operating point. At 2.832 GHz, $\beta_0 L = 34.37°$. Synchronous interaction between beam and circuit occurs when an input signal of this frequency is injected.

Note that the beam line happens to intersect the second passband near the upper band-edge (π-mode or $\beta_0 L = 180°$, at 15 GHz, where there is zero group velocity). This intersection shows strong possibility of band-edge oscillation [68-69]. Indeed, oscillations were observed

in ICEPIC at 15 GHz. Extensive studies, involving the Briggs-Bers Criterion [86], on band-edge oscillations have been done [68-69,87], where it is shown that the upper band-edge in general is more susceptible to oscillations than the lower band-edge [87]. Suppression of oscillations at the upper band-edge has been achieved with industrial proprietary techniques. This is an ongoing issue and will not be further considered here. The main purpose of this chapter is to reliably determine all of the Pierce parameters, including q, for the DoR TWA.

4.3 The Hot-Tube Dispersion Relation

We next place an annular sheet electron beam in the structure and derive the hot-tube dispersion relation. The beam is assumed to be monoenergetic with velocity v_0 and is guided by an infinite axial magnetic field so the beam motion is one-dimensional. The beam thickness τ is assumed to be much smaller than its radius, so an electron sheet is essentially assumed. This thin-beam assumption has been widely used with good results [36,74-75,83,88]. The four boundary conditions stated in the paragraph that contains Eq. (4.1) still hold, but we now add two more to account for the electron beam: (5) the tangential electric field must be continuous at the location of the sheet electron beam ($r = R$) and (6) the normal electric field suffers a discontinuity ($\frac{\sigma_n}{\varepsilon_0}$, where σ_n is the surface charge density of the electron beam at the nth space harmonic and ε_0 is the permittivity of free space) at $r = R$. With this and some mathematics, it can be shown that the hot-tube dispersion relation takes the form:

$$D(\omega,\beta_n) \equiv \frac{U'\left(\frac{\omega a}{c}\right)}{\left(\frac{\omega a}{c}\right)U\left(\frac{\omega a}{c}\right)}$$

$$- \sum_{n=-\infty}^{\infty} \frac{(sin\,\theta_n)^2}{\theta_n' \theta_n}$$

$$\cdot \left\{ \frac{\omega_p^2(\frac{\tau}{a})}{(\omega - \beta_n v_0)^2 - p_n^2 \omega_p^2 \tau R \frac{V(p_n R)}{V(p_n a)} W_n} \cdot \frac{R}{a} \cdot \left(\frac{V(p_n R)}{V(p_n a)} \right)^2 \right. \tag{4.9}$$

$$\left. + \frac{V'(p_n a)}{(p_n a) V(p_n a)} \right\} = 0$$

where

$$W_n = I_0(p_n R) K_0(p_n a) - I_0(p_n a) K_0(p_n R), \tag{4.10}$$

and $\omega_p^2 \equiv \frac{e^2 n_0}{m_e \gamma_0^3 \varepsilon_0}$ is the plasma frequency (squared), that includes the relativistic beam dynamics where $\gamma_0 = \frac{1}{\sqrt{1-\frac{v_0^2}{c^2}}}$ is the relativistic mass factor.

We may rewrite Eq. (4.9) in the equivalent form, when using the definition of *G* from Eq. (4.1),

$$G(\omega, \beta_0) = \sum_{n=-\infty}^{\infty} \frac{(sin\,\theta_n)^2}{\theta_n' \theta_n} \frac{\omega_p^2(\frac{\tau}{a})}{(\omega - \beta_n v_0)^2 - p_n^2 \omega_p^2 \tau R \frac{V(p_n R)}{V(p_n a)} W_n} \cdot \frac{R}{a} \cdot \left(\frac{V(p_n R)}{V(p_n a)} \right)^2 . \tag{4.9'}$$

When the beam is removed, $\omega_p \to 0$ and both Eqs. (4.9) and (4.9') reduce to the cold-tube dispersion relation, Eq. (4.1).

4.3.1 Pierce's Form and Identification of the Pierce Parameters

We may rewrite Eq. (4.9) into a more familiar and physically intuitive form:

$$(\omega - \beta_0 v_0)^2 = \omega_p^2 \cdot F^2, \tag{4.11}$$

where F^2 is the plasma frequency reduction factor, given in Eq. (4.12) below. If we set $F^2 = 1$, Eq. (4.11) is the familiar dispersion relation for the space-charge waves of a uniform electron beam drifting at velocity v_0 in free space. F^2 then provides a correction to this textbook case that accounts for the finite geometry of the beam and its surrounding structures. For the DoR TWA (Figure 4.1), the plasma frequency reduction factor may be extracted from the exact dispersion relation Eq. (4.9) and it has the form:

$$F^2 = \frac{\tau}{a}\left[\frac{\frac{(\sin\theta_0)^2}{\theta_0'\theta_0}\frac{R}{a}\left(\frac{V(p_0R)}{V(p_0a)}\right)^2}{G(\omega,\beta_0) - \sum_{n\neq 0}\frac{(\sin\theta_n)^2}{\theta_n'\theta_n}\frac{\omega_p^2(\frac{\tau}{a})}{(\omega-\beta_n v_0)^2 - p_n^2\omega_p^2\tau R\frac{V(p_nR)}{V(p_na)}W_n}\cdot\frac{R}{a}\cdot\left(\frac{V(p_nR)}{V(p_na)}\right)^2} + (p_0R)(p_0a)\frac{V(p_0R)}{V(p_0a)}W_0\right]. \tag{4.12}$$

When the exact hot-tube dispersion relation is written in the form of Eq. (4.11), resonance is said to occur when $F \to \infty$. Note that the function in Eq. (4.12) is singular ($F \to \infty$) when the denominator of the first term is zero, i.e. when

$$G(\omega,\beta_0) = \sum_{n\neq 0}\frac{(\sin\theta_n)^2}{\theta_n'\theta_n}\frac{\omega_p^2(\frac{\tau}{a})}{(\omega-\beta_n v_0)^2 - p_n^2\omega_p^2\tau R\frac{V(p_nR)}{V(p_na)}W_n}\cdot\frac{R}{a}\cdot\left(\frac{V(p_nR)}{V(p_na)}\right)^2. \tag{4.13}$$

For low beam currents, the plasma frequency is small and this condition of resonance becomes $G(\omega,\beta_0) = 0$; that is, there is resonance in this beam-circuit interaction at the natural modes of the cold structure [36,89]. However, for high beam currents, this circuit

resonance condition is modified by higher-order spatial harmonics of the *beam mode*, which is what gives rise to our new space-charge parameter *q*, as explicitly shown below.

Similar to the tape helix TWT that we studied in Chapter 3, near the operating point, the exact dispersion relation, Eqs. (4.11) or (4.9), always admits three numerical roots for β_0, with $\mathrm{Re}(\beta_0) > 0$, two of which are complex conjugates, and the third root is real, for all tube parameters that we tested. Thus, we may likewise cast the exact dispersion relation for the DoR TWA, Eq. (4.11), in Pierce form, as given in Eqs. (4.15a) and (4.15b) below.

To cast the exact hot-tube dispersion relation into a Pierce-like form analytically, we decompose this plasma frequency reduction factor into a singular part (singular at the now modified cold-tube circuit frequencies that satisfy Eq. (4.13)) R_S and a remainder part R_N [36]:

$$F^2(\omega, \beta_0) = \frac{R_S}{(\omega - \omega_1) - v_g(\beta_0 - \beta_{01}) + R_{N,beam}} + R_{N,circuit}, \tag{4.14}$$

where $\omega_1 = 2\pi f_1$ and β_{01} are given in Table 4.2, v_g is the group velocity ($v_g \equiv \frac{\partial \omega}{\partial \beta_0} = -\frac{\partial G(\omega,\beta_0)/\partial \beta_0}{\partial G(\omega,\beta_0)/\partial \omega}\Big|_{\omega_1,\beta_{01}}$) and $\frac{\partial G(\omega,\beta_0)}{\partial \omega}\Big|_{\omega_1,\beta_{01}}[(\omega - \omega_1) - v_g(\beta_0 - \beta_{01})]$ is the first-order Taylor expansion of the cold-tube dispersion relation $G(\omega,\beta_0)$ about the operating point (ω_1,β_{01}) (Note: $\partial G(\omega, \beta_0)/\partial \omega$ has been absorbed into R_S. See Eqs. (4.15a,b) and (4.16) below.). We emphasize that Eqs. (4.12) and (4.14) are equivalent. Substituting Eq. (4.14) into Eq. (4.11) and rearranging, we arrive at a form of the Pierce dispersion relation, which is exact,

$$[(\omega - \beta_0 v_0)^2 - \omega_p^2 R_{N,circuit}][(\omega - \omega_1) - v_g(\beta_0 - \beta_{01}) + R_{N,beam}] = \omega_p^2 R_S, \tag{4.15a}$$

which may be written as,

$$[(\omega-\beta_0 v_0)^2-4\omega^2 QC^3]\left[(\omega-\omega_1)-v_g(\beta_0-\beta_{01})+4\omega qC^3\right]=\frac{v_{ph}}{v_0}\omega^3C^3. \quad (4.15b)$$

Comparing Eq. (4.15a) with Eq. (4.15b), we see that in Eq. (4.14), $R_{N,circuit}$ gives rise to Q and $R_{N,beam}$ gives rise to q. Furthermore, $\omega_p^2 R_S=\frac{v_{ph}}{v_0}\omega^3C^3$, relating R_S to C^3. We stress that Eqs. (4.11), (4.15a), and (4.15b) are all exact, equivalent, hot-tube dispersion relations. They yield the same three roots of β_0 that were numerically obtained. Comparing Eqs. (4.15a) with (4.15b), and using Eq. (4.14), we may determine C, Q, and q as follows, for the exact dispersion relation Eqs. (4.11) and (4.15a),

$$C^3=\frac{v_0}{v_{ph}}\frac{\omega_p^2}{\omega^3}\frac{(sin\,\theta_0)^2}{\theta_0'\theta_0}\frac{R}{a}\left(\frac{V(p_0R)}{V(p_0a)}\right)^2\frac{(\frac{\tau}{a})}{\partial G/\partial\omega\big|_{\omega_1,\beta_{01}}} \quad (4.16)$$

$$4QC^3=\frac{\omega_p^2}{\omega^2}\left[F^2-\frac{R_S}{(\omega-\omega_1)-v_g(\beta_0-\beta_{01})-R_{N,beam}}\right] \quad (4.17)$$

$$4qC^3=\left(\omega\frac{\partial G}{\partial\omega}\Big|_{\omega_1,\beta_{01}}\right)^{-1}\sum_{n\neq0}\frac{(sin\,\theta_n)^2}{\theta_n'\theta_n}\frac{\omega_p^2(\frac{\tau}{a})}{(\omega-\beta_n v_0)^2-p_n^2\omega_p^2\tau R\frac{V(p_nR)}{V(p_na)}W_n}\cdot\frac{R}{a}\cdot\left(\frac{V(p_nR)}{V(p_na)}\right)^2 \quad (4.18)$$

Once more, it is clear from Eq. (4.18) that the new parameter q is due to the higher-order beam modes that are represented by the non-zero n's in the infinite sum. The complexity in the tape helix TWT treated in Chapter 3 prevents an explicit derivation of C, Q, and q, so the physical origin of q could not be identified for the tape helix TWT.

We may now compute each of the Pierce parameters C (or C^3 as is sometimes used in the literature) and Q (or QC). Note first that the Pierce parameters C, Q, and q as analytically expressed in Eqs. (4.16)-(4.18) are functions of ω and β. The next question of where to evaluate the functions (so that β_0 remains a cubic polynomial in Eq. (4.15b)) was studied

extensively for a TWT with a smooth dielectric waveguide and a sheet electron beam [35]. It was found that evaluating the Pierce parameters at the beam line $\beta_e = \frac{\omega}{v_0}$ gave the most accurate solutions when compared to the exact solution, and we shall use this approximation in the analytic theory for the DoR TWA. Note that for that "toy problem" of a dielectric TWT with smooth walls, the new space-charge parameter q was not present. This is because the smooth-walled dielectric TWT yields no spatial harmonics, hence there are no higher-order beam modes, i.e. $q = 0$.

From Eqs. (4.17) and (4.18), we note that both Q and q depend on the beam current, as in the tape helix TWT. Below, we further examine C, Q, and q for the DoR TWA, and present their numerical values.

4.3.1.1 The Pierce Coupling Constant, *C*

C (or C^3) is a parameter that measures the coupling between the electron beam and the waveguide circuit. Before the discovery of q, this parameter was calculated in two very different ways. In the first method, the coupling constant was extracted from an exact formulation of the space-charge wave on the SWS (see above). We shall denote this by C, which is Eq. (4.16). In the second method, which will be described in the next paragraph, the coupling constant was extracted from a consideration of the action of the beam on just the operating circuit mode. We shall denote this by C'. As seemingly different as these two methods (and hence values of the coupling constant) appear to be, the author has mathematically proven that both of these methods yield identical results. That is, $C = C'$. This proof will not be presented here, as the technique is similar to that given in Eqs. (D15) and (D16) in Appendix D of [36].

We now look at method 2 in more detail, for completeness, as it explicitly describes the physics of the action of the beam on just the operating circuit mode. We again begin with the exact inhomogeneous wave equation for the magnetic field obtained from Maxwell's Equations

$$\left[\vec{\nabla}^2 - \frac{1}{c^2}\frac{\partial^2}{\partial t^2}\right]\vec{H} = -\vec{\nabla}\times\vec{J}. \tag{4.19}$$

Taking the inner product of this equation with $\vec{H}^*$(the complex conjugate of the magnetic field $\vec{H}$), approximating the field with the vacuum field: $\vec{H} \approx \vec{H}_v$, and using the corresponding equation for the vacuum mode: $\vec{\nabla}^2\overrightarrow{H_v} = -\frac{\omega_c^2}{c^2}\overrightarrow{H_v}$ (Helmholtz equation), we may derive an approximate equation of the form from Eq. (4.19) [5,13,36]:

$$\omega^2 - \omega_c^2 = \iiint \overrightarrow{J_1}\left(\overrightarrow{E_1}\right)\cdot\overrightarrow{E_1^*}dV/\mathrm{U} \tag{4.20}$$

where $\overrightarrow{E_1}$ is the cold-circuit RF electric field, $\overrightarrow{J_1}$ is the AC beam current induced by the vacuum mode electric field $\overrightarrow{E_1}$, *U* is the normalized energy content in the vacuum mode, and the volume integral is taken over a period of the structure.

Note that setting the right-hand side of Eq. (4.20) equal to zero gives the cold-tube dispersion relation, which is Eq. (4.1), whose numerical solution is shown in Figure 4.2.

For the integral in Eq. (4.20), since $\overrightarrow{J_1}$ is assumed to be the linearized AC current response to the cold-tube RF $\overrightarrow{E_1}$ field, we take only the fundamental component of the space harmonics. After some mathematical rearrangement, we may derive from Eq. (4.20)

$$(\omega - \beta_0 v_0)^2 \cdot (\omega - \omega_c) = \omega^3 C'^3, \tag{4.21}$$

which is the Pierce dispersion relation to the lowest order. We have proven that: $C^3 = C'^3$. The actual proof, which involves showing that $R_S = R_S'$, has been rigorously performed by the author, where R_S and R_S' are the singular parts of the two approaches; see Eq. (4.14).

This derivation not only shows the nature of C as a coupling constant between the beam mode and the circuit mode but also illustrates that C measures the interaction at the fundamental of all space harmonics. Plots of the Pierce parameter C (or C^3) as a function of frequency (Figure 4.4) and as a function of DC beam current (Figure 4.5) are given below. The range of C (C^3), as can be seen in Figures 4.4 and 4.5, is within the range of typical values for this parameter. Furthermore, $C^3 \propto I_0$ in Figure 4.5, as expected (c.f. Eq. (1.21c) from Chapter 1). This gives confidence that we have correctly identified the parameter from our full hot-tube dispersion relation.

In any waveguide circuit, there are infinite passbands, and the presence of the beam excites all modes in these bands, to various degrees [36,89]. Although this type of interaction is much weaker, they may still play a significant role in determining the overall gain of a device. This residual interaction is characterized by QC, presented next.

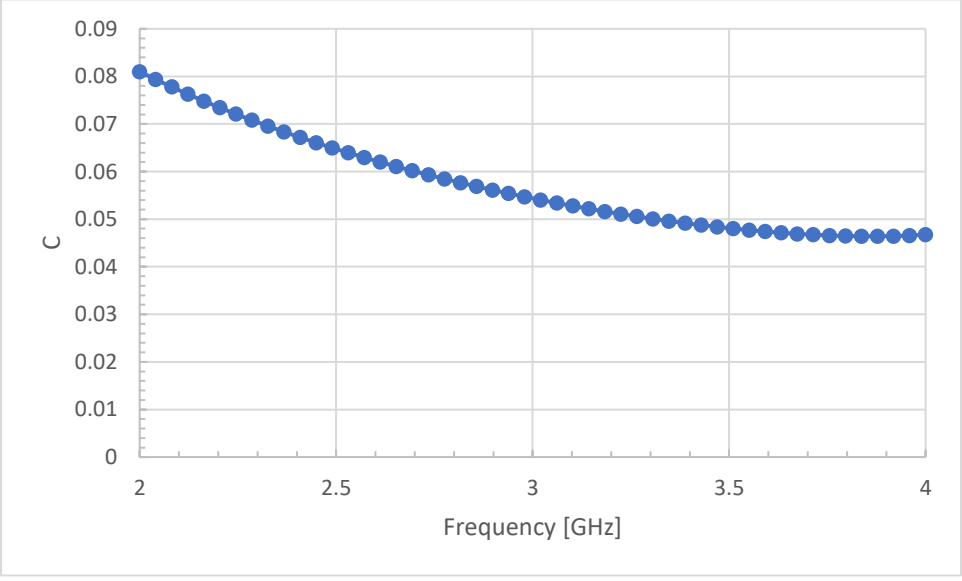

Figure 4.4. Plot of the Pierce Coupling Parameter as a function of frequency for the case study; I_0 = 50 A.

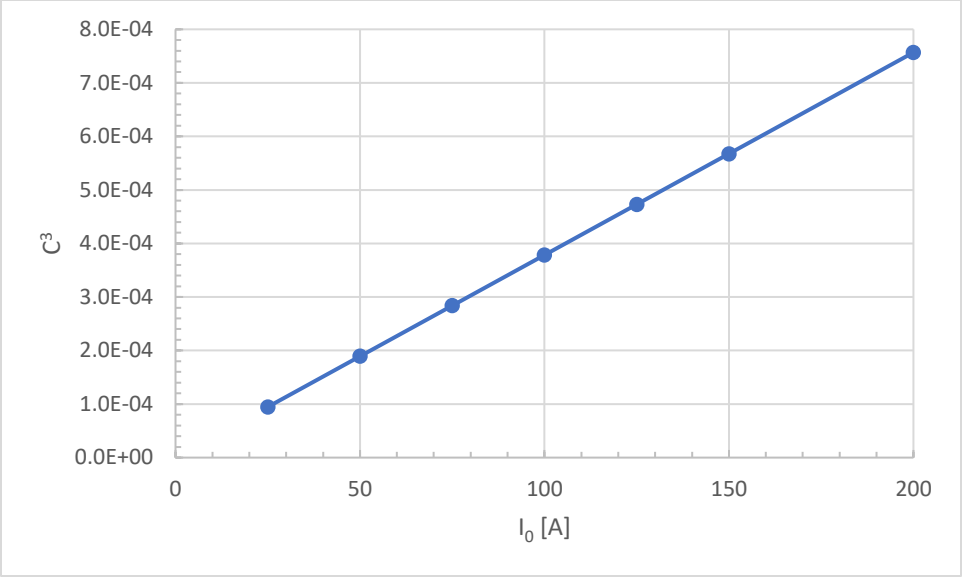

Figure 4.5. Plot of the Pierce Coupling Parameter as a function of DC beam current for the case study at 2.832 GHz.

4.3.1.2 Pierce's AC Space Charge Parameter, *QC*

We next investigate the so-called AC Space-Charge Parameter, usually denoted by *Q* or *QC*. This term has been the subject of much debate and has been calculated in several different ways [36,48-51]. Most of these traditional approaches employ some sort of approximation (e.g. using a simplified geometry: a perfectly conducting metallic cylinder or sheath helix instead of a full helix) or numerical backtracking technique from simulation data [90]. That is, the values of *QC* used are virtually all approximations. We look at one such approximation for *QC* for the Disk-on-Rod geometry and compare this to our exact analytical theory.

Consider first the limit $h \to 0$ in Figure 4.1. That is, the vane height vanishes and the disk-on-rod structure becomes a smooth coax. This is equivalent to the approximation used by Branch and Mihran [49], where the boundary of the periodic structure is replaced by a

smooth wall in the evaluation of *QC*. Equations (4.11) and (4.12) becomes, by taking only the $n = 0$ term and setting $\beta_0 = k_z$,

$$(\omega - k_z v_0)^2 = -\omega_p^2 \frac{\tau}{R} \frac{\pi (pR)^2}{2} Y_0^2(pR) \left[\frac{\left(\frac{J_0(pR)}{Y_0(pR)} - \frac{J_0(pb)}{Y_0(pb)} \right) \left(\frac{J_0(pR)}{Y_0(pR)} - \frac{J_0(pa)}{Y_0(pa)} \right)}{\frac{J_0(pb)}{Y_0(pb)} - \frac{J_0(pa)}{Y_0(pa)}} \right], \tag{4.22}$$

which is the dispersion relation for space-charge waves on an annular beam in a coaxial waveguide with inner wall radius *a* and outer wall radius *b* [49,74].

For the smooth coax case, Eq. (4.22) may be cast into the form:

$$[(\omega - k_z v_0)^2 - 4\omega^2 Q C^3] = 0, \tag{4.23}$$

where *QC* may then be readily extracted using Eq. (4.22), and this is basically the approach by Branch and Mihran in their formulation of *QC*. Because of the nature of the smooth coax, there can be no synchronous interaction between the circuit wave and the electron beam (analogous to the Branch & Mihran approximation for a helix TWT); there is no slow-wave structure. It is interesting to note that this *QC* term obtained for the smooth coax case was already built in to the hot-tube dispersion relation, Eq. (4.11). It is given by the last term, $(p_0 R)(p_0 a) \frac{V(p_0 R)}{V(p_0 a)} W_0$, in Eq. (4.12) (The first term in Eq. (4.12) tends to zero as $h \to 0$, in which case $G \to \infty$, as $U\left(\frac{\omega a}{c}\right) \to 0$).

To investigate the validity of this approximation, we plotted *QC* as a function of frequency for the disk-on-rod structure and for a smooth coax with inner radius equal to: (1) the rod radius *(a – h)* in Figure 4.1 and (2) the vane-tip radius *a*. The operating parameters are the same as above and the input DC beam current is 50 A. The results are shown below (Figure 4.6).

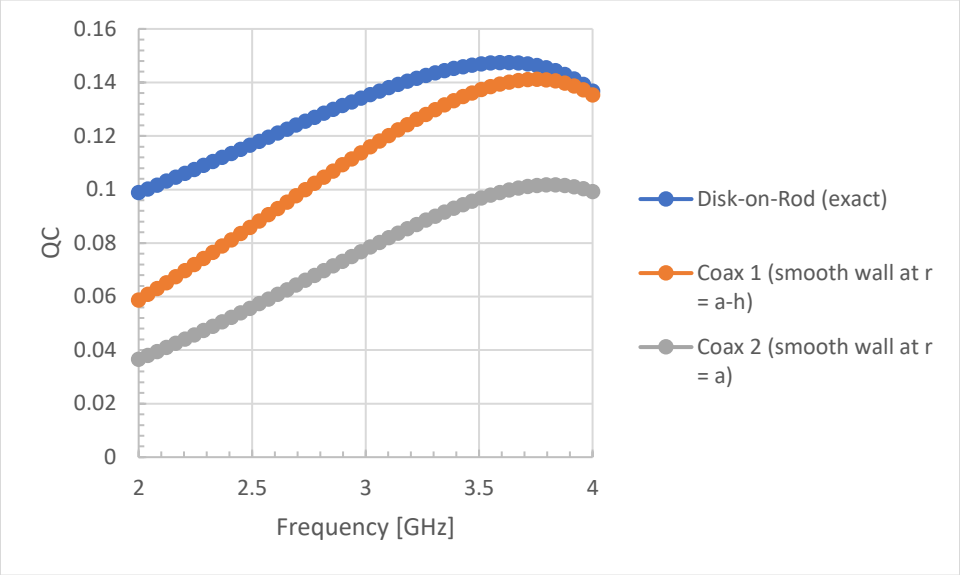

Figure 4.6. Plot of the AC Space-Charge Parameter *QC* as a function of frequency for the full Disk-on-Rod structure and for coax 1 (which has inner radius equal to the rod radius, $r = a\text{-}h$) and coax 2 (which has inner radius equal to the vane-tip radius, $r = a$); $I_0 = 50$ A.

This numerical test did not yield the expected results. Namely, it was expected that *QC* for the disk-on-rod geometry would lie between the *QC* curves of the two smooth coaxes, but as can be seen, the exact values of *QC* exceed the approximations except near the higher frequencies of the operating band, where the exact *QC* values happen to coincide with the coax 1 approximation. This shows that a simplified coax geometry for which *QC* may be easily calculated, as in Branch and Mihran, cannot fully capture the effects of the more complex geometry of the DoR TWA. We conclude that the resonance between beam and circuit wave at higher spatial harmonics and the extra fields introduced in the cavities must be accounted for in order to obtain an accurate value of the space-charge parameter *QC*.

4.3.1.3 The New Space-Charge Parameter, *q*

Lastly, we consider our newly discovered space-charge parameter *q*, which is the symmetric complement to Pierce's AC space-charge parameter *Q* and accounts for the effects

of higher-order beam modes on the circuit mode. See Eqs. (4.15b) and (4.18). This term, as mentioned for the tape helix TWT, becomes more prominent in the high current regime. Here, for the first time, we give a closed analytic form of this parameter (c.f. Eq. (4.18)). A plot of this parameter as a function of frequency is presented in Figure 4.7. At 2.832 GHz, q as a function of DC beam current is shown in Figure 4.8.

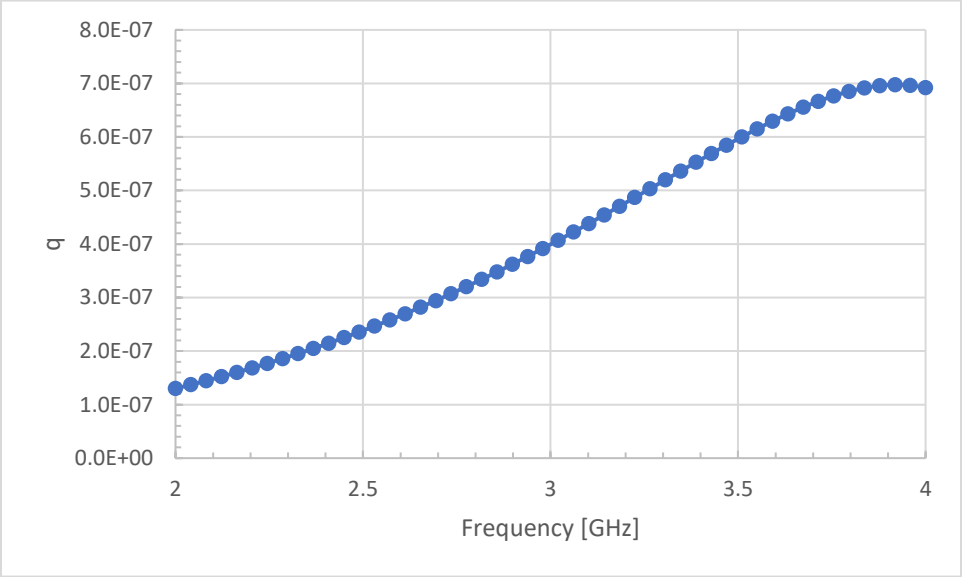

Figure 4.7. Plot of the new space-charge parameter q as a function of frequency for the case study; I_0 = 50 A.

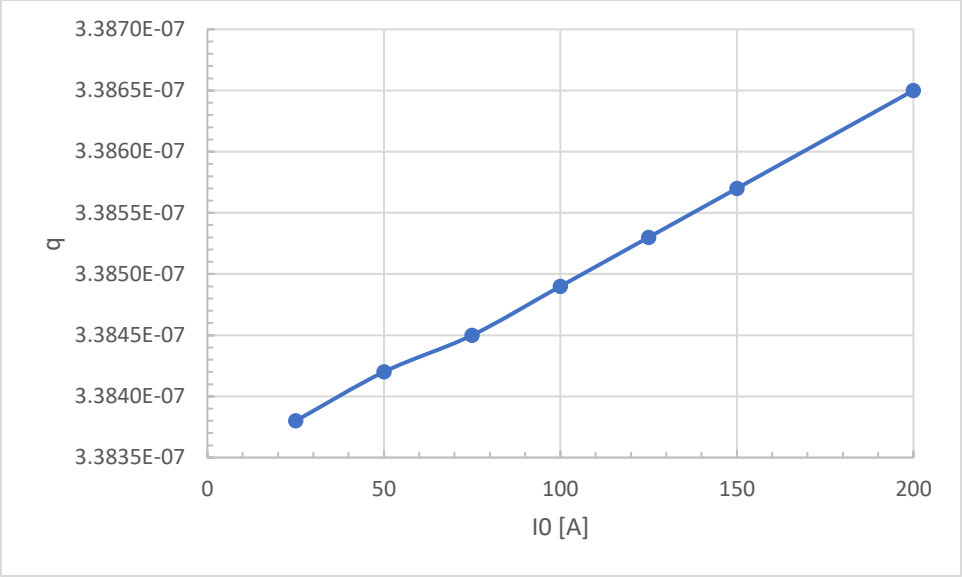

Figure 4.8. Plot of the new space-charge parameter *q* as a function of DC beam current for the case study at 2.832 GHz.

The values of *q* for this particular DoR TWA geometry are much smaller than expected. The underlying reason is unclear. One conjecture may be that the dispersion curves for this structure (c.f. Figure 4.1 and 4.2) are a lot more dispersive than those for a tape helix. Because of this, there is more of a detune between the beam modes from the other circuit modes, and the effect of the higher-order beam modes on the circuit modes are not as important in the DoR TWA. This issue remains to be examined.

4.3.2 Comparison with MAGIC and ICEPIC

Because there is no (immediate) way to identify the Pierce parameters in a simulation code, we compare the exponentiation rate obtained from the full hot-tube dispersion relation with the results of the simulation codes. Since this analytic theory only uses the spatial amplification rate of the unstable mode from the exact dispersion relation, *only one mode is considered*.

The (small-signal) spatial amplification rate $Im(\beta)$ as a function of DC beam current I_0 is plotted in Figure 4.9, which includes simulation results obtained by Dr. Brad Hoff and Dr. David Simon using two (2) different codes: ICEPIC [77] and MAGIC [78].

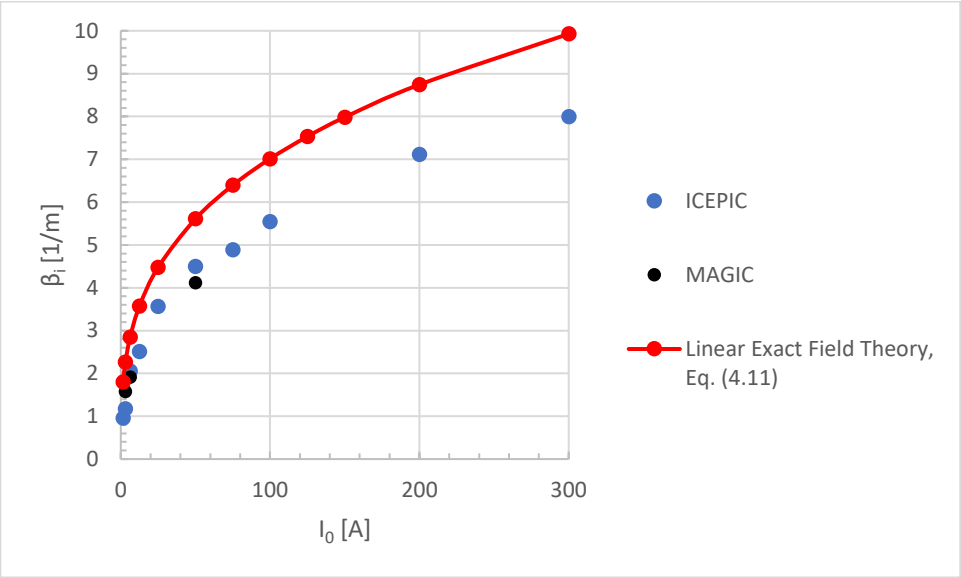

Figure 4.9. Plot of the small-signal spatial amplification rate as a function of DC beam current for the operating parameters in Tables 4.1 and 4.2.

Figure 4.9 shows that there is agreement in the general trend between theory, ICEPIC, and MAGIC. The discrepancy between simulation and field theory may lie in the approximations used to formulate the theory. Perhaps more importantly, the field theory shown in Figure 4.9 is a linear theory using only the most unstable mode in the equivalent Pierce three-wave theory, while simulation codes are fully non-linear and include launching loss [4] which involves all three waves in Pierce's three-wave theory. It is therefore difficult to extract the small-signal gain from simulation codes.

The frequency response of the spatial gain is shown in Figure 4.10, where the analytic theory is compared to ICEPIC.

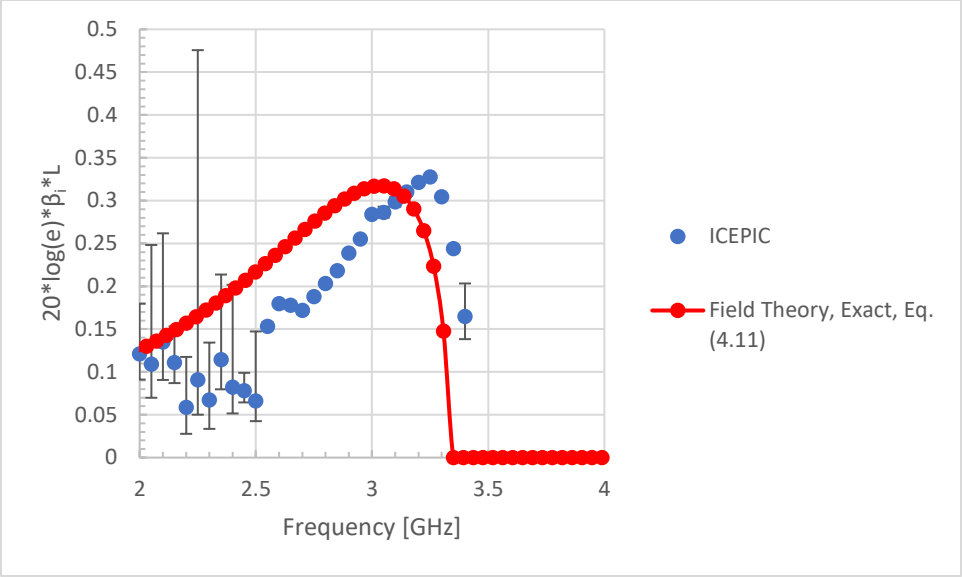

Figure 4.10. Frequency response of the Disk-on-Rod TWA for the operating parameters in Tables 4.1 and 4.2; $I_0 = 50$ A.

Again, there is agreement only in the trend between ICEPIC and the field theory. The ICEPIC results seem to be slightly shifted to higher frequencies when compared to theory. Nonlinearity and launching loss in the system may be the main reasons for the discrepancies.

4.4 Conclusions

In this chapter, we present an analysis of a Disk-on-Rod Traveling-Wave Amplifier. Both the cold-tube dispersion relation and the small-signal hot-tube dispersion relation for the problem were derived. For the case study, the numerical solution to the analytic cold-tube dispersion relation for both the fundamental and second passbands agreed well with simulations ran in both HFSS and ICEPIC, validating the analytic theory and the simulation codes. The small-signal hot-tube dispersion relation was formulated exactly and was cast into a Pierce-like three-wave dispersion relation, also exactly, from which analytical forms of the Pierce parameters C, Q, and q were extracted, all given analytically. For the DoR TWA, we

conclude that Q is due to higher-order circuit modes, whereas q is due to the higher-order beam modes.

A numerical analysis of each of these Pierce parameters was done. It was found that C (or C^3) behaved as expected as a function of input signal frequency and DC beam current. Comparisons of Q (or QC) with a standard Branch and Mihran approximation were also made, highlighting how such an approximation fails to capture the beam-circuit interaction in this complex geometry. The newly introduced space-charge parameter q was evaluated also for the first time. It was found that q was extremely small for this set-up, compared to those of the tape helix studied in the previous chapter. This result is unexpected, and the underlying reason is unknown.

Lastly, the numerical solution to the analytic hot-tube dispersion relation was computed and compared to simulation runs using MAGIC and ICEPIC, two PIC codes. The match between simulation and theory was only fair, but both exhibited the same trends. Disagreement may be due to the fact that the simulation codes are fully non-linear and contain all three modes of Pierce, whereas our theory is completely in the small-signal regime, using only the most unstable mode for spatial amplification among the three modes in Pierce theory.

Chapter 5 :
Summary and Future Work

5.1 Summary

In this thesis, the classical Pierce theory of traveling-wave tubes was critically re-examined. In particular, we focused on the interaction and coupling of the beam mode and the circuit mode. In doing so, we have provided several extensions to the basic theory much beyond the well-established small-signal theory of TWTs by Pierce.

In Chapter 2, we extended the classical Pierce theory to include second harmonic generation. This second harmonic of the input signal is generated dynamically with input only at the fundamental frequency. There are two possible sources for this harmonic generation: (1) from current crowding (including charge overtaking), a kinematic process similar to that found in klystron theory, and (2) from non-linear perturbations to the electron beam from the circuit wave. It turns out that the dynamical process (2) is much more important for a wideband TWT with regards to second harmonic RF power generation, and the governing equations modeling this have been derived. We discovered the important mechanism of synchronous excitation in both time and space of the second harmonic. For several test cases with an octave bandwidth tape helix TWT, including a realistic one with a spatial taper, the developed analytic theory was applied and excellent agreement was found with simulations using the non-linear CHRISTINE code.

In Chapter 3, an in-depth investigation into the most elusive Pierce parameter was performed. The so-called Pierce “AC space-charge” parameter Q has never been reliably

calculated for a realistic TWT. Here, we solved this problem exactly for a thin tape helix radially stratified by a dielectric layer(s); the stratified dielectric(s) approximately represents the support rods of the helix TWT. The exact analysis of this cold-tube circuit by Chernin et al. [34] is extended to include a centered, monoenergetic electron beam guided by an infinite axial magnetic field. The exact hot-tube dispersion relation is derived for the first time. From the numerical solution to this hot-tube dispersion relation (at a given input frequency), we always find three roots of the propagation constant which may then be cast in the form of Pierce's three-wave theory. From this, the Pierce parameters are unambiguously determined. It turns out that a new parameter that we call q has to be introduced to the traditional Pierce formulation to conform with the numerical results obtained from the exact theory. This new parameter appears as a modification to the circuit mode and acts as a detune to the circuit phase velocity (as much as 2% for the tape helix TWT, which is very significant) due to space-charge effects. Physically, this q modifies the cold circuit mode in the dispersion relation and serves as a symmetric complement to Pierce's Q, which modifies the beam mode.

In Chapter 4, we turned our attention to a problem of current interest to the Air Force Research Laboratory: a disk-loaded or Disk-on-Rod coaxial Traveling-Wave Amplifier driven by an annular electron beam. This set-up promises high power (due to the higher current of the annular electron beam) and moderately large bandwidth (by virtue of its slow-wave structure). To test the viability of such a device, we began a small-signal Pierce-like analysis. The cold-tube and the exact hot-tube dispersion relations have been derived, with the cold-tube results agreeing well with simulations ran in HFSS and ICEPIC. The analytical forms of the Pierce parameters: C, Q, and q have been extracted from the hot-tube dispersion

relation and are analytically given. This allows us to infer that Q is the modification of the beam mode due to the presence of higher-order circuit modes, whereas q is the modification of the circuit mode by the higher-order beam modes, both due to space-charge effects. Such a physical interpretation of Q and q is lacking for the thin tape helix TWT. The properties of these parameters were extensively studied. We found that q is surprisingly small numerically for the DoR TWA. The predicted gain from the analytic theory was also compared against the PIC simulation codes MAGIC and ICEPIC. There is only fair agreement, possibly due to the non-linear effects and launching loss (energy sharing between all of the three waves in the Pierce dispersion relation) that are in the code but are absent in the present analytic theory. Both theory and simulation predict the same trends, however.

5.2 Future Work

As stated in Chapter 2, the work on harmonic generation in a TWT was motivated in part by experiments at the University of Michigan Plasma, Pulsed Power, and Microwave Laboratory on a bi-frequency Recirculating Planar Magnetron (RPM) [53-54,59]. We started with a linear beam device like a TWT because it had a much better characterized beam than a magnetron. The method that was presented may be extended to other HPM devices. Thus, for future work, it will be interesting and challenging to apply the harmonic generation theory developed here to the bi-frequency RPM, or other HPM devices that employ an electron beam. Furthermore, it will also be interesting to consider what would happen if there was a non-zero input signal at the second harmonic frequency (in addition to the input signal at the fundamental frequency). This may be important because there are instances where the second or higher harmonics of the input signal are unwanted. To suppress these harmonics, one can

operate the device (a TWT, say) below saturation so as to not induce harmonic generation [5]. As shown here, harmonics may still arise even in the small-signal regime. Another method, by Wirth et al. [91], makes use of injecting a phase-appropriate signal at the harmonic frequency to cancel the undesired wave. Future work may follow this line of thought. Higher harmonic generation (i.e. keeping more terms in the expansion technique in Chapter 2) may also be investigated, as high harmonic generation may be desired in certain applications.

The discovery of the new space-charge parameter q that accounts for beam-loading on the circuit by taking into account the higher-order beam modes is expected to open a plethora of other questions. For example, what is the phenomenological origin of this parameter in general (recall: this q was discovered through numerical means)? In particular, why is the effect of q large for the tape helix TWT but small in the Disk-on-Rod TWT? How does this new parameter affect non-linear, large-signal theory? What are the values of Q and q for the backward wave mode in a tape helix TWT, and how do they affect the threshold condition in backward wave oscillations (BWO) as classically formulated by Johnson [57]?

The list of potential future work for the above two topics can go on. Common questions to both include: (1) how may the three-wave theories be modified to include the neglected backward wave? That is, what is the Pierce four-wave theory equivalent to the above? This issue is important to analyze the stability of TWT, especially near the band edges. (2) What will be the effects on q if there is cold-tube loss (non-zero Pierce loss parameter, d)? (3) How is q formulated for a beam with Brillouin flow instead of an immersed flow (with an infinite axial magnetic field as in this thesis)?

Each of Chapters 2, 3, and 4 contain novel, unexpected results. Much remains to be done.

Appendices

Appendix A

Modeling of a Mid-Stream Sever in a Traveling-Wave Tube

We model the mid-stream sever ($z_- < z < z_+$, $z_- = 2.667$ cm, $z_+ = 2.921$ cm, see Figure 2.2 of Chapter 2) in the test cases as a cylindrical drift tube that is perfectly conducting. We assume that the circuit electric field is completely cut off in the sever region (i.e., $E_C = 0$). Information from the pre-sever region to the post-sever region is transmitted only through the beam. The governing equation for the evolution of the beam within the sever region is:

$$\left(\frac{\partial}{\partial t} + v_0 \frac{\partial}{\partial z}\right) v(z,t) + \omega_q^2 s(z,t) = 0, \qquad z_- < z < z_+ \tag{A1}$$

Assuming $e^{j(n\omega_0)t}$ dependence for a signal of frequency $\omega = n\omega_0$, Eq. (A1) becomes

$$\left(jn\omega_0 + v_0 \frac{d}{dz}\right) v_n(z) + \omega_{qn}^2 s_n(z) = 0. \tag{A2}$$

Equation (A1) is just a statement of the (linearized) force law with space-charge effects and no circuit fields, as in the drift tube of a klystron [62]. Here, $\omega_q = \omega_p F$ is the reduced plasma frequency, where the plasma frequency reduction factor F was calculated using the method prescribed in Branch and Mihran [49] (in particular, the case where the pencil electron beam is concentric with a metallic cylinder). The initial conditions for Eq. (A2) are that $s_n(z)$ and $v_n(z)$ are continuous at $z = z_-$.

At the exit of the sever region ($z = z_+$), $s_n(z)$ and $v_n(z)$ are continuous. In addition, $E_C(z_+) = 0$, meaning that the circuit field is zero at $z = z_+$. These are the boundary conditions

for the post-sever region ($z > z_+$) for Eqs. (2.11) and (2.13) for n = 1, and for Eqs. (2.12) and (2.14) for n = 2 of Chapter 2.

Appendix B

Derivation of the Exact Dispersion Relation for an Electron Beam Interacting with the Electromagnetic Fields of a Thin Cylindrical Tape Helix

We consider an electron beam interacting with electromagnetic fields propagating on a thin tape helix that is supported by a stratified dielectric layer and enclosed by a perfectly conducting cylindrical shell, as shown in Figure 3.1 of Chapter 3. The exact ("cold-tube") dispersion relation governing waves propagating on such a helix in the absence of a beam was obtained by Chernin et al. [34]. In this Appendix, we show how to include self-consistent interactions of these waves with a mono-energetic electron beam centered on the axis of the helix. We will refer to the resulting dispersion relation as the "hot-tube" dispersion relation.

We assume that the beam is nonrelativistic with velocity $v_0 \ll c$, and has uniform density n_0 within radius R_b. We assume that the beam is confined by an infinite axial magnetic field so that the electron motion is limited to the axial ($\hat{z}$) direction.

We define the region occupied by the beam as "Region 0",

$$0 < r < R_b, \qquad Region\ 0 \tag{B1}$$

and the vacuum region between the beam and the helix as "Region 1",

$$R_b < r < a, \qquad Region\ 1 \tag{B2}$$

where a is the radius of the infinitesimally thin helix (see Figure 3.1 of Chapter 3). Beyond Region 1 ($r > a$), including the boundary conditions at the helix, the cold-tube analysis of Chernin et al. [34] carries over. Thus we focus here mainly on Regions 0 and 1.

In Region 0, Maxwell's equations may be combined to read,

$$\nabla^2 \overrightarrow{E_1} - \frac{1}{c^2}\frac{\partial^2 \overrightarrow{E_1}}{\partial t^2} = -\frac{e}{\epsilon_0}\vec{\nabla} n_1 + \mu_0 \frac{\partial \overrightarrow{J_1}}{\partial t} \tag{B3}$$

and

$$\nabla^2 \overrightarrow{H_1} - \epsilon_0 \mu_0 \frac{\partial^2 \overrightarrow{H_1}}{\partial t^2} = -\vec{\nabla} \times \overrightarrow{J_1} \tag{B4}$$

In Eqs. (B3) and (B4), $\overrightarrow{J_1} = -e(n_0 v_1 + n_1 v_0)\hat{z} \equiv J_1 \hat{z}$ is the AC electron current density, expressed in terms of the density perturbation n_1, and the (axial) velocity perturbation v_1.

Following reference [34], we write all quantities in the 'Floquet' form,

$$F^{(i)}(r, \theta, z, t) = \sum_{n=-\infty}^{\infty} F_n^{(i)}(r) e^{j\omega t + jn\theta - j\beta_n z} \tag{B5}$$

in the ith ($i = 0,1$) region. The nth term in the sum in Eq. (B5) is the nth space harmonic, the propagation constant of which is

$$\beta_n \equiv \beta + nk_H, \qquad n = 0, \pm 1, \pm 2, \ldots \tag{B6}$$

where $k_H = \frac{2\pi}{p}$ (p is the helix pitch; see Figure 3.1). β itself is unknown. Its value must be determined from the solution of the full dispersion relation (Eq. (B34), below), for a specified real value of frequency ω.

The perturbation quantities, n_1, v_1, and J_1, may be obtained from the linearized force law and the linearized continuity equation:

$$\left(\frac{\partial}{\partial t} + v_0 \frac{\partial}{\partial z}\right) v_1 = -\frac{e}{m_e} E_{1z} \tag{B7a}$$

$$\frac{\partial n_1}{\partial t} + \frac{\partial}{\partial z}(n_0 v_1 + n_1 v_0) = 0, \tag{B7b}$$

which yield, for the n[th] space harmonic,

$$v_{1n} = \frac{-\frac{e}{m_e} E_{1zn}}{j(\omega - \beta_n v_0)} \tag{B8a}$$

$$n_{1n} = \frac{\beta_n n_0}{\omega - \beta_n v_0} v_{1n} = \frac{-\frac{e}{m_e} \beta_n n_0}{j(\omega - \beta_n v_0)^2} E_{1zn} \tag{B8b}$$

$$J_{1n} = \frac{\frac{e^2}{m_e} \omega n_0}{j(\omega - \beta_n v_0)^2} E_{1zn} \tag{B8c}$$

The z-component of Eqs. (B3) and (B4) yields, upon using Eqs. (B8b) and (B8c),

$$r^2 \frac{d^2 E_{1zn}}{dr^2} + r \frac{dE_{1zn}}{dr} - (p_n^2 r^2 + n^2) E_{1zn} = 0 \tag{B9}$$

and

$$r^2 \frac{d^2 H_{1zn}}{dr^2} + r \frac{dH_{1zn}}{dr} - \left(\gamma_n^{(1)2} r^2 + n^2\right) H_{1zn} = 0, \tag{B10}$$

where

$$\gamma_n^{(1)2} \equiv \beta_n^2 - \frac{\omega^2}{c^2} \tag{B11}$$

$$p_n^2 \equiv \epsilon_{rn}^{(0)} \gamma_n^{(1)2}, \tag{B12}$$

$$\epsilon_{rn}^{(0)} \equiv 1 - \frac{\omega_p^2}{(\omega - \beta_n v_0)^2} \tag{B13}$$

and $\omega_p = \sqrt{\frac{e^2 n_0}{m_e \epsilon_0}}$ is the electron plasma frequency.

From Eqs. (B9) and (B10), we obtain the axial fields in Region 0,

$$E_{1z}^{(0)}(r,\theta,z,t) = \sum_{n=-\infty}^{\infty} E_{1zn}^{(0)}(r) e^{j\omega t + jn\theta - j\beta_n z} = \sum_{n=-\infty}^{\infty} A_n^{(0)} I_n(p_n r) e^{j\omega t + jn\theta - j\beta_n z} \quad \text{(B14)}$$

$$H_{1z}^{(0)}(r,\theta,z,t) = \sum_{n=-\infty}^{\infty} H_{1zn}^{(0)}(r) e^{j\omega t + jn\theta - j\beta_n z} = \sum_{n=-\infty}^{\infty} C_n^{(0)} I_n\left(\gamma_n^{(1)} r\right) e^{j\omega t + jn\theta - j\beta_n z} \quad \text{(B15)}$$

where $\left\{A_n^{(0)}, C_n^{(0)}\right\}$ are arbitrary constants and I_n is the n[th] order modified Bessel function of the first kind.

The other components of the hot-tube RF electric and magnetic fields may be obtained in terms of E_{1z} and H_{1z} using Maxwell's equations, $\vec{\nabla} \times \overrightarrow{E_1} = -j\omega \overrightarrow{B_1}$ and $\vec{\nabla} \times \overrightarrow{H_1} = \overrightarrow{J_1} + j\omega\epsilon_0 \overrightarrow{E_1}$:

$$E_{1rn}^{(0)} = \frac{j\beta_n}{\gamma_n^{(1)2}} A_n^{(0)} p_n I_n'(p_n r) - \frac{n\omega\mu_0}{\gamma_n^{(1)2} r} C_n^{(0)} I_n(\gamma_n^{(1)} r) \quad \text{(B16)}$$

$$E_{1\theta n}^{(0)} = -\frac{n\beta_n}{\gamma_n^{(1)2} r} A_n^{(0)} I_n(p_n r) - \frac{j\omega\mu_0}{\gamma_n^{(1)2}} C_n^{(0)} \gamma_n^{(1)} I_n'(\gamma_n^{(1)} r) \quad \text{(B17)}$$

$$H_{1rn}^{(0)} = \frac{n\omega\epsilon_0}{\gamma_n^{(1)2} r} A_n^{(0)} I_n(p_n r) + \frac{j\beta_n}{\gamma_n^{(1)2}} C_n^{(0)} \gamma_n^{(1)} I_n'(\gamma_n^{(1)} r) \quad \text{(B18)}$$

$$H_{1\theta n}^{(0)} = \frac{j\omega\epsilon_0}{\gamma_n^{(1)2}} A_n^{(0)} p_n I_n'(p_n r) - \frac{n\beta_n}{\gamma_n^{(1)2} r} C_n^{(0)} I_n(\gamma_n^{(1)} r) \quad \text{(B19)}$$

where the prime denotes differentiation of the modified Bessel function with respect to its argument. In passing we remark that the dielectric tensor for the present pencil beam model is

$$\overleftrightarrow{\epsilon} = \epsilon_0 \begin{pmatrix} 1 & 0 & 0 \\ 0 & 1 & 0 \\ 0 & 0 & \epsilon_r^{(0)} \end{pmatrix} \tag{B20}$$

where, for the nth space harmonic,

$$\epsilon_r^{(0)} = \epsilon_{rn}^{(0)}. \tag{B21}$$

For Region 1, the z-component of the RF electric and magnetic fields satisfies

$$\left[\frac{1}{r}\frac{\partial}{\partial r} r \frac{\partial}{\partial r} - \left(\gamma_n^{(i)2} + \frac{n^2}{r^2}\right)\right] F_n^{(i)}(r) = 0, \tag{B22}$$

where

$$\gamma_n^{(i)2} \equiv \beta_n^2 - \epsilon_r^{(i)} \frac{\omega^2}{c^2} \tag{B23}$$

and $\epsilon_r^{(i)} = 1$ and Eq. (B23) becomes Eq. (B11). (This notation is used to conform with that used in Ref. [34].) Thus, the solutions to Eq. (B22) may be written

$$\begin{aligned} E_{1z}^{(1)}(r,\theta,z,t) &= \sum_{n=-\infty}^{\infty} E_{1zn}^{(1)}(r) e^{j\omega t + jn\theta - j\beta_n z} \\ &= \sum_{n=-\infty}^{\infty} \left[A_n^{(1)} I_n\left(\gamma_n^{(1)} r\right) + B_n^{(1)} K_n\left(\gamma_n^{(1)} r\right)\right] e^{j\omega t + jn\theta - j\beta_n z} \end{aligned} \tag{B24}$$

$$\begin{aligned} H_{1z}^{(1)}(r,\theta,z,t) &= \sum_{n=-\infty}^{\infty} H_{1zn}^{(1)}(r) e^{j\omega t + jn\theta - j\beta_n z} \\ &= \sum_{n=-\infty}^{\infty} \left[C_n^{(1)} I_n\left(\gamma_n^{(1)} r\right) + D_n^{(1)} K_n\left(\gamma_n^{(1)} r\right)\right] e^{j\omega t + jn\theta - j\beta_n z} \end{aligned} \tag{B25}$$

where B_n and D_n, like A_n and C_n, are arbitrary constants and K_n is the n[th] order modified Bessel functions of the second kind. The other field components are found using Maxwell's equations:

$$\gamma_n^{(i)2} E_{1rn}^{(i)} = j\beta_n \frac{\partial}{\partial r} E_{1zn}^{(i)} - \frac{\omega n}{r} \mu_0 H_{1zn}^{(i)}$$

$$\rightarrow E_{1rn}^{(1)} = \frac{j\beta_n}{\gamma_n^{(1)}} \left[A_n^{(1)} I_n'\left(\gamma_n^{(1)} r\right) + B_n^{(1)} K_n'\left(\gamma_n^{(1)} r\right) \right] \tag{B26}$$

$$- \frac{\omega n}{\gamma_n^{(1)2} r} \mu_0 \left[C_n^{(1)} I_n\left(\gamma_n^{(1)} r\right) + D_n^{(1)} K_n\left(\gamma_n^{(1)} r\right) \right]$$

$$\gamma_n^{(i)2} E_{1\theta n}^{(i)} = -\frac{n\beta_n}{r} E_{1zn}^{(i)} - j\omega\mu_0 \frac{\partial}{\partial r} H_{1zn}^{(i)}$$

$$\rightarrow E_{1\theta n}^{(1)} = -\frac{n\beta_n}{\gamma_n^{(1)2} r} \left[A_n^{(1)} I_n\left(\gamma_n^{(1)} r\right) + B_n^{(1)} K_n\left(\gamma_n^{(1)} r\right) \right] \tag{B27}$$

$$- \frac{j\omega\mu_0}{\gamma_n^{(1)}} \left[C_n^{(1)} I_n'\left(\gamma_n^{(1)} r\right) + D_n^{(1)} K_n'\left(\gamma_n^{(1)} r\right) \right]$$

$$\gamma_n^{(i)2} H_{1rn}^{(i)} = \epsilon^{(i)} \omega \frac{n}{r} E_{1zn}^{(i)} + j\beta_n \frac{\partial}{\partial r} H_{1zn}^{(i)}$$

$$\rightarrow H_{1rn}^{(1)} = \frac{\epsilon_0 \omega}{\gamma_n^{(1)2}} \frac{n}{r} \left[A_n^{(1)} I_n\left(\gamma_n^{(1)} r\right) + B_n^{(1)} K_n\left(\gamma_n^{(1)} r\right) \right] \tag{B28}$$

$$+ \frac{j\beta_n}{\gamma_n^{(1)}} \left[C_n^{(1)} I_n'\left(\gamma_n^{(1)} r\right) + D_n^{(1)} K_n'\left(\gamma_n^{(1)} r\right) \right]$$

$$\gamma_n^{(i)2} H_{1\theta n}^{(i)} = j\epsilon^{(i)} \omega \frac{\partial}{\partial r} E_{1zn}^{(i)} - \frac{n\beta_n}{r} H_{1zn}^{(i)} \tag{B29}$$

$$\rightarrow H_{1\theta n}^{(1)} = \frac{j\epsilon_0\omega}{\gamma_n^{(1)}}\left[A_n^{(1)} I_n'\left(\gamma_n^{(1)} r\right) + B_n^{(1)} K_n'\left(\gamma_n^{(1)} r\right)\right]$$

$$- \frac{n\beta_n}{\gamma_n^{(1)2} r}\left[C_n^{(1)} I_n\left(\gamma_n^{(1)} r\right) + D_n^{(1)} K_n\left(\gamma_n^{(1)} r\right)\right]$$

The boundary conditions between the beam (Region 0) and vacuum (Region 1) are:

$$E_{1zn}^{(0)}(r = R_b) = E_{1zn}^{(1)}(r = R_b) \tag{Bi}$$

$$H_{1zn}^{(1)}(r = R_b) - H_{1zn}^{(0)}(r = R_b) = 0 \tag{Bii}$$

$$E_{1rn}^{(1)}(r = R_b) - E_{1rn}^{(0)}(r = R_b) = 0 \tag{Biii}$$

$$H_{1rn}^{(0)}(r = R_b) = H_{1rn}^{(1)}(r = R_b) \tag{Biv}$$

$$E_{1\theta n}^{(0)}(r = R_b) = E_{1\theta n}^{(1)}(r = R_b) \tag{Bv}$$

$$H_{1\theta n}^{(1)}(r = R_b) - H_{1\theta n}^{(0)}(r = R_b) = 0 \tag{Bvi}$$

Eqs. (Bi)-(Bvi) state that all components of the RF electric and magnetic fields are continuous; this must be so since there is no surface charge or surface current on the beam-vacuum boundary by the assumption of 1-D motion (infinite axial magnetic field) [71]. Of the six boundary conditions, only four are needed; the remaining two are redundant.

Using Eqs. (Bi)-(Bvi), we may express one undetermined constant for the electric field (e.g. $A_n^{(1)}$) and one undetermined constant for the magnetic field (e.g. $C_n^{(1)}$) in terms of the other constants, i.e. $\left\{A_n^{(1)}, C_n^{(1)}\right\} = f\left(A_n^{(0)}, C_n^{(0)}, B_n^{(1)}, D_n^{(1)}\right)$.

The dimensionless logarithmic derivatives for the electric and magnetic fields are defined to be:

$$l_{En}^{(i)} \equiv \frac{1}{\gamma_n^{(i)} E_{zn}^{(i)}} \frac{\partial E_{zn}^{(i)}}{\partial r}\Bigg]_{r\to a} \tag{B30a}$$

$$l_{Hn}^{(i)} \equiv \frac{1}{\gamma_n^{(i)} H_{zn}^{(i)}} \frac{\partial H_{zn}^{(i)}}{\partial r}\Bigg]_{r\to a}. \tag{B30b}$$

For Region 1, Eqs. (B30a) and (B30b) become

$$l_{En}^{(1)} = \frac{A_n^{(1)} I_n'\left(\gamma_n^{(1)} a\right) + B_n^{(1)} K_n'\left(\gamma_n^{(1)} a\right)}{A_n^{(1)} I_n\left(\gamma_n^{(1)} a\right) + B_n^{(1)} K_n\left(\gamma_n^{(1)} a\right)} \tag{B31a}$$

$$l_{Hn}^{(1)} = \frac{C_n^{(1)} I_n'\left(\gamma_n^{(1)} a\right) + D_n^{(1)} K_n'\left(\gamma_n^{(1)} a\right)}{C_n^{(1)} I_n\left(\gamma_n^{(1)} a\right) + D_n^{(1)} K_n\left(\gamma_n^{(1)} a\right)}. \tag{B31b}$$

Using the results from Eqs. (Bi)-(Bvi), we may write all of the undetermined variables in terms of $A_n^{(1)}$ in Eq. (B31a) and $C_n^{(1)}$ in Eq. (B31b). This gives:

$$l_{En}^{(1)} = \frac{I_n'\left(x_n^{(1)}\right) K_n\left(y_n^{(1)}\right) - I_n\left(y_n^{(1)}\right) K_n'\left(x_n^{(1)}\right) + F I_n(p_n R_b) K_n'\left(x_n^{(1)}\right)}{I_n\left(x_n^{(1)}\right) K_n\left(y_n^{(1)}\right) - I_n\left(y_n^{(1)}\right) K_n\left(x_n^{(1)}\right) + F I_n(p_n R_b) K_n\left(x_n^{(1)}\right)} \tag{B32a}$$

$$l_{Hn}^{(1)} = \frac{I_n'\left(x_n^{(1)}\right)}{I_n\left(x_n^{(1)}\right)}, \tag{B32b}$$

where $x_n^{(1)} \equiv \gamma_n^{(1)} a$ and $y_n^{(1)} \equiv \gamma_n^{(1)} R_b$, and

$$F \equiv \frac{1}{\left[(p_n R_b) I_n'(p_n R_b) K_n\left(y_n^{(1)}\right) - y_n^{(1)} I_n(p_n R_b) K_n'\left(y_n^{(1)}\right)\right]}. \tag{B32ai}$$

$l_{En}^{(1)}$ contains the information about the beam in the parameter F. If the beam is removed, then $\omega_p \to 0 \Rightarrow \epsilon_{rn}^{(0)} \to 1 \Rightarrow p_n \to \gamma_n^{(1)}$ and $F \to 1$, and the equations from [34] are recovered, namely,

$$l_{En}^{(1)} = l_{Hn}^{(1)} = \frac{I_n'\left(x_n^{(1)}\right)}{I_n\left(x_n^{(1)}\right)}. \tag{B33a,b}$$

The rest of the calculation of the fields and boundary conditions at the helix and beyond follows Ref. [34]. The final result for the small-signal hot-tube dispersion relation is

$$D(\beta; \omega) = \det(M) = 0, \tag{B34}$$

where the matrix M is given by:

$$M_{ll'} = (-1)^l j^{l+l'} \sum_{n=-\infty}^{\infty} \begin{pmatrix} J_l(\alpha_n) & 0 \\ 0 & \frac{l+1}{\alpha_n} J_{l+1}(\alpha_n) \end{pmatrix} \widetilde{Z_n} \begin{pmatrix} J_{l'}(\alpha_n) & 0 \\ 0 & \frac{l'+1}{\alpha_n} J_{l'+1}(\alpha_n) \end{pmatrix} \tag{B34a}$$

for $l, l' = 0,1,2, \ldots$ J here is the l^{th} (l'^{th}) order Bessel function of the first kind. Its argument, α_n, is $\alpha_n \equiv \frac{w}{2}\left[\frac{n}{a \sin\psi} + \beta \cos\psi\right]$. The matrix $\widetilde{Z_n}$ is defined to be

$$\widetilde{Z_n} \equiv R Z_n \begin{pmatrix} 0 & 1 \\ -1 & 0 \end{pmatrix} R^{-1} \tag{B34b}$$

where R is the rotation matrix

$$R \equiv \begin{pmatrix} \cos\psi & \sin\psi \\ -\sin\psi & \cos\psi \end{pmatrix} \tag{B34c}$$

and Z_n is the impedance matrix

$$Z_n \equiv \left(Y_n^{(2)} - Y_n^{(1)}\right)^{-1} \tag{B34d}$$

defined in terms of the admittance matrices

$$Y_n^{(i)} \equiv \frac{-j\beta_n c}{\varsigma_0 \gamma_n^{(i)} l_{Hn}^{(i)} \omega a} \begin{pmatrix} n & \dfrac{n^2\beta_n}{\gamma_n^{(i)2} a} - \epsilon_r^{(i)} \dfrac{\omega^2}{c^2} \dfrac{a}{\beta_n} l_{Hn}^{(i)} l_{En}^{(i)} \\ -\dfrac{\gamma_n^{(i)2} a}{\beta_n} & -n \end{pmatrix} \tag{B34e}$$

where $\varsigma_0 \equiv \mu_0 c$ is the impedance of free space.

Bibliography

[1] A. S. Gilmour, Jr., *Principles of Traveling Wave Tubes*, Second Edition, Artech Print on Demand (1994).

[2] A. S. Gilmour, Jr., *Klystrons, Traveling Wave Tubes, Magnetrons, Crossed-Field Amplifiers, and Gyrotrons*, First Edition, Artech House (2011).

[3] J. R. Pierce, *Traveling Wave Tubes*, Van Nostrand: New York, NY, USA (1950).

[4] G. W. Gewartowski and H. A. Watson, *Principles of Electron Tubes*, Van Nostrand: Princeton, NJ, USA (1966).

[5] Shulim E. Tsimring, *Electron Beams and Microwave Vacuum Electronics*, John Wiley & Sons, Inc.: Hoboken, NJ, USA (2007).

[6] R. Kompfner, *The Invention of Traveling Wave Tube*, San Francisco Press, San Francisco, CA (1964).

[7] Nils E. Lindenblad, "Electron discharge device system," U.S. Patent 2300052, 1942.

[8] National Academy of Science, online: http://www.nasonline.org/publications/biographical-memoirs/memoir-pdfs/pierce-john-r.pdf.

[9] Andrew V. Haeff, "Device for and method of controlling high frequency currents," U.S. Patent 2064469, 1936 and U.S. Patent 2233126, 1941.

[10] L3 Technologies: Electron Devices Division website: http://www2.l3t.com/eti/products/twt_design.htm.

[11] R. H. Abrams, B. Levush, A. A. Mondelli, and R. K. Parker, "Vacuum Electronics for the 21st Century," IEEE Microwave Magazine, Vol. 2, Issue: 3, pp. 61-72, Sept. 2001. doi: 10.1109/6668.951550.

[12] Z. Huang and K. J. Kim, "Review of x-ray free electron laser theory," Phys. Rev. Special Topics - Accelerator and Beams **10**, 034801 (2007). doi: 10.1103/PhysRevSTAB.10.034801.

[13] L. Schachter, "Beam-wave interaction in periodic and quasi-periodic structures," 2nd Ed., Springer-Verlag: Berlin, Germany (2011).

[14] C. W. Roberson and P. Sprangle, "A review of free-electron lasers," Phys. Fluids B **1**, 3 (1989).

[15] T. C. Marshall, *Free Electron Lasers*, Macmillan: New York (First edition, January 1985).

[16] H. P. Freund and T. M. Antonsen, *Principles of Free-electron Lasers (2nd Edition)*, Springer, US (1996).

[17] V. Kumar and K. J. Kim, "Analysis of Smith-Purcell free-electron lasers," Phys. Rev. E **73**, 026501 (2006). doi: 10.1103/PhysRevE.73.026501.

[18] P. Zhang, L. K. Ang, and A. Gover, "Enhancement of coherent Smith-Purcell radiation at terahertz frequency by optimized grating, prebunched beams, and open cavity," Phys. Rev. Special Topics - Accelerators and Beams **18**, 020702 (2015). doi: 10.1103/PhysRevSTAB.18.020702.

[19] V. L. Granatstein and I. Alexeff, *High power microwave sources*, Artech House: Boston (1987).

[20] K. R. Chu, "The electron cyclotron maser," Rev. Mod. Phys. **76**, 2, 489-540 (2004).

[21] R. J. Barker, J. H. Booske, N. C. Luhmann, and G. S. Nusinovich, *Modern microwave and millimeter-wave power electronics*, IEEE Press: Piscataway, New Jersey (2005).

[22] J. Benford, J. A. Swegle, and E. Schamiloglu, *High-power microwaves*, 3rd ed., CRC Press: New York (2016).

[23] M. Thumm, *State-of-the-art of high power gyro-devices and free electron masers*, KIT Scientific Publishing, 2016.

[24] G. S. Nusinovich, *Introduction to the physics of gyrotrons*, Johns Hopkins University Press: Baltimore (2004).

[25] Y. S. Tan and R. Seviour, "Wave energy amplification in a metamaterial-based traveling-wave structure," EPL **87** 34005 (2009). doi: 10.1209/0295-5075/87/34005.

[26] D. Shiffler, J. Luginsland, D. M. French, and J. Watrous, "A Cerenkov-like Maser Based on a Metamaterial Structure," IEEE Transactions on Plasma Science, Vol. 38, No. 6, pp. 1462-1465, June 2010. doi: 10.1109/TPS.2010.2046914.

[27] S. C. Yurt, A. Elfrgani, M. I. Fuks, K. Ilyenko, and E. Schamiloglu, "Similarity of Properties of Metamaterial Slow-Wave Structures and Metallic Periodic Structures," IEEE Transactions on Plasma Science, Vol. 44, No. 8, pp. 1280-1286, August 2016. doi: 10.1109/TPS.2016.2535305.

[28] J. R. Pierce, “Coupling of Modes of Propagation”, Journal of Applied Physics **25**, 179 (1954). doi: 10.1063/1.1721599.

[29] H. A. Haus and W. P. Huang, “Coupled-Mode Theory,” Proc. IEEE, Vol. 79, No. 10, pp. 1505-1518, October 1991.

[30] Francis F. Chen, *Introduction to Plasma Physics and Controlled Fusion, Volume 1: Plasma Physics (2nd Edition)*, Plenum Press: New York (1984).

[31] Paul M. Bellan, *Fundamentals of Plasma Physics*, Cambridge University Press: New York (2006).

[32] Simon Ramo, John R. Whinnery, and Theodore Van Duzer, *Fields and Waves in Communication Electronics*, Third Edition, John Wiley & Sons, Inc.: New York (1994).

[33] Marvin Chodorow and Charles Susskind, *Fundamentals of Microwave Electronics*, McGraw-Hill: New York (1964).

[34] D. Chernin, T. M. Antonsen, Jr., and B. Levush, “Exact Treatment of the Dispersion and Beam Interaction Impedance of a Thin Tape Helix Surrounded by a Radially Stratified Dielectric,” IEEE Transactions on Electron Devices, Vol. 46, No. 7, pp. 1472-1483, July 1999.

[35] D. H. Simon, P. Wong, D. Chernin, Y. Y. Lau, B. Hoff, P. Zhang, C. F. Dong, and R. M. Gilgenbach, “On the evaluation of Pierce parameters C and Q in a traveling wave tube,” Physics of Plasmas **24**, 033114 (March 2017). doi: 10.1063/1.4978474.

[36] Y. Y. Lau and D. Chernin, “A review of the ac space charge effect in electron-circuit interactions,” Phys. Fluids B, VOL. 4, NO. 11, pp. 3473-3497, November 1992. doi: 10.1063/1.860356.

[37] S. J. Cooke, C-L Chang, T. M. Antonsen, Jr., D. P. Chernin, and B. Levush, “Three-Dimensional Modeling of AC Space Charge for Large Signal TWT Simulation,” IEEE Transactions on Electron Devices, Vol. 52, No. 5, pp. 764-773, May 2005. doi: 10.1109/TED.2005.845870.

[38] C. K. Birdsall and G. R. Brewer, “Traveling Wave Tube Characteristics for Finite Values of C,” IRE Trans. PGED, ED-1, pp. 1-11, August 1954.

[39] Thomas M. Antonsen, Jr., Pedro Safier, David P. Chernin, and Baruch Levush, “Stability of traveling-wave amplifiers with reflections,” IEEE Transactions on Plasma Science, Vol. 30, No. 3, pp. 1089–1107, June 2002. doi: 10.1109/TPS.2002.801563.

[40] David Chernin, Ian Rittersdorf, Y. Y. Lau, Thomas M. Antonsen, Jr., and Baruch Levush, "Effects of Multiple Internal Reflections on the Small-Signal Gain and Phase of a TWT," IEEE Transactions on Electron Devices, Vol. 59, No. 5., pp. 1542-1550, May 2012. doi: 10.1109/TED.2012.2186141.

[41] John H. Booske and Mark C. Converse, "Insights From One-Dimensional Linearized Pierce Theory About Wideband Traveling-Wave Tubes With High Space Charge," IEEE Transactions on Plasma Science, Vol. 32, No. 3, pp. 1066-1072, June 2004. doi: 10.1109/TPS.2004.828790.

[42] A. Nordsieck, "Theory of the Large Signal Behavior of Traveling-Wave Amplifiers," Proceedings of the I.R.E., Vol. 41, Issue: 5, pp. 630-637, June 1953.

[43] P. K. Tien, L. R. Walker, and V. M. Wolontis, "A Large Signal Theory of Traveling-Wave Amplifiers," Proceedings of the I.R.E., Vol. 43, Issue: 3, pp. 260-277, March 1955.

[44] J. E. Rowe, "A Large-Signal Analysis of the Traveling-Wave Amplifier: Theory and General Results," IRE Transactions—Electron Devices, Vol. 3, Issue: 1, pp. 39-56, January 1956.

[45] A. J. Giarola, "A Theoretical Description for the Multiple-Signal Operation of a TWT," IEEE Transactions on Electron Devices, VOL. ED-15, NO. 6, pp. 381-395, June 1968.

[46] N. J. Dionne, "Harmonic Generation in Octave Bandwidth Traveling-Wave Tubes," IEEE Transactions on Electron Devices, VOL. ED-17, NO. 4, pp. 365-372, April 1970.

[47] C. F. Dong, P. Zhang, D. Chernin, Y. Y. Lau, B. W. Hoff, D. H. Simon, P. Wong, G. B. Greening, and R. M. Gilgenbach, "Harmonic Content in the Beam Current in a Traveling-Wave Tube," IEEE Transactions on Electron Devices, Vol. 62, No. 12, pp. 4285-4292, December 2015. doi: 10.1109/TED.2015.2490584.

[48] T. M. Antonsen, Jr. and B. Levush, "CHRISTINE: A Multifrequency Parametric Simulation Code for Traveling Wave Tube Amplifiers," NRL report NRL/FR/6840-97-9845, April 1997.

[49] G. M. Branch and T. G. Mihran, "Plasma Frequency Reduction Factors in Electron Beams," IRE Transactions—Electron Devices, Vol. 2, No. 2, pp. 3-11, 1955.

[50] D. Dialetis, D. Chernin, T. M. Antonsen, Jr., and B. Levush, "An Improved Representation of AC Space-Charge Fields in Steady-State Simulation Codes for Linear-Beam Tubes," IEEE Transactions on Electron Devices, Vol. 54, No. 4, pp. 888-892, April 2007. doi: 10.1109/TED.2007.891858.

[51] S. K. Datta and L. Kumar, "A Simple Closed-Form Formula for Plasma-Frequency Reduction Factor for a Solid Cylindrical Electron Beam," IEEE Transactions on Electron Devices, Vol. 56, No. 6, pp. 1344-1346, June 2009. doi: 10.1109/TED.2009.2017649.

[52] T. M. Antonsen, Jr. and B. Levush, "Traveling-Wave Tube Devices with Nonlinear Dielectric Elements," IEEE Transactions on Plasma Science, Vol. 26, No. 3, pp. 774-786, June 1998.

[53] G. B. Greening, N. M. Jordan, S. C. Exelby, D. H. Simon, Y. Y. Lau, and R. M. Gilgenbach, "Multi-frequency recirculating planar magnetrons," Applied Physics Letters, Vol. 109, No. 7, 074101, August 2016. doi: 10.1063/1.4961070.

[54] Geoffrey B. Greening, PH. D Thesis, University of Michigan, 2017.

[55] B. W. Hoff and D. M. French, "Particle-in-Cell Simulations of a Multiple Beam S-Band Disk-on-Rod TWT Amplifier," IEEE Transactions on Plasma Science, Vol. 44, No. 8, pp. 1287-1290, August 2016. doi: 10.1109/TPS.2016.2547344.

[56] B. W. Hoff and D. M. French, "Simulations of a Disk-on-Rod TWT Driven by an NLTL-Modulated Electron Beam," IEEE Transactions on Plasma Science, Vol. 44, No. 8, pp. 1265-1269, August 2016. doi: 10.1109/TPS.2016.2519407.

[57] H. R. Johnson, "Backward-Wave Oscillators," Proceedings of the IRE, Vol. 43, Issue: 6, pp. 684-697, June 1955.

[58] A. Jassem, P. Y. Wong, Y. Y. Lau, "A Re-Examination of Johnson's Theory of Backward Wave Oscillation in a Traveling Wave Tube," IEEE International Conference on Plasma Science (ICOPS) 2018, Denver, CO, June 2018.

[59] Geoffrey B. Greening, Steven C. Exelby, Drew A. Packard, Nicholas M. Jordan, Y. Y. Lau, and Ronald M. Gilgenbach, "Harmonic Frequency Locking in the Multifrequency Recirculating Planar Magnetron," IEEE Transactions on Electron Devices, March 2018. doi: 10.1109/TED.2018.2810240.

[60] X. Meng, Y. Gong, T. Tang, H. Gong, and G. Travish, "The research of 140ghz high harmonic traveling wave tube," in 2016 IEEE International Vacuum Electronics Conference (IVEC), Apr. 2016, pp. 1–2. [Online]. Available: http://doi.org/10.1109/IVEC.2016.7561832.

[61] C. B. Wilsen, Y. Y. Lau, D. P. Chernin, and R. M. Gilgenbach, "A Note on Current Modulation From Nonlinear Electron Orbits," IEEE Transactions on Plasma Science, Vol. 30, No. 3, pp. 1176-1178, June 2002. doi: 10.1109/TPS.2002.801571.

[62] Y. Y. Lau, D. P. Chernin, C. Wilsen, and R. M. Gilgenbach, "Theory of Intermodulation in a Klystron," IEEE Transactions on Plasma Science, Vol. 28, No. 3, pp. 959-970, June 2000.

[63] M. Friedman, J. Krall, Y. Y. Lau, and V. Serlin, "Externally modulated intense relativistic electron beams," Journal of Applied Physics, Vol. 64, No. 7, pp. 3353-3379, October 1988.

[64] D. R. Nicholson, *Introduction to Plasma Theory*, p.31, New York: Wiley, 1983.

[65] S. K. Datta, P. K. Jain, M. D. Raj Narayan, and B. N. Basu, "Nonlinear Eulerian Hydrodynamical Analysis of Helix Traveling-Wave Tubes," IEEE Transactions on Electron Devices, Vol. 45, No. 9, pp. 2055-2062, September 1998.

[66] J. G. Wöhlbier, J. H. Booske, and I. Dobson, "The Multifrequency Spectral Eulerian (MUSE) Model of a Traveling Wave Tube," IEEE Transactions on Plasma Science, Vol. 30, No. 3, pp. 1063-1075, June 2002. doi: 10.1109/TPS.2002.801603.

[67] Y. V. Gulyaev, V. F. Kravchenko, and A. A. Kuraev, "Vavilov-Cherenkov Amplifiers with Irregular Electrodynamic Structures," Physics-Uspekhi, VOL. 47, NO. 6, pp. 583-599, June 2004. doi: 10.1070/PU2004v047n06ABEH001748.

[68] D. M. H. Hung, I. M. Rittersdorf, P. Zhang, D. Chernin, Y. Y. Lau, T. M. Antonsen, Jr., J. W. Luginsland, D. H. Simon, and R. M. Gilgenbach, "Absolute Instability near the Band Edge of Traveling-Wave Amplifiers," Physical Review Letters **115**, 124801 (2015). doi: 10.1103/PhysRevLett.115.124801.

[69] A. P. Kuznetsov, S. P. Kuznetsov, A. G. Rozhnev, E. V. Blokhina, and L. V. Bulgakova, "Wave Theory of a Traveling-Wave Tube Operated Near the Cutoff," Radiophysics and Quantum Electronics, VOL. 47, NOs. 5-6, pp. 356-373, 2004.

[70] I. M. Rittersdorf, T. M. Antonsen, Jr., D. Chernin, and Y. Y. Lau, "Effects of Random Circuit Fabrication Errors on the Mean and Standard Deviation of Small Signal Gain and Phase of a Traveling Wave Tube," IEEE J. Electron Device Soc., Vol. 1, No. 5, pp. 117-128, May 2013. doi: 10.1109/JEDS.2013.2273794.

[71] Simon Ramo, "The Electronic-Wave Theory of Velocity-Modulation Tubes," Proceedings of the I.R.E., Vol. 27, Issue: 12, pp. 757-763, December 1939.

[72] Lester M. Field, "Some slow-wave structures for traveling-wave tubes," Proc. IRE, Vol. 37, No. 1, pp. 34-40, January 1949.

[73] L. M. Field, "Traveling wave tube," U.S. Patent 2645737, July 14, 1953.

[74] Y. Y. Lau, "Some design considerations on using modulated intense annular electron beams for particle acceleration," Journal of Applied Physics, Vol. 62, No. 2, pp. 351-356, July 1987. doi: 10.1063/1.339803.

[75] M. Friedman, "Propagation of an intense relativistic electron beam in an annular channel," Journal of Applied Physics, Vol. 80, No. 3, pp. 1263-1267, August 1996. doi: 10.1063/1.362976.

[76] Peng Zhang, Ágúst Valfells, L. K. Ang, J. W. Luginsland, and Y. Y. Lau, "100 years of the physics of diodes," Applied Physics Reviews **4**, 011304 (2017).

[77] R. E. Peterkin and J. W. Luginsland, "A virtual prototyping environment for directed-energy concepts," *Comput. Sci. Eng.*, vol. 4, no. 2, pp. 42-49, March 2002.

[78] B. Goplen, L. Ludeking, D. Smith, and G. Warren, "User-configurable MAGIC for electromagnetic PIC calculations," Comput. Phys. Commun., vol. 87, no. 1–2, pp. 54–86, May 1995.

[79] Y. Y. Lau and L. R. Barnett, "Theory of a Low Magnetic Field Gyrotron (Gyromagnetron)," *International Journal of Infrared and Millimeter Waves*, Vol. 3, No. 5, pp. 619-744, 1982.

[80] Matthew Franzi, Ronald Gilgenbach, Y. Y. Lau, Brad Hoff, Geoff Greening, and Peng Zhang, "Passive mode control in the recirculating planar magnetron," Physics of Plasmas **20**, 033108 (2013). doi: 10.1063/1.4794967.

[81] D. H. Simon, Y. Y. Lau, G. Greening, P. Wong, B. Hoff, and R. M. Gilgenbach, "Stability of Brillouin flow in the presence of slow-wave structure," Physics of Plasmas **23**, 092101 (2016). doi: 10.1063/1.4961917.

[82] David P. Chernin, Private communication.

[83] Chiping Chen, "Piercetype dispersion relation for an intense relativistic electron beam interacting with a slowwave structure," Physics of Plasmas, Vol. 1, No. 1, pp. 167-170, January 1994. doi: 10.1063/1.870547.

[84] David H. Simon, Private communication.

[85] ANSYS HFSS: High Frequency Electromagnetic Field Simulation, Available: http://www.ansys.com.

[86] R. J. Briggs, *Electron Stream Interactions with Plasmas*, (MIT Press, Cambridge, MA, 1964); A. Bers, *Handbook of Plasma Physics*, edited by M. N. Rosenbluth and R. Z. Sagdeev (North-Holland, New York, 1983).

[87] Foivos Antoulinakis, Patrick Wong, Abhijit Jassem, and Y. Y. Lau, "Re-examination of Absolute Instability Near Band Edges in a Traveling Wave Tube," IEEE International Vacuum Electronics Conference (IVEC), Monterey, CA, April 2018.

[88] R. J. Briggs, “Space charge waves on a relativistic, unneutralized electron beam and collective ion acceleration,” Physics of Fluids **19**, No. 8, pp. 1257-1258, August 1976. doi: 10.1063/1.861611.

[89] Peng Zhang, Brad Hoff, Y. Y. Lau, D. M. French, and J. W. Luginsland, “Excitation of a Slow Wave Structure,” Physics of Plasmas **19**, 123104 (2012).

[90] Brad W. Hoff, David S. Simon, David M. French, Y. Y. Lau, and Patrick Wong, “Study of a high power sine waveguide traveling wave tube amplifier centered at 8 GHz,” Physics of Plasmas **23**, 103102 (2016). doi: 10.1063/1.4964141.

[91] Michael Wirth, Aarti Singh, John Scharer, and John Booske, “Third-Order Intermodulation Reduction by Harmonic Injection in a TWT Amplifier,” IEEE Transactions on Electron Devices, Vol. 49, No. 6, pp. 1082-1084, June 2002.